Higgs Exempt No-Scale Supersymmetry

by

Jason Lott Evans

A dissertation submitted in partial fulfillment
of the requirements for the degree of
Doctor of Philosophy
(Physics)
in The University of Michigan
2009

Doctoral Committee:

Professor James Daniel Wells, Chair
Professor Dante Eric Amidei
Professor Ratindranath Akhoury
Professor Charles R. Doering
Assistant Professor Aaron Thomas Pierce

TABLE OF CONTENTS

LIST OF FIGURES

Figure

LIST OF APPENDICES

Appendix

CHAPTER I

Introduction

The Standard Model (SM) has been one of the great triumphs of science. It has consistently predicted all collider phenomenology thus far. However, the Higgs particle, which is responsible for mass, has not yet been observed and is not completely understood. One difficulty of the SM is associated with the Higgs' scalar nature. In a quantum theory, the mass of a scalar particle will receive corrections that are proportional to the scale where any new physics arises. Because the cut-off scale of the SM is the Planck scale, $M_{\rm Pl}$, the natural mass of the SM Higgs boson "should be" of order the Planck scale. A Higgs particle of this mass cannot replicate experimental predictions. The data prefers a Higgs mass similar to the electroweak scale. This disparity between the preferred experimental and theoretical Higgs mass in the SM is known as the hierarchy problem. To remedy this instability of the Higgs mass, there must be some new physics at or around 1 TeV. If the scale of new physics is larger than 1 TeV, the quantum corrections become large and the hierarchy problem still exists.

Cosmology presents other challenges to our current understanding of the universe. Of the energy budget of the universe, approximately five percent is composed of known particles, with the majority of this energy being in baryons. Although baryons make up a very small percentage of the total energy budget, it is not known why there are so many. This large abundance can only be achieved if some mechanism is able to create an asymmetry

between baryons and anti-baryons in the early universe. The other seventy five percent of the energy budget is either dark energy or dark matter for which there is no good candidates in the SM. However, supersymmetry provides a good candidate for dark matter of the weakly interacting massive particle (WIMP) type[1].

1.1 The Hierarchy Problem of the Standard Model

There are two main techniques for stabilizing the Higgs mass at or around the electroweak scale: increasing the number of dimensions or extending the symmetries of the SM[2]. With extra dimensions, the Planck scale can be pushed down to around a TeV. A Planck scale this small means the effective theory of gravity is only defined up to the TeV scale. An effective theory with a cut around a TeV gives acceptably small corrections to the Higgs mass. The other technique for stabilizing the hierarchy (symmetry) protects the Higgs mass from the radiative corrections of the high scale physics, i.e. gravity.

Supersymmetry, a symmetry capable of stabilizing the hierarchy, relates fermions and bosons. The minus sign appearing in fermion loop calculations leads to a cancellation with contributions from boson loops. To see how this cancellation arises we look at some of the properties of supersymmetry. The generators of a supersymmetric transformation interchange bosons and fermions as follows

$$Q|\mathbf{Fermion}\rangle = |\mathbf{Boson}\rangle \qquad Q|\mathbf{Boson}\rangle = |\mathbf{Fermion}\rangle. \tag{1.1}$$

Because the generators of supersymmetry exchange fermions and bosons without changing their representation under the other symmetries, a supersymmetric theory will have bosons and fermions with the exact same quantum numbers. This means every fermion in the SM must have a corresponding boson with the same representation under the SM gauge groups. In the case of matter fermions, this partner is a spin zero boson, for the spin 1 bosons,

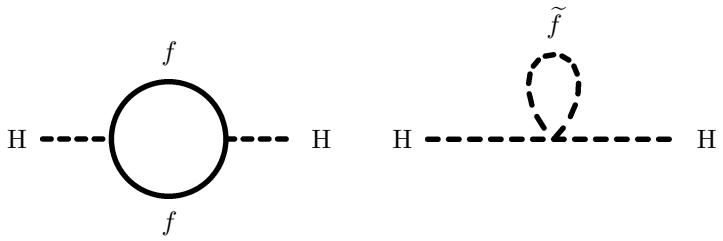

Figure 1.1: This figure contains the Feynman diagrams for, a) a fermionic contribution to the Higgs mass, b) a scalar contribution to Higgs mass.

this partner particle is a spin 1/2 fermion. For local supersymmetry (supergravity), there is also a spin 3/2 fermion (gravitino) and a spin 2 boson (gravition).

For the Lagrangian of supersymmetry to be invariant under supersymmetric transformations, the couplings of the bosons and fermions must be related. If this were not the case, there would exist some supersymmetric transformation (interchanging bosons and fermions) that would give a Lagrangian with different couplings and thus it would not be invariant. The relationship among the couplings forced by supersymmetry leads to a cancellation among the diagrams. For example, in supersymmetry the diagrams like those in Fig. 1.1 would cancel exactly if the fermion and boson in these loops had equal masses. In fact, all diagrams that contribute to the mass of the Higgs have some sort of cancellation and the hierarchy is stable.

To preserve the invariance of the SUSY Lagrangian, the masses of the supersymmetric particles must also be related. The bosons and fermions of a given multiplet turn out to have the same masses. Experiment has not as of yet seen any evidence of these supersymmetric particles. If they exist, these superpartners must be heavier than their corresponding SM counterpart in order to evade experimental constraints. The broken degeneracy of the fermion and boson masses required by experiment forbids supersymmetry from being an exact symmetry of nature. Instead, supersymmetry must be broken at the electroweak scale. However, certain forms of broken supersymmetry can stabilize the hierarchy. Having a stable hierarchy will place strong constraints on the SUSY breaking mechanism. A broken

supersymmetry with a stable hierarchy has been softly broken. Supersymmetry is softly broken by the introduction of any or all of the following operators to the Lagrangian

$$\mathcal{L}_{\mathbf{soft}} = -\frac{1}{2}\left(M_a\lambda^a\lambda^a + A^{ijk}\phi_i\phi_j\phi_k + B^{ij}\phi_i\phi_j\right) + \text{c.c.} - m_i^j\phi^{i*}\phi_j \tag{1.2}$$

where the couplings A^{ijk}, B^{ij} and m_i^j are only constrained by gauge invariance. These couplings introduce new diagrams contributing to the mass of the Higgs. However, these new diagrams are only logarithmically sensitive to higher mass scales. With this logarithmic sensitivity, the Higgs mass is still sufficiently protected[1]. The diagrams involving only supersymmetry preserving interactions from the superpotential, which give the quadratic divergences, are modified as well. Fortunately, this modification does not disrupt the cancellation of the quadratic divergences. The lack of observed superpartners with masses $\lesssim 100\,\text{GeV}$ then places a lower bound on the soft masses in Eq. (1.2).

An obvious first try for breaking supersymmetry would be a Higgs type mechanism involving only renormalizable interactions[3]. In this case, the soft masses arise from directly coupling fields that break supersymmetry to minimal supersymmetric standard model (MSSM) fields. The difficulty with this mechanism is that it leads to scalars that are lighter then their fermionic partners. This can be seen by examining the mass matrices of supersymmetry. The mass matrices are as follows: the fermion mass matrix is

$$M_{1/2} = \begin{pmatrix} W_{ab} & -\sqrt{2}g_B D_{Ba} \\ -\sqrt{2}D_{Ab} & 0 \end{pmatrix}, \tag{1.3}$$

for the state

[1] Here we have assumed that the highest possible cut off for the SM is the Planck scale.

$$\Psi = \begin{pmatrix} \psi^a \\ \\ \lambda_A \end{pmatrix} \tag{1.4}$$

and the scalar mass matrix is

$$M_0^2 = \begin{pmatrix} M_{1/2}^\dagger M_{1/2} + D_A^a D_{Ab} + D_{Ab}^a D_A & W^{\dagger abc} W_c + D_A^a D_A^b \\ W_{abc} W^{\dagger c} + D_{Aa} D_{Ab} & M_{1/2} M_{1/2}^\dagger + D_{Aa} D_A^b + D_{Aa}^b D_A \end{pmatrix}, \tag{1.5}$$

W is the superpotential, and $D_A = g_A Q_a^\dagger (T_A)_b^a Q^b$. The above scalar mass matrix is for the state

$$\Phi = \begin{pmatrix} Q^a \\ \\ Q_a^\dagger \end{pmatrix}. \tag{1.6}$$

The subscripts (superscripts) a, b, c etc. correspond to derivatives with respect to the fields $Q_a^\dagger$ (Q^a). As an example, we consider the mass matrix of the up type squarks in the basis $(\tilde{u}, \tilde{u}^\dagger)$. The off-diagonal components of the scalar mass matrix will be zero because mass terms of the type $\tilde{u}\tilde{u}$ are forbidden by the gauge symmetries. With the gauge groups of the standard model preserved, $\langle D_{Ab} \rangle = \langle D_A^a \rangle = 0$. Examining the fermion and scalar mass matrices with these constraints we see they differ by a term $D_{Ab}^a D_A = g_A T_b^a D_A$. If $\tilde{u}_a T_b^a = -|\lambda| \tilde{u}_b$, which will be the case for at least one particle, the mass of the scalar will be less than the corresponding fermion. Scalar particles lighter than their fermionic partner are excluded for all flavors except possibly the top.

Clearly, a renormalizable low-scale supersymmetric theory cannot meet the necessary conditions placed on supersymmetry breaking. This difficulty can be evaded by introducing a hidden sector. In this hidden sector, supersymmetry breaking occurs and is then

transmitted to the visible sector through non-renormalizable operators. This hidden sector, where supersymmetry breaking occurs, cannot be charged under the gauge groups of the SM. Otherwise, we are back to the situation with light scalars.

Without any knowledge of the hidden sector or high-scale physics, it is still possible to write a Lagrangian with non-renormalizable interactions leading to SUSY breaking in the visible sector. A generic set of SUSY breaking contributions to the Lagrangian are

$$\begin{aligned}\Delta\mathcal{L} \quad &= \int d^4\theta \left\{ \frac{(z_Q)^i{}_j}{M^2} X^\dagger X Q^\dagger Q + \cdots \right. \\ &\qquad \left. + \frac{b}{M} X H_u H_d + \frac{b'}{M} X^\dagger X H_u H_d + \text{h.c.} \right\} \\ &\quad + \int d^2\theta \left[\frac{s_1}{M} X W_1^\alpha W_{1\alpha} + \cdots \right] + \text{h.c.} \\ &\quad + \int d^2\theta \left[\frac{a_{ij}}{M} X Q^i H_u (U^c)^j + \cdots \right].\end{aligned} \tag{1.7}$$

When the F term of the X field obtains a vacuum expectation value (vev), these terms will be exactly those found in Eq. (1.2) with the masses being of order $M_{SUSY} \sim \langle F_X \rangle / M$

1.2 Minimal Supersymmetric Standard Model

The simplest supersymmetric model (minimal matter content) capable of reproducing the SM predictions is known as the minimal supersymmetric standard model (MSSM). This is an effective theory that contains only the particles of the standard model (SM) and their superpartners, plus an extra Higgs boson. The extra Higgs boson is needed for anomaly cancellation. The superpotential for the MSSM is

$$\mathcal{W} = \mu H_u H_d + \lambda^l_{ij} L_i e_j + \lambda^d_{ij} Q_i d_j H_d + \lambda^u_{ij} Q_i u_j H_u \tag{1.8}$$

where $Q_i,\ L_i,\ u_i,\ d_i,\ , e_i$ are matter chiral superfields with obvious notation, and H_u, H_d are the Higgs bosons. In the supersymmetric limit the MSSM only has one more

coupling than the SM, μ. However, each of these fields will have a soft mass and possibly a trilinear coupling that breaks supersymmetry and introduces many more free parameters. Because there is no symmetry to prevent flavor mixing in these couplings, flavor violation will be quite large in a generic MSSM. Only approximately diagonal scalar masses at the electroweak scale will give acceptable flavor violation.

1.3 Flavor Changing Neutral Currents of Supersymmetric Theories

Although the soft breaking terms of supersymmetry are constrained by gauge invariance, they are still quite generic. They can still lead to observations that contradict experimental findings. Besides a lower bound on the size of the scalar masses, there are constraints on the off-diagonal components.

Flavor changing neutral currents in supersymmetry can arise from non-diagonal soft masses [5]. These non-diagonal scalar mass matrices lead to a misalignment between the interaction basis and mass basis of the scalar particles. This misalignment allows the scalars to change flavor as they propagate. With flavor violating propagators, loop diagrams will lead to flavor violation in the decay of SM leptons. The difficulty with large off-diagonal components of the slepton mass matrices is flavor changing neutral currents such as $\ell_i \to \ell_j \gamma$. In the SM, lepton flavor violating amplitudes are quite small because they are suppressed by $(m_\nu/m_W)^2$ [4], where m_ν is the neutrino mass and m_W is the mass of the W. With the neutrinos having eV scale masses and the W being of order 100 GeV, lepton number is only marginally violated in the SM. These dangerously large flavor violating processes can be suppressed by either taking very large soft masses, or by some sort of alignment of the soft masses at the low scale. Models of supersymmetry breaking such as gauge mediation are specifically designed to suppress these flavor changing processes. Because supersymmetry breaking in these models occurs through gauge interactions, the sfermion mass matrices are diagonal when the SM fermions are in the interaction basis.

In these models, the only flavor violation present at the electroweak scale will be due to renormalization group (RG) running. With the Yukawa matrices of the SM approximately diagonal[2], the sfermion masses remain diagonal in the course of renormalization group evolution (RGE) and no new flavor violation emerges.

Another possibility for creating diagonal low scale sfermion masses, discussed in more detail later, is no-scale type models. In no-scale type models, the sfermion mass matrices are zeroed at some high scale boundary. The low scale masses are then entirely the consequence of renormalization group (RG) running. Because the dominant contribution to the RG running of the sfermions is from the gauginos, the induced sfermion mass matrices are predominantly diagonal. One complication of pure no-scale models is that the lightest super partner is charged (LSP).

1.4 R Parity and Dark Matter

A supersymmetric theory that is natural and constrained only by gauge invariance will have problems with proton stability. Unless there is some symmetry to prevent the following operators from appearing in the superpotential [6],

$$\mathcal{W}_{\not R_p} = -\epsilon_i L_i \cdot H_2 + \frac{1}{2}\lambda_{ijk} L_i \cdot L_j \bar{E}_k + \lambda'_{ijk} L_i \cdot Q_j \bar{D}_k + \frac{1}{2}\lambda''_{ijk} \bar{U}_i \bar{D}_j \bar{D}_k, \tag{1.9}$$

the lifetime of the proton will be too small[3] . Several combinations of interactions from the previous equations can produce diagrams leading to proton decay. These amplitudes have tree level diagrams that are proportional to $\lambda\lambda''$ or $\lambda'\lambda''$, where the indices have been suppressed. There are three possible symmetries that forbid these interactions and stabilize the proton: baryon conservation (B), lepton conservation (L), and R parity. If lepton number is conserved then $\lambda, \lambda' = 0$, and if baryon number is conserved $\lambda', \lambda'' = 0$.

[2]The Yukawa coupling of the quarks are not diagonal. However, if the corrections to the scalars are proportional to the Yukawa couplings, they will give acceptable amounts of flavor changing neutral currents. This is referred to as minimal flavor violation.

[3]Other dangerous processes from these terms are: $n - \bar{n}$ oscillation, large neutrino masses, neutrinos less β decay, etc.[6]

Imposing R parity, discussed below, excludes all couplings in Eq. (1.9). It is interesting to note that if R parity is imposed, the perturbative superpotential conserves both baryon number and lepton number. At this point, it may be unclear which of these symmetries is best. However, the best candidate is R parity. If R parity is conserved, supersymmetry can also explain the dark matter of the universe.

R parity distinguishes the particles of the SM from their superpartners. Every particle of the SM model has a positive R parity, and every superpartner has a negative R parity. Under the assumption of R parity conservation, only operators with positive R parity are allowed in the Lagrangian. Because the Higgs is the only scalar field of the SM, it is the only scalar with positive R parity. This allows it to be paired with SM fermions for the Yukawa terms. Other Yukawa terms, and any trilinear terms not involving the Higgs, will be forbidden. With R parity imposed, a good way to determine the interactions allowed by supersymmetry is to take the SM interactions and replace two of the particles by superpartners. The interactions that involve an odd number of superpartners will not be allowed. Because of this, the scalar particles of supersymmetry can only decay to a SM particle and a superpartner particle. Due to kinematic constraints, the lightest superpartner (LSP) is then stable and cannot decay. In certain regions of parameter space, this LSP has the right relic abundance to be dark matter.

1.5 The Vacuum Structure of Supersymmetry

In the SM, there is only one fundamental scalar particle: the Higgs boson. This leads to a fairly simple potential. Because scalar particles are singlets under the Lorentz transformation, they can obtain a vacuum expectation value (vev) without breaking Lorentz invariance. However, the Higgs is not a singlet under $SU(2) \times U(1)$ and its vev breaks the electroweak symmetry.

Supersymmetry, on the other hand, has many scalar particles. These scalar particles

lead to a very complicated potential. This complexity can lead to many minima that are deeper than the SM minimum [7, 8, 9, 10, 11, 12]. These minima are generated by either negative cubic terms coming from the trilinear soft breaking terms, or large negative soft masses. If these soft terms lead to deep minima with squark and/or slepton vevs, the true minimum of SUSY will break $SU(3)$ and/or $U(1)_{em}$. These minima are referred to as charge and color breaking (CCB) minima. For transitions to these CCB minima which are second order, or very weakly first order, the universe would have quickly transitioned to the true minimum. In this case, the ground state would not be symmetric under $SU(3) \times U(1)_{em}$. Models with these type of minima and phase transitions can be excluded. However, if the transition is strongly first order, it may take longer than the age of the universe and these points cannot be excluded.

1.6 Higgs Exempt No-Scale Supersymmetry

Here, we study the phenomenology of the minimal supersymmetric standard model (MSSM) subject to vanishing scalar soft mass terms (no-scale boundary conditions). With vanishing scalar soft terms, the low scale scalar masses are generated through renormalization group (RG) running. Because only the gauginos have large boundary masses, the dominant RG contribution to the scalar masses will be to the diagonal components. This running leads to scalar mass matrices with diagonal components that are much larger than the off-diagonal components. Unless the scalar masses are large, this approximate diagonality is needed to suppress the supersymmetric contribution to the flavor violation.

The Higgs bosons are flavorless and do not lead to flavor mixing. This allows us to generalize the study of no-scale boundary conditions by including non-vanishing Higgs boson soft masses, as well as a Higgs boson bilinear B term. Inspired by grand-unified theories, we take our input scale to be M_{GUT}, and demand universal gaugino masses at this scale.[4]

[4]For the case of non-universal gaugino masses but vanishing Higgs soft terms, see [13].

In these type of models, electroweak symmetry breaking is due to radiative corrections. After imposing consistent electroweak symmetry breaking, the independent parameters of this theory, which we call Higgs Exempt No-Scale (HENS) supersymmetry[14], are

$$M_{1/2},\ \tan\beta,\ m^2_{H_u},\ m^2_{H_d},\ sgn(\mu), \tag{1.10}$$

where $M_{1/2}$ is the universal gaugino mass at M_{GUT}, $\tan\beta$ is the ratio of the Higgs boson expectation values, $m^2_{H_u}$ and $m^2_{H_d}$ are the soft Higgs masses at M_{GUT}, and $sgn(\mu)$ is the sign of the supersymmetric Higgs bilinear μ term. More details about this model are contained in Chapter II.

First, we will outline the parameter space of HENS models by imposing constraints from electroweak symmetry breaking, $b \to s\gamma$, and the LEP bounds on the Higgs mass. We will also emphasize the regions of parameter space that have a neutralino LSP, and determine in which regions this LSP could be a good candidate for thermal dark matter. Because the scalar masses are small at the high scale, the sleptons in these models tend to be quite light. The light sleptons lead to large cross sections for reactions producing leptons. In fact, HENS models will have a distinctively large 4ℓ signal.

By including right-handed neutrinos, flavor violation is reintroduced. However, unlike other models, HENS models can suppress this new source of flavor violation by taking $m^2_{H_u} \to 0$. In mSUGRA models for example, m_0^2 and A_0 must be small in order to prevent large flavor violation. However, this tends to lead to a stau LSP. Inclusion of these right-handed neutrinos in the HENS model also has an up side. Right-handed neutrinos provide a mechanism for explaining the baryon asymmetry through leptogenesis.

Because much of the parameter space of HENS models have large negative Higgs masses, it is plagued by unbounded from below (UFB) directions, and charge and color breaking (CCB) minima. Requiring the SM vacuum to be stable on time scales longer than the age of the universe will lead to strong constraints on the parameter space, especially for large

$\tan\beta$.

CHAPTER II

Low-Scale Higgs Exempt No-Scale Supersymmetry

2.1 Generating Small Scalar Soft Terms

The motivation for examining models with vanishing scalar masses is primarily data driven. These type of models provide a simple and elegant explanation for the small amount of flavor violation in supersymmetry. Even though our choice of boundary masses are experimentally driven, they can arise from several theoretical constructions. In this chapter we describe some of these theoretical models and discuss how they can be modified to allow for non-vanishing soft masses for the Higgs bosons.

2.1.1 No-Scale Supergravity

We start by considering a model with all scalar masses small. After which, we will consider methods to generalize to non-zero Higgs masses. Vanishing scalar soft terms have traditionally been associated with no-scale models [15]. These models are attractive because the gravitino mass, and therefore the scale of supersymmetry breaking, is determined dynamically. The basic assumption underlying no-scale constructions is that the effective superspace Kähler density and superpotential have the form [16, 17, 18, 19]

$$\begin{aligned} \mathcal{F} &= -3\,M_{\rm Pl}^2 + f(X) + f^\dagger(X^\dagger) + g(\Phi,\Phi^\dagger), \\ \mathcal{W} &= W(\Phi), \end{aligned} \tag{2.1}$$

where X is a hidden sector field, Φ represents a visible sector field, and W is a holomorphic cubic function. To see how this Kähler density and superpotential leads to vanishing scalar masses, we derive the potential for this setup[15]. For this analysis, we take $M_{\rm Pl} = 1$. The Kähler potential from the above functions is

$$\mathcal{G} = 3\ln\left(-3 + f(X) + f^\dagger(X^\dagger) + g(\Phi, \Phi^\dagger)\right) + F(\Phi) + F^\dagger(\Phi^\dagger), \tag{2.2}$$

where $F(\Phi) = \ln \mathcal{W}$. The scalar potential in terms of a generic Kähler potential is

$$V = -e^{-\mathcal{G}}\left(3 + \mathcal{G}^i(\mathcal{G}^{-1})^j_i \mathcal{G}_j\right), \tag{2.3}$$

where

$$\mathcal{G}_i = \tfrac{\partial \mathcal{G}}{\partial \phi_i}, \quad \mathcal{G}^i = \tfrac{\partial \mathcal{G}}{\partial \phi_i}, \quad \mathcal{G}^j_i = \tfrac{\partial^2 \mathcal{G}}{\partial \phi_i \partial \phi_i}. \tag{2.4}$$

In the above expression, we denote $\{X, \Phi\}$ by ϕ_l, with $\phi_1 = X$. Using the no-scale Kähler potential, we can simplify this generic expression for the potential. For convenience, we define the derivative of the Kähler potential with respect to the function $f(X)$ as $\mathcal{G}_f$, which obeys the relationships

$$\mathcal{G}_f^2 = 3\mathcal{G}_{ff} = 3\mathcal{G}_{ff^*}. \tag{2.5}$$

Using these relationships, the derivatives in Eq. (2.4) of the no-scale Kähler potential become

$$\begin{aligned} \mathcal{G}_i &= \mathcal{G}_f\left(f_i + g_i\right) + F_i(\Phi), \\ \mathcal{G}^j &= \mathcal{G}_f\left(f^{*i} + g^{*i}\right) + F^{i\dagger}(\Phi^\dagger), \\ \mathcal{G}^j_i &= \tfrac{1}{3}\mathcal{G}_i\mathcal{G}^j + \mathcal{G}_f g^j_i. \end{aligned} \tag{2.6}$$

It will also be useful to define the projection operator

$$\alpha_i = \frac{\mathcal{G}_f}{\mathcal{G}_{ff^*}} \frac{f^i}{|f^X|^2}. \tag{2.7}$$

This projection operator's only non-vanishing term is the one corresponding to the X direction. From this projection operator, we find that

$$\alpha_i \mathcal{G}^i_j = \mathcal{G}^j - F^{\dagger j}, \tag{2.8}$$

which can be manipulated to the form

$$\mathcal{G}^j (\mathcal{G}^{-1})^i_j = \alpha_i + F^{\dagger j} (\mathcal{G}^{-1})^i_j. \tag{2.9}$$

Contracting the remaining index in the above expression gives

$$\mathcal{G}^j (\mathcal{G}^{-1})^i_j \mathcal{G}_i + 3 = F^{\dagger j} (\mathcal{G}^{-1})^i_j \mathcal{G}_i. \tag{2.10}$$

Taking the complex conjugate of Eq. (2.7) and doing a similar analysis as above, leads to $F^{\dagger j} (\mathcal{G}^{-1})^i_j \mathcal{G}_i = F^{\dagger j} (\mathcal{G}^{-1})^i_j F_i$. This then gives the potential

$$V = -e^{-\mathcal{G}} F^{\dagger j} (\mathcal{G}^{-1})^i_j F_i. \tag{2.11}$$

If we chose $g(\Phi, \Phi^\dagger) = \sum_i \Phi_i \Phi^{\dagger i}$, the potential can be further simplified to give

$$V = e^{-2/3 G_0} \sum_i \left| \frac{\partial \mathcal{W}}{\partial \phi_i} \right|^2 \tag{2.12}$$

where G_0 is the same as $\mathcal{G}$ without the superpotential contribution.

With the definition in Eq. (2.1), there are no supersymmetry breaking terms in Eq. (2.12), and the potential is flat in the X direction. Although the scalar masses are zero in this construction, the gaugino masses can be non-zero as long as the gauge kinetic function is non-trivially dependent on X. The gaugino mass term for a non-trivial gauge kinetic function is

$$e^{-1} \mathcal{L}_{FM} = \frac{1}{4} e^{-\mathcal{G}/2} \mathcal{G}^\ell (\mathcal{G}^{-1})^k_\ell f^*_{\alpha\beta,k} \bar{\lambda}^\alpha_R \lambda^\beta_R = \frac{e^{-\mathcal{G}/2}}{4} \frac{\mathcal{G}_{X^*}}{\mathcal{G}_{XX^*}} \left(\frac{\partial f_{\alpha\beta}}{\partial X} \right) \bar{\lambda}^\alpha_R \lambda^\beta_R. \tag{2.13}$$

From the above expression, we see that the gaugino masses should be of order the gravitino mass, $m_{3/2} = e^{-\mathcal{G}/\in}$, which is not yet determined. However with a gaugino mass term,

there are one-loop corrections to the potential. These corrections lift the potential in the X direction and fix the value of $m_{3/2}$ to lie close to the electroweak scale. Furthermore, no scalar masses arise at the tree level. In this scenario, the electroweak scale is determined dynamically by the large top Yukawa coupling [17].

It is difficult to maintain $m_{3/2} \sim M_W$ in no-scale models if there are other larger scales in the theory. Because of the radiative corrections, the physics at these larger scales can contribute to the effective potential for $m_{3/2}$ [19]. If such large scales exist, such as in a GUT, the heavy sector must be completely sequestered from the supersymmetry breaking, since in the supersymmetric limit, they must not alter the effective potential. Within a GUT where the Higgs superfields are components of complete multiplets that also contain heavy fields, it is therefore essential to prevent these GUT multiplets from obtaining a supersymmetry breaking mass. Having separated the Higgs boson in this way, it is natural to sequester the other chiral multiplets as well. This is the origin of the vanishing scalar soft terms in no-scale models. Gaugino masses can be induced by a non-minimal kinetic function for those and only those components of the GUT vector multiplet that remain light. Thus if the Higgs multiplets are components of a larger GUT multiplet, of which some components develop GUT scale masses, it is not possible to generate soft masses for the Higgs fields without destabilizing $m_{3/2}$. On the other hand, soft Higgs masses might be possible in more general unification scenarios in which the Higgs fields do not belong to complete GUT multiplets [20].

The form of the no-scale Kähler density and superpotential, Eq. (2.1), is an input to these models. Such a form does arise to lowest order in several string- and M-theory constructions, but is typically corrected at higher orders [21]. More generally, a superspace Kähler density in which the visible and hidden sectors appear as disjoint terms, as in Eq. (2.1), is said to be *sequestered* [22]. A sequestered Kähler density and superpotential

guarantees that no direct soft terms are generated. This is a necessary ingredient for anomaly mediation [22].

2.1.2 Gaugino Mediation

It is possible to suppress scalar masses using extra dimensions. This is done by constraining the SM model matter fields and hidden sector fields to reside on spatially separated branes. Because these branes are spatially separated, they cannot directly communicate with each other. Once supersymmetry is broken on the hidden sector brane, the only way to communicate it to the visible sector is through loops containing fields from the bulk. In this case, the scalar masses are loop suppressed relative to the messenger particles living in the bulk.

In gaugino mediation[23], the gauge fields live in the bulk and are the messengers of supersymmetry breaking. Supersymmetry breaking in the hidden sector takes the form of a gaugino mass. Note, this mass term is only relevant on the hidden sector brane. The loops contributing to the supersymmetry breaking masses must then traverse the bulk between the hidden sector and the visible sector. This bulk propagator will lead to an exponential suppression. (This fact will be relevant when we calculate the scalar masses.) The contribution to the action from the mass term for the gauginos is

$$S = \int d^n x \delta(y - L) \int d^2\theta \left[\frac{X}{M} W^\alpha W_\alpha + h.c. \right], \tag{2.14}$$

where the delta function arises because X is constrained to live on the hidden sector brane. It also plays a role in supersymmetry breaking through a non-zero F term. Integrating over the extra dimensions, the gaugino kinetic term becomes non-canonical. Redefining the guagino fields brings the kinetic term back to a canonical form. We now discuss the simplest example of 5 dimensions. If supersymmetry breaking is to be communicated from the hidden sector to the visible sector, the gaugino profile must be non-zero on both branes. These boundary conditions can only be satisfied if the Kaluza Klein (KK) decomposition of

the gaugino is purely a cosine, assuming flat extra dimensions. The zero mode of a cosine expansion is flat. When the integral over this flat profile is done, the kinetic term gets an L coefficient where L is the size of the extra dimension. To return the Lagrangian to a canonical form, the gaugino fields are redefined as $\lambda_4^0 \to \lambda_4^0/L^{-1/2}$. Because the integral over the gaugino mass term has a delta function, the gaugino mass term is unaffected by the integration. The redefinition of the gaugino fields then leads to a $1/L$ coefficient multiplying the gaugino mass term. The 4-d gaugino mass term is then

$$m_{\tilde{\lambda}} = \frac{F_S}{M}\frac{1}{ML}. \tag{2.15}$$

Next, we show that the scalar masses are loop suppressed relative to this value.

To understand why the scalar masses are suppressed, we examine their loop contributions. An important factor in the loop calculation is the bulk propagator of the gauginos. To calculate the propagator, we will need to determine the free field Green's function $\langle 0|\psi\bar{\psi}|0\rangle$. To find this Green's function we need to first determine the form of the 5-d free fermion field for the gauginos. Since the gauginos mass is constrained to the hidden sector brane, the field equations for the gauginos in the bulk are for a massless fermion. They have the form

$$\gamma^M \partial_M \Psi = 0, \tag{2.16}$$

where γ^M with $M = \mu = 0, 1, 2, 3$ are the standard gamma matrices, and $M = 4$ is the matrix $\gamma_5 = \gamma_0\gamma_1\gamma_2\gamma_3$. To solve this equation, we break the gaugino spinor into its left and right handed components,

$$\Psi = \begin{pmatrix} \chi_\alpha \\ \bar{\psi}^{\dot{\alpha}} \end{pmatrix}. \tag{2.17}$$

With this decomposition, Eq. (2.16) becomes a set of coupled differential equations

$$-i\bar{\sigma}^{\mu}\partial_{\mu}\chi_n - \partial_5\bar{\psi}_n = 0, \tag{2.18}$$

$$-i\sigma^{\mu}\partial_{\mu}\bar{\psi}_n + \partial_5\chi_n = 0.$$

To further simplify these equations, we will assume that the expression for the gaugino fields can be separated into a function of the extra dimension multiplied by a four dimensional function as

$$\sum_n g_n(y)\chi_n(x), \tag{2.19}$$

$$\sum_n f_n(y)\bar{\psi}_n(x).$$

Note that the left and right handed components can have different profiles in the extra dimension. This is not only allowed, but will be necessary to meet the boundary conditions of the Z_2 orbifold we impose. The spinor structure is all contained in the 4-d fields. Because we wish $\bar{\psi}_n, \chi_n$ to behave like the familiar massive 4-d fermions, we impose the following equations of motion

$$-i\bar{\sigma}^{\mu}\partial_{\mu}\chi_n + m_n\bar{\psi}_n = 0, \tag{2.20}$$

$$-i\sigma^{\mu}\partial_{\mu}\bar{\psi}_n + m_n\chi_n = 0.$$

With these equations imposed, the $f_n(y)$ and $g_n(y)$ satisfy the following equations of motion

$$g_n' - m_n f_n = 0, \tag{2.21}$$

$$f_n' + m_n g_n = 0.$$

After decoupling these equations, they can be solved giving

$$g_n(y) = A_n\cos(m_n y) + B_n\sin(m_n y), \tag{2.22}$$

$$f_n(y) = B_n\cos(m_n y) - A_n\sin(m_n y). \tag{2.23}$$

As previously mentioned, the Z_2 parity of the orbifold in the extra dimension will impose boundary conditions on the above fields. By requiring that the left and right handed components of the fermions transform differently under this Z_2 parity, the right handed spinor vanishes on the SM brane. The profile of the right-handed fermion must be zero on the SM brane because the 4-d gaugino is a Majorana fermion and not a full Dirac fermion. The boundary conditions forced by these requirements gives the extra dimensional profile

$$f_n(y) = \sqrt{\frac{2}{L}}\cos(m_n y), \tag{2.24}$$

$$g_n(y) = \sqrt{\frac{2}{L}}\sin(m_n y). \tag{2.25}$$

To find the other coefficient, we have also normalized the fields.

Because we imposed Eq. (2.21), the expression for the 4-d fermion fields will be in the familiar form which can be found in [24]. Combining the previous expressions for the extra dimensional profiles with what we know about 4-d fermions, the 5-d free fermion field is

$$\begin{aligned}\Psi(x,y) = \quad & \textstyle\sum_{n,s}\sqrt{\frac{2}{L}}\left[P_L\cos(m_n y) + P_R\sin(m_n y)\right] \\ & \times\textstyle\int\frac{d^3p}{(2\pi)^3}\frac{1}{\sqrt{E_p}}\left(a^s_{p,n}u^s(p)e^{-ipx} + b^{s\dagger}_{p,n}v^s(p)e^{ipx}\right).\end{aligned} \tag{2.26}$$

Since the 5-d field is separable, the Green's functions will also be separable. Using this expression for the fermion fields, the bulk propagator for the gauginos will be

$$\begin{aligned}\mathcal{P}(q,x,y) = \langle 0|\Psi\bar{\Psi}|0\rangle = & \textstyle\sum_{n,m}\sqrt{\frac{2}{L}}\left[P_L\frac{\cos(m_n y)}{\sqrt{2}^{\delta^{n,0}}} + P_R\sin(m_n y)\right] \\ & \times\textstyle\frac{\delta_{m,n}(\not{q}+m_n)}{q^2-m_n^2}\sqrt{\frac{2}{L}}\left[P_R\frac{\cos(m_m y)}{\sqrt{2}^{\delta^{m,0}}} + P_L\sin(m_m y)\right].\end{aligned} \tag{2.27}$$

Performing the sum, we find[37]

$$\mathcal{P}(q;0,L) = \frac{P_L\not{q}}{q\sinh(qL)}. \tag{2.28}$$

Now that we have the bulk propagators for the fermions, we approximate the loop diagrams leading to the soft masses in the visible sector. This contribution to the soft masses will

be of the form

$$g_5^2 \left(\frac{F_S}{M^2}\right)^2 \times \int \frac{d^4q}{2\pi^4} \mathrm{Tr}\left[\frac{1}{\not{q}} \mathcal{P}(q;0,L) C \mathcal{P}^T(q;,L,L) C^{-1} \mathcal{P}(q;L,0)\right]. \tag{2.29}$$

where C is the charge conjugation matrix. Because the propagators in the above expression are exponentially suppressed, any numerical factors arising from integrating will be at most order one and are likely smaller. With only one mass scale in Eq. (2.29), we can then approximate the size of the scalar mass

$$m_{\tilde{\phi}}^2 \sim \frac{g_5^2}{16\pi^2} \left(\frac{F_S}{M^2}\right)^2 \frac{1}{L^3} = \frac{g_4^2}{16\pi^2} m_{\tilde{\lambda}}^2. \tag{2.30}$$

The last equality comes from the relation between the 4-d and 5-d couplings $g_5^2/L = g_4^2$. From the above expression, it is clear that the scalar masses in gaugino mediation are indeed loop suppressed relative to the gaugino masses.

With just the gauginos in the bulk, the Higgs masses are suppressed. However if the Higgs bosons are moved into the bulk, they can be given a mass term on the hidden brane. The Higgs masses then become a free parameter of the effective 4-d theory as well.

2.1.3 Conformal Sequestering

Another way to achieve HENS type boundary conditions is through conformal running. The suppression of the scalar masses, in this case, is realized in a four dimensional setup through strongly-coupled conformal dynamics. The strongly-coupled theory is hidden from the visible sector by conformal running [25, 26]. The conformal running suppresses the interactions between the hidden and visible sector. This effectively sequesters the hidden sector. In a strongly-coupled theory near a fixed point, the wave function renormalization will run towards $Z = 1$ in the IR. Because the visible sector is weekly coupled, it is equivalent to a small perturbation of the strongly-coupled sector. In this case, the visible sector fields can be viewed as background fields. The non-renormalizable operators between

these background fields and the hidden sector fields lead to the soft breaking terms. Because the visible fields are just background fields, they can be subsumed into the wave function renormalization of the strongly coupled fields. The soft masses are then suppressed as the conformal running dampens out any perturbations away from $Z = 1$. To make this more clear, we will give an example [26] of a theory with an IR fixed point. In this example, we find that the soft masses are suppressed. This toy model will also highlight when the conformal dynamics are incapable of suppressing the soft masses.

Our discussion will follow in part the appendix of [26]. The starting point is the Lagrangian of supersymmetric QCD with N colors and F flavors in the holomorphic basis,

$$\mathcal{L}_{hol} = ZQ^{\dagger}_{hol}Q_{hol}|_D + (\tau \mathcal{W}_\alpha \mathcal{W}^\alpha)|_F, \tag{2.31}$$

whose one loop gauge coupling is

$$\tau(\mu) = \tau(M) + \frac{b}{8\pi^2}\ln\left(\frac{\mu}{M}\right), \qquad b = 3N - F. \tag{2.32}$$

From the above Lagrangian, it may appear that the only possible conformal theory would be for $3N - F = 0$. The fact that other conformal theories exist becomes apparent through the rescaling, $Q_{hol} \to Z^{-1/2}Q$ and $Q^{\dagger}_{hol} \to Z^{-1/2}Q^{\dagger}$. Because this rescaling is anomalous, the gauge coupling is shifted by $-\frac{F}{8\pi^2}\ln Z$ due to the Konishi[28] anomaly. In the basis where the fields are canonical, the gauge coupling is then

$$\tau(\mu) = \tau(M) + \frac{b}{8\pi^2}\ln\left(\frac{\mu}{M}\right) - \frac{F}{8\pi^2}\ln Z(\mu). \tag{2.33}$$

With the wave function renormalization

$$Z(\mu) = Z(M)\left(\frac{\mu}{M}\right)^{2\gamma_Q}, \qquad 2\gamma_Q = \tfrac{3N-F}{F}, \tag{2.34}$$

the gauge coupling, $\tau(\mu)$, is scale independent and we see that we have a conformal theory. In this basis, it appears that the entire kinetic term is suppressed and not just the perturbations away from $Z = 1$. To see how the soft masses are sequestered as compared to the

kinetic term, it will be easier to start in a basis where the kinetic terms are normalized. With the kinetic terms canonical, the only running parameter is the gauge coupling. A theory is conformal at a point where its beta function goes to zero. This point is known as a fixed point.

The beta functions can be expanded about the couplings fixed point values as follows

$$\beta = \beta'_*(\tau - \tau_*) + \cdots . \tag{2.35}$$

For the fixed point to be stable, $\beta'_* \geq 0$. Using this expansion of the beta function, the coupling is found to be

$$\tau(\mu) = \tau(M) + \left(\frac{\mu}{M}\right)^{\beta'_*} (\tau(M) - \tau_*) . \tag{2.36}$$

In this expression, τ_* is the gauge coupling at the fixed point, and M is the renormalization scale. With this expression for the coupling, the Lagrangian in a basis having canonically normalized fields is

$$\mathcal{L} = \left(Q^\dagger Q\right)\Big|_D + \left(\left[\tau(M) + \left(\frac{\mu}{M}\right)^{\beta'_*} (\tau(M) - \tau_*)\right] \mathcal{W}_\alpha \mathcal{W}^\alpha\right)\Big|_F . \tag{2.37}$$

Near the IR fixed point, the theory will become conformal. By redefining the fields in the previous expression, we can change to a basis where the coupling is constant. When the fields are redefined as $Q = \sqrt{R}Q'$ and $Q^\dagger = \sqrt{R}Q'^\dagger$, the coupling in the previous expression is shifted by $\frac{F}{8\pi^2}\ln(R)$ because of the Konishi[28] anomaly. Because the R now appears in the coupling, the running of the coupling, $\tau(\mu)$, can be cancelled by R. The R that gives a constant coupling τ_* is

$$R(\mu) = [R(M)]^{\left(\frac{\mu}{M}\right)^{\beta'_*}} . \tag{2.38}$$

The Lagrangian, with the above wave function renormalization, is

$$\mathcal{L} = [R(M)]^{\left(\frac{\mu}{M}\right)^{\beta'_*}} \left(Q^\dagger Q\right)|_D + (\tau_* \mathcal{W}_\alpha \mathcal{W}^\alpha)|_F . \tag{2.39}$$

In this basis, it is clear that the coupling is constant or conformal. However, it is less clear what happens to the coefficient of the kinetic term. If the wave function renormalization is expanded about its canonical value, we find

$$R(\mu) = 1 + \left(\frac{\mu}{M}\right)^{\beta'_*} (R(M) - 1)\,. \tag{2.40}$$

In this basis, it is clear that the conformal running in the hidden sector tends to suppress any deviations from a canonical kinetic term.

The consequences of this can be seen by considering the following $\int d^4\theta$ term

$$\int d^4\theta \, \left(1 + \frac{c(\mu_0)}{M}\Phi^\dagger\Phi\right) Q^\dagger Q. \tag{2.41}$$

In the above equation, M is the messenger scale, Q is a hidden sector field, and Φ_i is a visible sector field. If we now regard the terms in front of the $Q^\dagger Q$ as the wave function renormalization, the expansion in Eq. (2.40) gives

$$\int d^4\theta \, Z_Q * \left(1 + \frac{c(\mu_0)}{M}\left(\frac{\mu}{M}\right)^{\beta'_*}\Phi^\dagger\Phi\right) Q^\dagger Q. \tag{2.42}$$

This tells us that the approximate running of the coupling $c(\mu)$ will be

$$c(\mu) \simeq c(\mu_0)\left(\frac{\mu}{M}\right)^{\beta'_*}. \tag{2.43}$$

In order for $c(\mu)$ to be sufficiently squashed, strong dynamics are needed. Otherwise, the exponent β'^* would be too small, and the suppression of $c(\mu)$ would be insufficient.

If there is a global non-anomalous symmetry in the hidden sector, the sequestering discussed above may break down. To understand this, we must consider a more complicated hidden sector with many fields. The lack of sequestering from this global symmetry becomes apparent from the expansions of the anomalous dimension and beta function. The

expansion of the anomalous dimensions about the fixed point value of the couplings can be written as

$$\frac{d}{dt}\Delta \ln Z_i = \left.\frac{\partial \gamma_i}{\partial \alpha_k}\right|_* \Delta\alpha_k, \tag{2.44}$$

with

$$\tfrac{d}{dt}\Delta \ln Z_i = \gamma_i - \gamma_i^*, \qquad \Delta \ln Z_i = \ln Z_i - \gamma_i^* t, \qquad \Delta\alpha_k = \alpha_k - \alpha_k^*. \tag{2.45}$$

In the above expression, α_k are the gauge couplings of the conformal theory, $t = \ln \mu$, and γ_i is the anomalous dimension. The deviation of the couplings from the fixed point value, $\Delta\alpha_k$, can be expressed in terms of $\Delta \ln Z_i$. This is done by expanding the beta function about the anomalous dimension at the fixed point and then integrating. If this is done, we get

$$\Delta\alpha_i = \left.\frac{\partial \beta_i}{\partial \gamma_j}\right|_* \Delta \ln Z_j. \tag{2.46}$$

Combining this expression with that found in Eq. (2.44), we find a set of coupled first order differential equations for the wave function renormalization of

$$\frac{d}{dt}\Delta \ln Z_i = \left.\frac{\partial \gamma_i}{\partial \alpha_k}\right|_* \left.\frac{\partial \beta_k}{\partial \gamma_j}\right|_* \Delta \ln Z_j = L_{ij}\Delta \ln Z_j. \tag{2.47}$$

This set of equations is solved by diagonalizing the matrix L_{ij} and then integrating. Each wave function renormalization runs as $\Delta \ln Z_k \propto e^{\lambda_i t}$, where the λ_i's are the eigenvalues of L_{ij}, and $t = \ln(\mu)$. If the matrix L_{ij} in the previous expression has a zero eigenvalue, there will be some combination of fields whose wave function renormalization will not be affected by the conformal running. This combination of fields is not sequestered. The interaction of these non-sequestered fields will leave some of the soft masses generic and large. These zero eigenvalues in the matrix L_{ij} arise from unbroken non-anomalous global symmetries in the hidden sector(See last two references of [25].).

Next, the mass hierarchies from conformal sequestering are examined. Recently it was pointed out that the Higgs mass, unlike the other scalar masses, is not suppressed in conformally sequestered theories[27, 29]. Instead, it is the combination $m^2_{H_{u,d}} + \mu^2$ which is sequestered[1]. This gives

$$m^2_{H_{u,d}} = -\mu^2. \tag{2.48}$$

In order to explain the origin of the above relationship, the appendix of[27] will be reviewed below. A fairly general Lagrangian with one chiral super field, or one linear combination of chiral super fields, and one real super field interacting with the hidden sector is

$$\int d^4\theta H^\dagger H \left(1 + x\frac{\chi}{M_*} + x^\dagger\frac{\chi}{M_*} + x^\dagger x\frac{\chi^\dagger\chi}{M_*^2} + r\frac{R}{M_*^2}\right) \tag{2.49}$$

where χ is a hidden sector chiral super field with complex coupling x, and R is a real super field with real coupling r.

These contributions to the Lagrangian can be factorized giving

$$\int d^4\theta \tilde{H}^\dagger \tilde{H} \left(1 + r\frac{R}{M_*}\right) \tag{2.50}$$

with terms of order $\left(\frac{\chi}{M_*}\right)^3$ neglected and

$$\tilde{H} = H\left(1 + x\frac{\chi}{M_*}\right). \tag{2.51}$$

If we redefine the fields according to the previous expression, the only supersymmetry breaking in Eq. (2.50) will be from R. The Lagrangian in Eq. (2.50) is the same as that from Eq. (2.41). Taking a strongly coupled hidden sector as in Eq. (2.41), the coupling r will run like

$$r(\mu) \simeq r(M_*)\left(\frac{\mu}{M_*}\right)^{\beta'_*}. \tag{2.52}$$

[1]This result is model independent for any conformal running that suppresses the scalar masses but not the gauginos masses [29].

If the strongly coupled conformal running occurs over a large enough energy range, and β'_* is order one, the coupling r will be negligible. The Lagrangian in this case is well approximated by Eq. (2.50) with $r = 0$. When $r = 0$, the supersymmetry breaking mass for H is $m^2_{\tilde{H}} = 0$. To determine the supersymmetry breaking mass of H, m^2_H, we return to the H basis

$$\int d^4\theta H^\dagger H \left(1 + x\frac{\chi}{M_*} + x^\dagger \frac{\chi}{M_*} + x^\dagger x \frac{\chi^\dagger \chi}{M_*^2}\right). \tag{2.53}$$

In this form, it may appear that the H field has both a supersymmetry breaking scalar mass, and supersymmetry preserving mass. However, the mass contribution from $\frac{\chi}{M_*}$ cancels with the mass term from $\frac{\chi^\dagger \chi}{M_*^2}$. Just as expected, the total mass for H cancels. Even though the two mass terms cancel, the trilinear term arising from $\frac{\chi}{M_*}$ is non-zero. Although we only considered one Higgs field, this calculation generalizes to a two Higgs boson scenario and gives the result found in Eq. (2.48). In the two Higgs boson scenario there are also B_μ terms. These turn out to be suppressed.

Another way to sequester the scalar masses through conformal running is to include contact terms in the superpotential that have hidden and visible sector fields. In this set up, a partial sequestration of soft terms, as well as an explanation for the Yukawa hierarchy, can also be obtained from the direct interaction of the strong conformal dynamics with the visible sector [30, 31, 32]. In these constructions, there is a new gauge group G_c that approaches a strongly-coupled fixed point in the IR. The MSSM fields are not charged under G_c, but they do couple to fields that are in the form of a cubic Yukawa operators in the superpotential. As the theory flows towards the fixed point, the MSSM fields develop large anomalous dimensions which suppress their corresponding (physical) Yukawa couplings. Since different (linear combinations of) fields develop distinct anomalous dimensions, related to their effective superconformal R charges, a Yukawa hierarchy can be generated in this way [30]. The conformal running also produces a general suppression of

the soft scalar masses, as well as a hierarchy of trilinear A terms that mirrors the Yukawa couplings [30, 31, 32, 33]. Conversely, the gaugino masses are largely unaffected because they do not couple directly to the strongly-coupled sector. The third generation multiplets and the Higgs multiplets must also be shielded from the conformal running effects to avoid suppressing the top quark Yukawa coupling. As a result, the third generation and the Higgs soft masses do not get suppressed. Thus, the spectrum from visible sector conformal running is similar to one we shall consider, but augmented by third generation soft masses and A terms. There may also be additional contributions to the soft masses if there are non-anomalous, continuous, abelian global symmetries. We expect the phenomenology of both scenarios of conformal sequestering to be similar over much of the allowed parameter space.

2.1.4 The Scale of M_c

From the discussion above, we see that a Higgs Exempt No-Scale (HENS) soft mass spectrum can arise from gaugino mediation with the Higgs multiplets in the bulk, or from conformal running in the hidden sector up to additional contributions to the third generation states. Before proceeding, however, let us comment on our choice of M_{GUT} as the input scale for the soft spectrum. In gaugino mediation, the input scale is on the order of the compactification scale, M_c.[2] For visible-sector conformal running, the input scale for the soft spectrum is the scale at which the conformal running ceases, which we will also call M_c. Our motivation to set $M_c = M_{GUT}$ is partly conventional, but is also motivated by gauge unification and our wish to strongly suppress the scalar soft masses.

In both cases, gauge unification can be preserved with $M_c < M_{GUT} \sim 2\times10^{16}$ GeV, but the process will be more complicated than in the standard picture. In gaugino mediation, Kaluza-Klein states appear above M_c and can lead to an accelerated power-law running [34].

[2] $M_c := 1/R$, is less than the cutoff of the theory.

With conformal dynamics in the visible sector, the SM gauge coupling beta functions will be modified by the large anomalous dimensions of the MSSM fields. Gauge unification will still occur, albeit at a lower scale, provided the conformal dynamics respects a global symmetry into which the SM gauge group can be embedded [35]. Thus, in each case having M_c below M_{GUT} can induce an effective unification of the SM gauge couplings below the apparent unification scale $M_{GUT} \simeq 2 \times 10^{16}$ GeV. This is problematic for many GUT completions of the MSSM, which predict baryon and lepton number violation. Typically, some additional structure is needed if M_c is much smaller than M_{GUT}. This motivates us to consider $M_c \geq M_{GUT}$.

It is clear that gauge unification can also be maintained with $M_c \geq M_{GUT}$. If M_c is larger than M_{GUT}, the renormalization group running from M_c down to M_{GUT} will induce non-vanishing (flavor-universal) soft masses at M_{GUT}. The size of these corrections from running above M_{GUT} depends on the precise GUT completion of the theory, but even for minimal GUT models they can be significant, on the order of [36]

$$\begin{aligned} \Delta A &\simeq \frac{2\alpha_G}{\pi} C_A \ln\left(\frac{M_c}{M_{GUT}}\right) M_{1/2}, \\ \Delta m^2 &\simeq \frac{2\alpha_G}{\pi} C_{m^2} \ln\left(\frac{M_c}{M_{GUT}}\right) M_{1/2}^2, \end{aligned} \tag{2.54}$$

where $\alpha_G \simeq 1/24$ is the GUT coupling, and C_A and C_{m^2} are dimensionless constants on the order of or slightly larger than unity. These contributions can be large enough for an acceptable low-energy spectrum to be obtained [36].

On the other hand, in both gaugino mediation and conformal sequestering, M_c cannot be more than about an order of magnitude above M_{GUT} because the suppression of soft terms (and Yukawa couplings) requires a separation of scales. Let M_{in} be the scale at which conformal running begins in the case of conformal dynamics, or the UV cutoff of the extra-dimensional gauge theory in gaugino mediation. Presumably $M_{in} \leq M_{\rm Pl} = 2.4 \times 10^{18}$ GeV. The amount of suppression of the soft scalar terms from conformal running is expected to

be an order-one power of M_c/M_{in}, whereas the required suppression is typically on the order of 10^{-4} [31]. An even stronger upper bound on M_c can be obtained if the conformal dynamics are responsible for the small electron Yukawa coupling as in Ref. [30]. The condition for this is

$$y_e \simeq \left(\frac{3\times 10^{-6}}{\cos\beta}\right) \simeq \left(\frac{M_c}{M_{in}}\right)^{(\gamma_L+\gamma_E)/2}, \tag{2.55}$$

where γ_i denote the anomalous dimensions of L and E^c, which are generally smaller than 2. If we take this bound seriously, M_c can be at most only slightly larger than M_{GUT}. In gaugino mediation, flavor-mixing contact interactions between the MSSM chiral multiplets and hidden sector operators, arising from bulk states with masses above the UV cutoff scale, are suppressed by a factor of $\exp(-M_{in}/M_c)$ [37]. Again this factor must be less than about 10^{-4} to avoid various experimental flavor constraints, which translates into M_c being within an order of magnitude larger than M_{GUT} (for $M_{in} = M_{\rm Pl}$).

Given the above considerations, we will set $M_c = M_{GUT}$, and not concern ourselves with the precise mechanism by which the scalar soft terms are suppressed. While beyond the scope of the present work, it also interesting to speculate that the breaking of the GUT symmetry is related to the geometry of the extra dimension, or the escape from conformal running. Such a construction would further justify our choice of $M_c = M_{GUT}$. Finally, let us also note that within particular models there is typically some residual flavor violation due to an incomplete suppression of the scalar terms at M_c. The amount of flavor suppression can be close to the level probed by current experiments. However, without specifying a particular model, it is not possible to perform an analysis of the constraints due to flavor physics. Thus, we assume as our starting point that at the scale $M_c = M_{GUT}$, all scalar masses except those of the Higgs bosons are precisely zero and that corrections to that assumption are inconsequential to the phenomenology discussed below.

2.2 Mass Spectrum and Constraints

2.2.1 One-Loop Analysis

The essential features of the HENS mass spectrum are well illustrated by a simple one-loop analysis. At this order, the ratio M_a/g_a^2, $a = 1, 2, 3$, is scale invariant for all three gaugino masses. If the gauge couplings unify and the gaugino masses are universal at M_{GUT}, it follows that at lower scales Q, $M_a(Q) = [g_a(Q)/g_{GUT}]^2 M_{1/2}$. For $Q = 1$ TeV, this gives

$$M_1 \simeq (0.43)\, M_{1/2},\ M_2 \simeq (0.83)\, M_{1/2},\ M_3 \simeq (2.6)\, M_{1/2}. \tag{2.56}$$

The one-loop running of the scalar soft masses is given by [2, 38]

$$(4\pi)^2 \frac{dm_i^2}{dt} \simeq X_i - 8 \sum_a C_i^a\, g_a^2\, |M_a|^2 + \frac{6}{5}\, g_1^2\, Y_i\, S, \tag{2.57}$$

where X_i depends on the soft masses and A terms and is usually proportional to Yukawa couplings, C_i^a is the quadratic Casimir for the representation i under gauge group a, and

$$S = (m_{H_u}^2 - m_{H_d}^2) + tr_F(m_Q^2 - 2m_U^2 + m_E^2 + m_D^2 - m_L^2), \tag{2.58}$$

with the trace above running over flavors.

At one-loop order, the RG equation for the S term is particularly simple,

$$(4\pi)^2 \frac{dS}{dt} = \frac{66}{5} g_1^2\, S. \tag{2.59}$$

Because of this simple form, the effect of the S-term on the low-scale soft masses is to simply shift the value they would have with $S = 0$ by the amount

$$\Delta m_i^2 = -\frac{Y_i}{11}\left[1 - \left(\frac{g_1}{g_{GUT}}\right)^2\right] S_{GUT} \simeq -(0.052)\, Y_i\, S_{GUT}, \tag{2.60}$$

where $S_{GUT} = (m_{H_u}^2 - m_{H_d}^2)$ evaluated at M_{GUT}.

Neglecting Yukawa effects, the low-scale slepton soft masses at $Q = 1$ TeV are

$$m_L^2 \simeq \left[(0.68)\, M_{1/2}\right]^2 + \frac{1}{2}(0.052)\, S_{GUT}, \tag{2.61}$$

$$m_E^2 \simeq \left[(0.39)\, M_{1/2}\right]^2 - (0.052)\, S_{GUT}. \tag{2.62}$$

If mixing effects are small, the physical slepton masses will be close to $\sqrt{m_L^2}$ and $\sqrt{m_E^2}$, up to the $U(1)_Y$ D-term contributions. The mass of the lightest neutralino is usually close to M_1 (under the assumption of gaugino universality) unless μ is relatively small.

Comparing Eq. (2.61) with Eq. (2.56), we see that for $S_{GUT} \geq 0$, m_E^2 is less than M_1 and the lightest superpartner tends to be a mostly right-handed slepton. On the other hand, if $S_{GUT} < 0$, the right-handed slepton soft mass is pushed up relative to M_1, allowing for a mostly Bino neutralino LSP. For S_{GUT} very large and negative, the LSP can be a mostly left-handed slepton. Relative to the sleptons and the electroweak gauginos, the squarks and gluino are very heavy because the $SU(3)_c$ gauge coupling grows large in the infrared.

2.2.2 Parameter Space Scans

To confirm the simple analysis given above, we have performed a scan over the HENS parameter space using SuSpect 2.34 [39]. This code performs the renormalization group running at two-loop order with one-loop threshold effects, and includes radiative and mixing corrections to the physical particle masses. We take $\alpha_s(M_Z) = 0.118$ [40] and $m_t = 171.4$ GeV [41] in our analysis. For each model parameter point we require consistent electroweak symmetry breaking, and superpartner masses above the LEP II and Tevatron bounds ($m_{\chi_1^0},\ m_{\tilde{\nu}} > 46$ GeV, $m_{\tilde{l}} > 90$ GeV, $m_{\chi_1^\pm} > 104$ GeV). We also impose the lower-energy constraints

$$\begin{aligned} \Delta\rho &\in [-8,\, 24] \times 10^{-4}\ [40] \\ BR(b \to s\gamma) &\in [3.0,\, 4.0] \times 10^{-4}\ [42] \\ \Delta a_\mu &\in [-5,\, 50] \times 10^{-10}\ [40] \end{aligned} \tag{2.63}$$

These ranges correspond approximately to the 95% *c.l.* allowed values, although we have allowed a slightly larger range for Δa_μ. The constraint from the muon magnetic moment is particularly interesting in HENS scenarios, and we shall discuss it more extensively below.

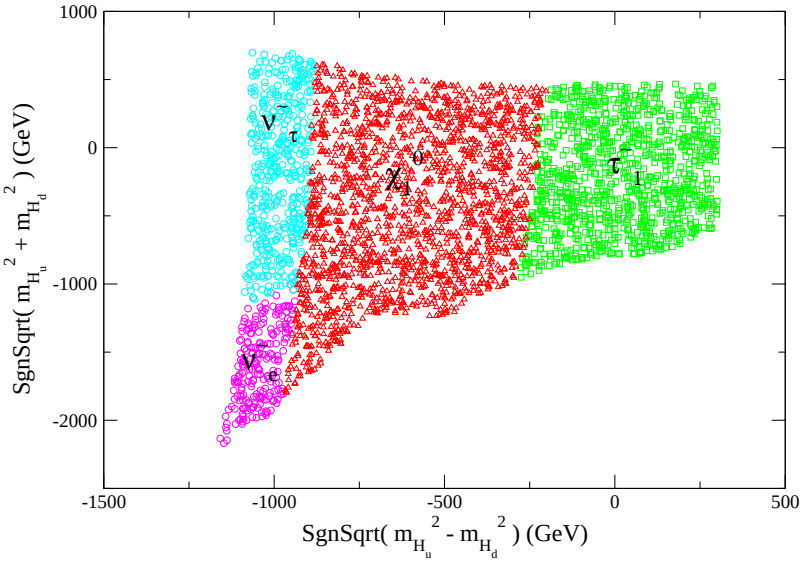

Figure 2.1: Allowed parameter regions for $\tan\beta = 10$ and $M_{1/2} = 300\,\mathrm{GeV}$. The differently colored regions in the figure indicate the identity of the lightest superpartner. The quantities $m^2_{H_u}$ and $m^2_{H_d}$ are evaluated at the input scale M_{GUT}.

In the immediate analysis we do not include the LEP II bound on the lightest Higgs boson mass. We will discuss this constraint below as well.

Figures 2.1, 2.2, and 2.3 show the allowed regions of $m^2_{H_u}(M_{GUT})$ and $m^2_{H_d}(M_{GUT})$, for $(\tan\beta,\ M_{1/2})$ equal to (10, 300 GeV), (10, 500 GeV), and (30, 500 GeV), subject to the constraints described above. The soft Higgs masses in these plots are re-expressed in terms of the more convenient combinations $SgnSqrt(m^2_{H_u} - m^2_{H_d})(M_{GUT}) = S_{GUT}/\sqrt{|S_{GUT}|}$, and $SgnSqrt(m^2_{H_u} + m^2_{H_d})(M_{GUT})$, where $SgnSqrt$ denotes the signed square root ($SgnSqrt(x) = sign(x)\sqrt{|x|}$). Also shown in these plots is the identity of the lightest superpartner at each allowed parameter point.

These figures confirm our previous approximate analysis. When S_{GUT} is positive or zero, the LSP is a mostly right-handed stau or selectron. As S_{GUT} becomes more negative, a neutralino becomes the LSP, while for very large and negative values of S_{GUT} the LSP is a sneutrino. For extremely large positive or negative values of S_{GUT}, one of the slepton

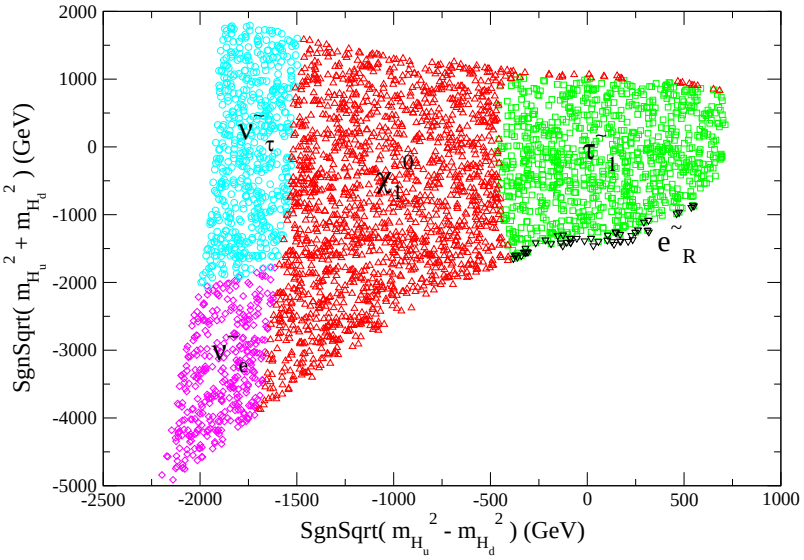

Figure 2.2: Allowed parameter regions for $\tan\beta = 10$ and $M_{1/2} = 500\,\mathrm{GeV}$. The differently colored regions in the figure indicate the identity of the lightest superpartner. The quantities $m^2_{H_u}$ and $m^2_{H_d}$ are evaluated at the input scale M_{GUT}.

soft masses becomes tachyonic. The allowed parameter region is cut off at larger positive values of $(m^2_{H_u}+m^2_{H_d})(M_{GUT})$ because $|\mu|^2$ only has a negative solution, implying that electroweak symmetry breaking is not possible.[3] Note that in Fig. 2.2, there is a thin strip along the upper border of the allowed region in which the LSP is a neutralino. In this strip, the μ term is smaller than M_1 and the neutralino LSP is mostly Higgsino. For larger negative values of $(m^2_{H_u}+m^2_{H_d})(M_{GUT})$, $M^2_{A^0} \to 0$ and the parameter space gets cut off by the bound from $BR(b \to s\gamma)$. As $(m^2_{H_u}+m^2_{H_d})(M_{GUT})$ becomes even smaller, electroweak symmetry breaking ceases to occur.

The effects of the τ Yukawa coupling and left-right mixing can be seen by comparing Figs. 2.2 and 2.3. In the models we are considering, the value of the Yukawa-dependent term in Eq. (2.57) for the right-handed stau soft mass is

$$X_{E_3} \simeq 2|y_\tau|^2\, m^2_{H_d}. \tag{2.64}$$

[3] In fact, the parameter space is cut before μ reaches zero by the $BR(b \to s\gamma)$ and the chargino mass constraints.

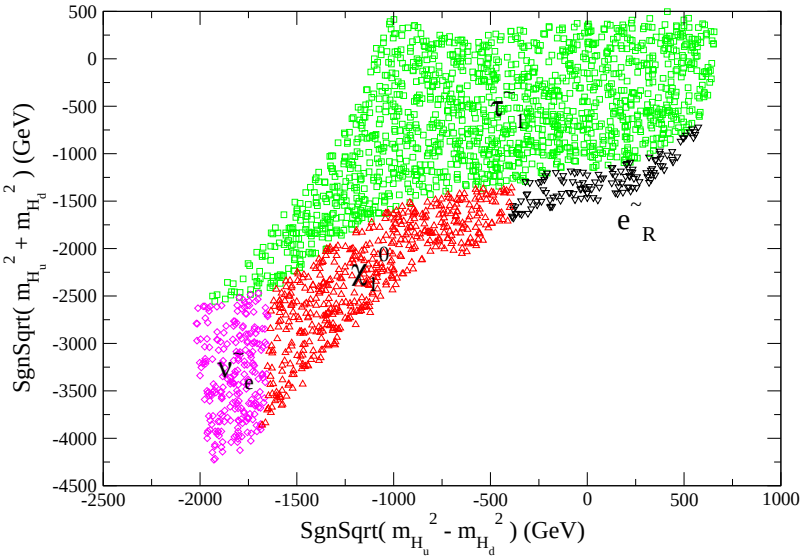

Figure 2.3: Allowed parameter regions for $\tan\beta = 30$ and $M_{1/2} = 500\,\mathrm{GeV}$. The differently colored regions in the figure indicate the identity of the lightest superpartner. The quantities $m^2_{H_u}$ and $m^2_{H_d}$ are evaluated at the input scale M_{GUT}.

The left-right mixing is also proportional to the τ Yukawa. As $\tan\beta$ increases, so too does the τ Yukawa, and therefore also the Yukawa effect on the running and the mixing. Left-right mixing tends to push the lighter stau mass lower, and for this reason it is more difficult to obtain a neutralino LSP at larger values of $\tan\beta$. However, there is also a competing effect from the influence of the τ Yukawa on the running of $m^2_{E_3}$. When $m^2_{H_d}$ is large and negative, the X_{E_3} term increases the value of $m^2_{E_3}$ at low energies. Thus, a selectron or an electron sneutrino is the LSP in some parts of the parameter space.

2.2.3 Constraints from $(g-2)_\mu$

Since the sleptons in HENS models are relatively light, the corrections to the anomalous magnetic moment of the muon, $a_\mu = (g-2)_\mu/2$ can be significant [43]. Currently, the measured value of a_μ exceeds the SM prediction by about two standard deviations [40],

$$\Delta a_\mu = a_\mu^{exp} - a_\mu^{SM} = (22 \pm 10) \times 10^{-10}. \tag{2.65}$$

This result is suggestive of new physics.

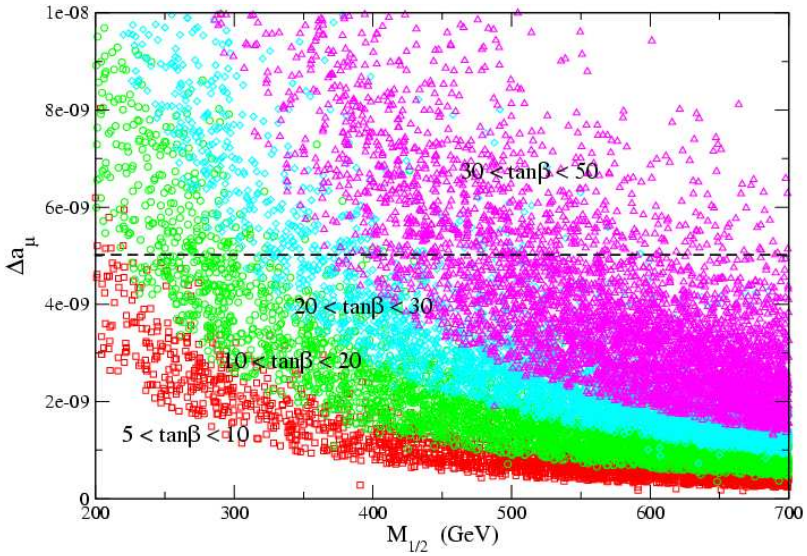

Figure 2.4: Δa_μ^{SUSY} as a function of $M_{1/2}$ for several ranges of $\tan\beta$, and $sgn(\mu) > 0$. The spread of points come from scanning over the acceptable input values of $m^2_{H_u}$ and $m^2_{H_d}$. The red points indicate $\tan\beta \in [5, 10)$, the green points $\tan\beta \in [10, 20)$, the blue points $\tan\beta \in [20, 30)$, and the magenta points $\tan\beta \in [30, 50)$. The dashed line represents a contribution to the anomalous magnetic moment that is 3σ large than the experimental value.

In the MSSM, there are additional contributions to $(g-2)_\mu$ from loops involving a virtual chargino and muon sneutrino, and loops with a virtual neutralino and smuon. For the HENS scenarios we are studying, in which all masses scale predominantly with $M_{1/2}$ and the gaugino masses are universal (and assumed real and positive), the leading supersymmetry contribution to a_μ is proportional to $\tan\beta$, scales roughly as $M_{1/2}^{-2}$, and has a sign equal to the sign of the μ term, $sgn(\mu)$ [44]. Given the tension between the measured value of Δa_μ and the SM prediction, $sgn(\mu) > 0$ is strongly favored. Indeed, we find that negative $sgn(\mu)$ is only possible for very large values of $M_{1/2}$. Conversely, if $sgn(\mu)$ is positive the new supersymmetric contribution can help to explain this possible discrepancy between the SM prediction and experiment.

The value of Δa_μ^{SUSY} is shown as a function of $M_{1/2}$ in Fig. 2.4. In generating this figure, we have taken $sgn(\mu) > 0$, and have scanned over input values of $m^2_{H_u}$ and $m^2_{H_d}$

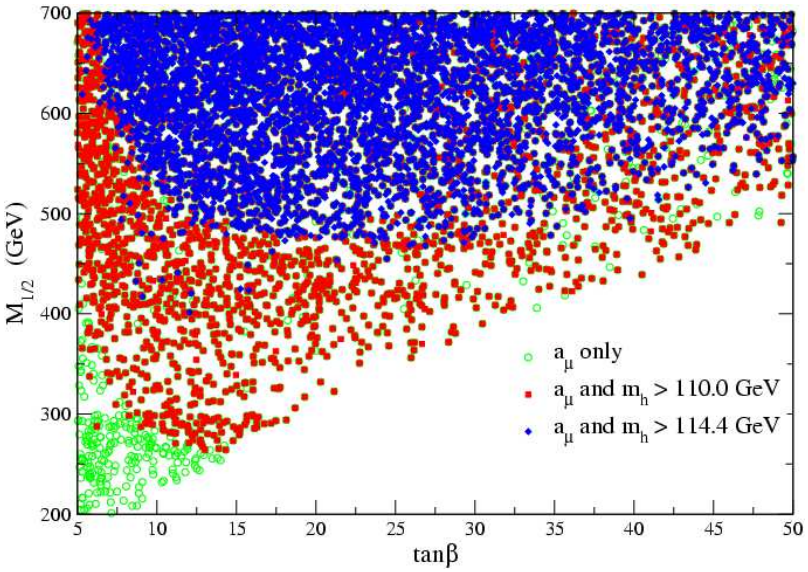

Figure 2.5: Scatter plot in the $M_{1/2} - \tan\beta$ plane of solutions that respect the bounds of $\Delta a_\mu^{SUSY} < 50 \times 10^{-10}$ and $m_h > 114.4\,\text{GeV}$. Due to uncertainty in the top quark mass, and the theoretical uncertainty in the computation of m_h, a more conservative constraint on this theoretically computed value of m_h is 110 GeV, which is also shown in the figure.

at M_{GUT}. The distribution for $sgn(\mu) < 0$ looks the same, except the sign of Δa_μ is opposite. With $sgn(\mu) > 0$, the new physics contribution is frequently too large, and from this we obtain a lower bound on $M_{1/2}$ as a function of $\tan\beta$. For $\tan\beta = 10$, this bound is $M_{1/2} \gtrsim 250$ GeV, while for $\tan\beta = 30$, it increases to $M_{1/2} \gtrsim 400$ GeV.

2.2.4 Constraints from the Higgs Boson Mass

A further constraint on HENS models, and one we have not yet imposed, is that the SM Higgs boson mass should exceed the LEP II bound [45],

$$m_h > 114.4 \text{ GeV}. \tag{2.66}$$

This bound also applies to the lightest CP-even Higgs boson in much of the parameter space of the MSSM. However at tree-level in the MSSM, the lightest CP-even Higgs boson has a mass below M_Z. It is only because of large loop corrections to the mass, predominantly due to the scalar tops, that this Higgs state can be raised above the LEP II bound. With

vanishing input scalar soft masses, the stop masses scale predominantly with $M_{1/2}$. The Higgs boson mass bound therefore imposes a further lower bound on the universal input gaugino mass.[4]

The combined bounds on $M_{1/2}$ as a function of $\tan\beta$ from the conditions $\Delta a_\mu < 50 \times 10^{-10}$ and $m_h > 110.0$ (114.4) GeV are shown in Fig. 2.5. We impose a slightly weaker 110 GeV lower bound on the Higgs boson mass than the 114 GeV LEP II bound to account for various uncertainties associated with the theoretical computation of m_h. We have taken $m_t = 171.4$ GeV in our analysis[5]. At smaller $\tan\beta$, less than about 15, the Higgs mass bound imposes the stronger constraint, while the upper bound on Δa_μ is more significant for values of $\tan\beta > 15$. For any value of $\tan\beta$, $M_{1/2}$ must be greater than about 300 GeV if we impose the weaker Higgs mass bound ($m_h > 110.0$ GeV), and larger than about 500 GeV to satisfy the stronger bound ($m_h > 114.4$ GeV). Note that as $M_{1/2}$ grows, the phenomenological constraints on the model tend to weaken, but usually at the cost of increased fine-tuning in the Higgs sector [47].

[4] One could increase the Higgs mass by introducing a SM singlet Higgs field to the spectrum, but this introduces tensions with grand unification [46].

[5] Larger values of m_t would increase the loop contribution to the mass of the Higgs boson and weaken the bound on $M_{1/2}$

CHAPTER III

Dark Matter

In order to give a more complete picture of the HENS model, the work of a collaborator on dark matter is included here[59]. In a previous chapter, we found that much of the HENS parameter space allowed by other constraints was plagued by a slepton or sneutrino LSP. If R parity is conserved, the relic abundance of these particles as the LSP would be too large to meet experimental constraints. The experimental constraints for a stable charged particle are quite strong [48]. Although neutral, the sneutrino is also ruled out as a dark matter candidate. The direct detection rates for a sneutrino LSP in this case would be much too high if $m_{\tilde{\nu}} \sim 100\,\mathrm{GeV}$ [49]. If the gravitino is the LSP, and a slepton is the next to lightest superpartner (charged or not), it could still give a consistent picture of dark matter [51]. We will briefly discuss this possibility below. However, our focus will be on standard cosmology and we will thus concentrate on a neutralino LSP [50].

The neutralino relic density for various points in the HENS parameter space were determined using DarkSUSY 4.1 [52]. The computation is fully relativistic and includes coannhilation.

In Figures 3.1 and 3.2, the relic density of a neutralino LSP in the HENS model is plotted for $\tan\beta = 10$, $\mu > 0$, and $M_{1/2} = 300, 500$ GeV respectively. The Higgs masses are free parameters and are scanned over their allowed ranges. The standard cosmological picture is examined. The black points in the figures do not have a neutralino LSP and will be

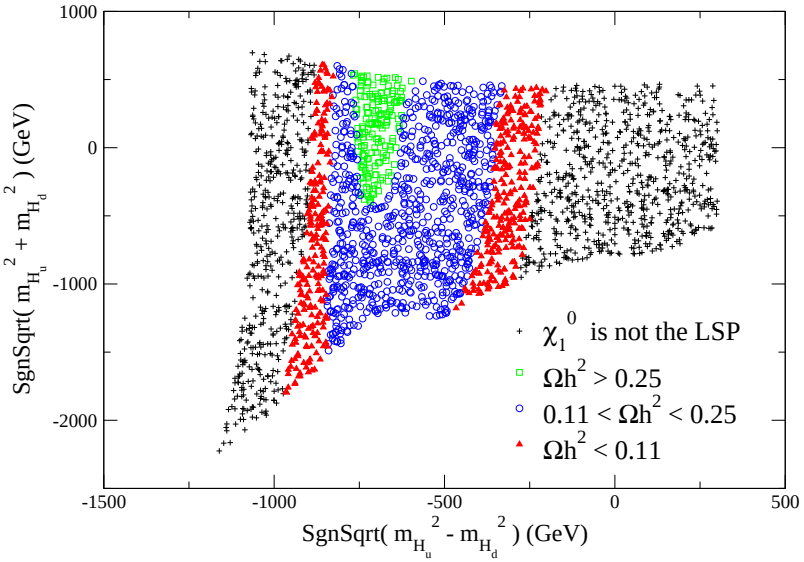

Figure 3.1: Neutralino LSP relic density for $\tan\beta = 10$, $M_{1/2} = 300$ GeV, and $sgn(\mu) > 0$. The region in which the lightest neutralino is not the LSP is denoted by the black plus signs. The red triangles indicate parameter points where the neutralino LSP relic density is less than $\Omega h^2 < 0.11$. In the blue and green regions, the neutralino LSP relic density exceeds this value.

discussed later. The red triangles are points with an acceptably small relic abundance for the LSP, $\Omega h^2 < 0.11$. This is to be compared with the observed dark matter density [53],

$$\Omega h^2 = 0.1045^{+0.0072}_{-0.0095} \text{ (WMAP only)}. \tag{3.1}$$

The other plotted points have a relic abundance that is too large. However, a late-time injection of entropy could reduce relic abundance of these points and they could still give acceptable amounts of neutralino dark matter [54].

The contours of constant relic abundance seen in Figs. 3.1-3.2 can be understood in terms of the mass spectrum of the HENS model. The LSP in the plotted regions is predominantly Bino except for a small strip on the upper border where the LSP is mostly Higgsino. With a Bino LSP, the most efficient annihilation cross section will be $\chi\chi \to f\bar{f}$ through a t channel sfermion $\tilde{f}$. Because the sleptons are light in the HENS model, this scattering cross section will be largest for sleptons. The other possible decay channels for a

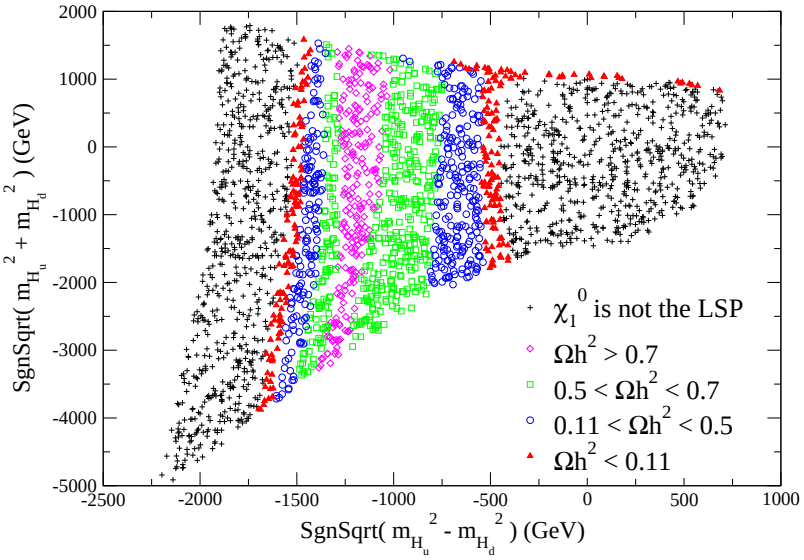

Figure 3.2: Neutralino LSP relic density for $\tan\beta = 10$, $M_{1/2} = 500$ GeV, and $sgn(\mu) > 0$. The region in which the lightest neutralino is not the LSP is denoted by the black plus signs. The red triangles indicate parameter points where the neutralino LSP relic density is less than $\Omega h^2 < 0.11$. In the blue, green, and magenta regions, the neutralino LSP relic density exceeds this value.

neutralino LSP require a large Higgsino or Wino component. With the LSP mostly Bino, the other annihilation channels are inefficient because they are suppressed by small components in the mixing matrices. The small annihilation cross section leads to a neutralino relic density that is quite large.

On the left and right borders, other processes for suppressing the neutralino relic abundance become possible. In these border regions, the LSP and slepton mass have similar sizes. Because their masses are nearly degenerate, they will freeze out at approximately the same time and temperature. Similar freeze out temperatures will lead to similar freeze out densities. The total scattering cross section for a Bino like LSP and slepton is much larger than that for two Bino like LSP's. This enhanced cross section, along with similar number densities for the Bino like LSP and sleptons, allow the LSP's to be annihilated efficiently. This reduction of the LSP number density puts the relic density at or below the

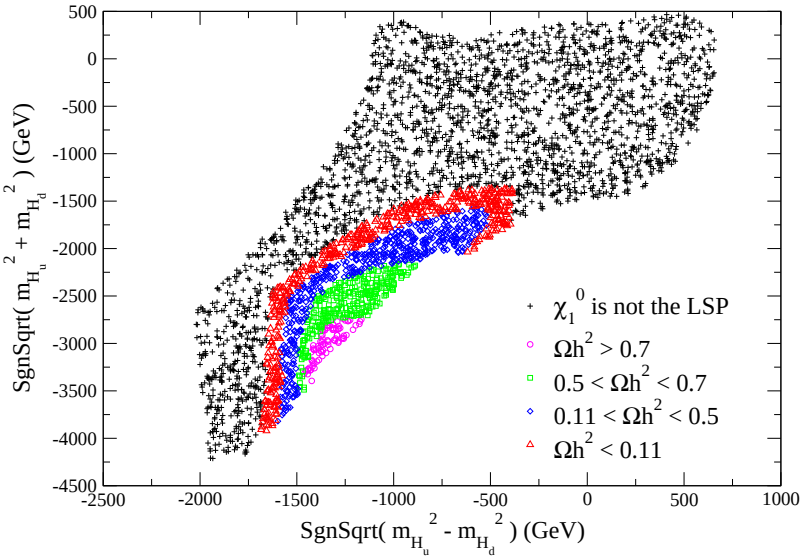

Figure 3.3: Neutralino LSP relic density for $\tan\beta = 30$, $M_{1/2} = 500$ GeV, and $sgn(\mu) > 0$. The region in which the lightest neutralino is not the LSP is denoted by the black plus signs. The red triangles indicate parameter points where the neutralino LSP relic density is less than $\Omega h^2 < 0.11$. In the blue, green, and magenta regions, the neutralino LSP relic density exceeds this value.

experimental limits. As is seen in the figures, if their mass difference becomes too large, this reduction in the LSP number density from co-annihilation ceases and the relic density is too large.

The strip along the upper boarder has a relic density that is sufficiently small as well. In this region the μ parameter becomes small. As μ becomes small, the LSP develops a significant Higgsino component. In this case, the LSP can annihilate through a t channel gauge boson and in some regions co-annihilate as well. Since the annihilation through gauge bosons is much more efficient, the correct relic density can be obtained.

Even though a slepton LSP would annihilate quickly, the regions having a slepton LSP (labelled by black plus signs in Figs. 3.1-3.2) are still problematic. Even with their large annihilation rates, the relic abundance, which will be of order $\Omega h^2 \sim 10^{-3} - 10^{-2}$, would be too large. This very small relic abundance is ruled out for charged particles like

sleptons [48]. If the LSP is the sneutrino, a neutral particle, it can be ruled out by direct searchs for dark matter [55].

These points, with a slepton lighter than the lightest neutralino, may still be acceptable if the true LSP is a gravitino. Because the gravitino couples very weakly, the lightest slepton would still freeze out as though it were the LSP. Once a sufficient amount of time passes, the slepton would decay to the gravitino. In this case, the LSP relic density is related to the next to lightest superpartner (NLSP) density as [51]

$$\Omega_{3/2}^{decay} h^2 = \frac{m_{3/2}}{m_{\tilde{l}}} \Omega_{\tilde{l}} h^2, \tag{3.2}$$

where $m_{3/2}$ is the gravitino mass. In the regions we are considering, the dark matter produced from these subsequent decays is too small to account for all the dark matter. However, these points are no longer excluded because of too much dark matter. The gravitino could still be the dominant source of dark matter for these points if there were other sources such as thermal production after inflationary reheating [56], or non-thermal production through heavy particle decays [57]. If the gravitino is the LSP, and the NLSP is a slepton, the gravitino mass is constrained. A gravitino mass $m_{3/2} \gtrsim 100$ MeV would disrupt big-bang nucleosynthesis and thus can be ruled out[1] [58].

Lastly, we examine the effect of changing $\tan\beta$ on the dark matter predictions. For smaller values of $\tan\beta$, the change is minimal. However, for larger values there is no longer a region with a mostly Higgsino LSP. This occurs because the large Yukawa coupling drives the stau slepton mass down unless $m_{H_d}^2$ is large and negative. The regions where the lightest neutralino is mostly Higgsino only occur for small values of $m_{H_{u,d}}^2$. This region now has a stau LSP. The only possible way to enhance the LSP cross section for large $\tan\beta$ is from co-annihilation. This enhancement will occur on the border between the slepton LSP and neutralino LSP as it did before, and can be seen in Fig. 3.3.

[1] The constraints for a sneutrino NLSP are not quite so strong.

The cross sections for direct and indirect detection of a neutralino LSP were also calculated. They were found to be outside of the current experimental limits. However, some regions of parameter space were found to be within reach of the next generation experiments[59]

CHAPTER IV

Collider Phenomenology

In HENS scenarios, the sleptons and the electroweak gauginos are generally very light relative to the squarks and the gluino. If the lightest neutralino is the LSP, which we assume throughout this section, the distinguishing feature of these scenarios at colliders are multi-lepton events with missing E_T. In this section we discuss the prospects for discovery and identification of HENS models at the Tevatron and the LHC.

4.1 Trilepton Signature at the Tevatron

The most promising search channel at the Tevatron is the trilepton signal with missing transverse energy (E_T) [60, 61, 62]. This can be induced, for example, by the electroweak production of $\chi_2^0 \chi_1^\pm$, with subsequent cascades of the form $\chi_2^0 \to \tilde{\ell}_L^* \ell^- \to \chi_1^0 \ell^+ \ell^+$ and $\chi_1^+ \to \tilde{\nu}_{\ell'} \ell'^+ \to \chi_1^0 \nu_{\ell'} \ell'^+$. For $M_{1/2} \geq 300$ GeV, the significant source of SUSY events comes from the electroweak production of gauginos, making this channel a copious and clean one. In HENS scenarios, the χ_2^0 and $\chi_1^\pm$ states tend to be mostly Wino and have two-body decays into left-handed sleptons. Because of this feature, the branching fractions of the abovementioned decay cascades can be significant, leading to a sizeable trilepton cross-section. Indeed, the mass spectrum derived from HENS models is close to being optimal for trilepton production.

To estimate the effective Tevatron trilepton cross-sections, we have simulated SUSY

production from $p\bar{p}$ collisions at $\sqrt{s} = 1.96$ TeV using ISAJET 7.74 [63]. Following the treatment in Ref. [62], we use the ISAJET subroutines CALSIM and CALINI (in the ISAPLT package) as a simple detector model with coverage in the range $-4 < \eta < 4$, and calorimeter cells of size $\Delta\eta \times \Delta\phi = 0.1 \times 0.262$. To simulate energy resolution uncertainties, the electromagnetic calorimeter cells are smeared by an amount $0.15/\sqrt{E/\mathrm{GeV}}$, while the hadronic calorimeter cells are smeared by an amount $0.7/\sqrt{E/\mathrm{GeV}}$. We define jets as hadronic clusters with $E_T > 15$ GeV within a cone of size $\Delta R = 0.7$, and use the GETJET subroutine to perform the clustering. Isolated leptons are defined to be e's or μ's having $p_T > 5$ GeV, with net visible hadronic activity $E_T < 2$ GeV within a cone of size $\Delta R = 0.4$ about the lepton direction.

We focus on a particular set of cuts, corresponding to the HC2 set in Ref. [62], that is well-suited to the HENS mass spectrum [61, 64]. In each event, we require three isolated leptons with $p_T(\ell_{1,2,3}) > 20,\ 15,\ 10$ GeV, and $|\eta(\ell_{1,2,3})| < 2.5$. In addition to this, the total missing E_T must exceed 25 GeV, the invariant mass of same-flavor opposite-sign dileptons must lie in the range 12 GeV $< m_{\ell\ell} <$ 81 GeV, and the transverse invariant mass between each lepton and the missing E_T vector must lie outside the range 60 GeV $< m_T(\ell, \not{E}_T) <$ 85 GeV. The dilepton invariant mass veto is designed to remove background events from off-shell Z and γ decays, while the m_T veto removes leptons from W decays. With these cuts, the SM background is estimated to be 0.49 fb [62], and is due mostly to the remaining W^*Z^* and $W^*\gamma^*$ events in which both off-shell gauge bosons decay leptonically.

In Fig. 4.1 we show the trilepton cross-section subject to the cuts for $M_{1/2} = 300$ GeV and $\tan\beta = 10$. This value of $M_{1/2}$ is about as small as possible within the model given the lower bound on the light Higgs boson mass, and represents a best-case scenario at the Tevatron. Note that for considerably larger values of $\tan\beta$, the constraint from the anomalous magnetic moment of the muon requires larger values of $M_{1/2}$ as well, as can

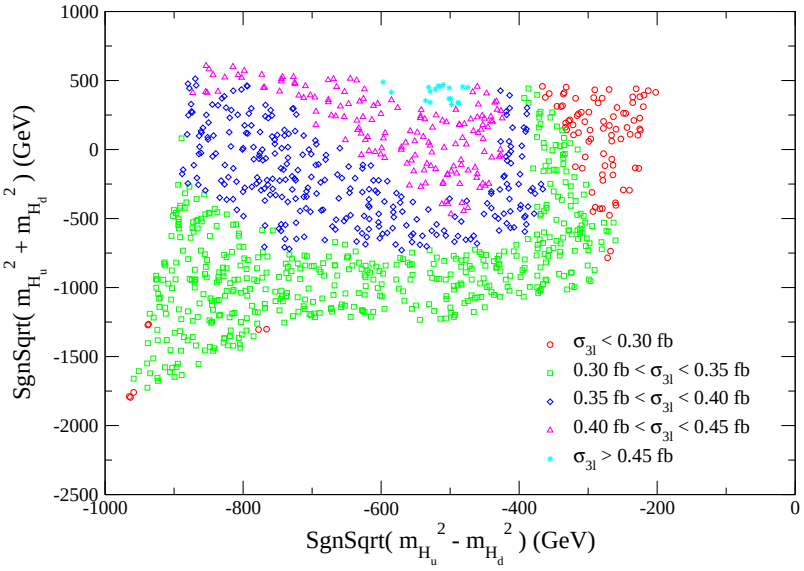

Figure 4.1: Trilepton cross-sections after HC2 cuts at the Tevatron for $M_{1/2} = 300$ GeV and $\tan\beta = 10$. The estimated background is $0.49\,fb$ [62].

be seen in Fig. 2.5. Like in the previous plots, the values of $m^2_{H_u}$ and $m^2_{H_d}$ in Fig. 4.1 are those at the input scale, $M_c = M_{GUT}$.

The dependence of the trilepton cross-section on $m^2_{H_u}$ and $m^2_{H_d}$ can be understood in terms of the mass spectrum. Except in the upper-right portion of the allowed parameter space, the effective cross-section increases smoothly from bottom to top as the value of μ decreases. In most of the parameter space, μ is larger than M_2 and the χ^0_2 and $\chi^\pm_1$ states are mostly Wino. As μ approaches M_2, these states develop a larger Higgsino fraction and their masses are reduced by the mixing. The heavier chargino and neutralino states become lighter as well. On account of these effects, the total gaugino cross section is increased leading to more trilepton events. This pattern is broken in the upper right corner of the parameter space because the mass of the χ^0_2 state approaches the left-handed slepton masses from above, again due to Higgsino mixing. When this mass difference becomes small, the branching fraction for $\chi^2_0 \to \tilde{\ell}_L \ell$ goes down. The leptons produced by the cascades become

relatively soft as well. Since this decay mode plays a prominent role in the trilepton signal subject to the HC2 cuts, the effective cross-section falls off rapidly when the decay fraction is suppressed. The effective cross-section in this region can be increased by using slightly weaker lepton p_T cuts, such as the SC2 set discussed in Ref. [62], but at the expense of an increase in background.

The effective trilepton cross-sections shown in Fig. 4.1 fall within the range of 0.2–0.5 fb. Given the estimated background of 0.49 fb, the signal significance level is marginal. For example, the Poisson probability P_p for a total of ten events, corresponding to the maximal expected signal and background with 10 fb^{-1}, is about $P_p = 0.016$. While this is unfortunately not enough for a discovery, an excess of clean trilepton events at the Tevatron would provide a tantalizing hint of a light HENS scenario. We also note that other event signatures involving leptons can be searched for in these scenarios. Of particular noteworthiness is the same-sign dilepton signature, which has small standard model background.

4.2 Signals at the LHC

If nature is supersymmetric and has a HENS spectrum, the prospects for discovery at the LHC with 10 fb^{-1} of data are excellent provided $M_{1/2}$ is less than about 700 GeV. To quantify this, we focus on six inclusive LHC SUSY search channels, classified by the number of isolated leptons in the event: $0\ell + \not{E}_T + jets$; $1\ell + \not{E}_T + jets$; $2\ell\ OS + \not{E}_T + jets$; $2\ell\ SS + \not{E}_T + jets$; $3\ell + \not{E}_T + jets$; $\geq 4\ell + \not{E}_T + jets$ [65, 66]. (Here, OS and SS refer to opposite-sign and same-sign dileptons, respectively.) Besides an excess of events in these channels, which is expected in many SUSY scenarios, the relative numbers of events within different channels can point towards small input scalar soft masses.

Supersymmetric events at the LHC were simulated using ISAJET 7.74 [63]. We use the ISAJET subroutines CALSIM and CALINI (in the ISAPLT package) as a simple detector model with coverage in the range $|\eta| < 5$, and calorimeter cells of size $\Delta\eta \times \Delta\phi =$

0.05×0.05. A gaussian smearing of the calorimeter cells is included to simulate energy resolution uncertainties. The electromagnetic calorimeter cells are smeared by an amount $0.1/\sqrt{E/\mathrm{GeV}} \oplus 0.01$, where $\oplus$ denotes addition in quadrature. Hadronic calorimeter cells are smeared by an amount $0.5/\sqrt{E/\mathrm{GeV}} \oplus 0.03$ for $|\eta| < 3$, and $1.0/\sqrt{E/\,\mathrm{GeV}} \oplus 0.07$ for $|\eta| > 3$. We define jets as clusters with $E_T > 100$ GeV and $|\eta| < 3$ within a cone of size $\Delta R = 0.7$, and use the GETJET subroutine to perform the clustering. Isolated leptons are defined to be e's or μ's having $p_T > 10$ GeV and $|\eta| < 2.5$, with total visible activity $E_T < 5$ GeV within a cone of size $\Delta R = 0.3$ about the lepton direction.

For all channels studied, we choose a cut energy $E_T^c = 200$ GeV and demand that each event have at least two hard jets, $n_j \geq 2$, with $E_T > E_T^c$, as well as missing transverse energy $\not{E}_T > E_T^c$. This cut substantially reduces the SM backgrounds relative to the SUSY signals.[1] We also require that the transverse sphericity of the event satisfies $S_T > 0.2$ to reduce the dijet background [67]. In zero-lepton events, we demand that the transverse angle between the missing momentum vector and the nearest jet must lie in the range $30^\circ < \Delta\phi(\not{E}_T, j) < 90^\circ$. In the one-lepton channel, we require a single isolated lepton with $p_T > 20$ GeV, as well as $M_T(\ell, \not{E}_T) > 100$ GeV to reduce the leptonic W background. For events with two or more isolated leptons, we demand that $p_T(\ell_{1,2}) > 20$ GeV for the two hardest leptons.

The cross sections after cuts for $M_{1/2} = 500$ GeV and $\tan\beta = 10$ are given in Fig. 4.2 for five sample points. For comparison, the SM backgrounds are estimated to be about $400\,fb$, $26\,fb$, $9\,fb$, $0.25\,fb$, $0.1\,fb$, and $0.002\,fb$ for the 0ℓ, 1ℓ, 2ℓ OS, 2ℓ SS, 3ℓ, and 4ℓ channels respectively [65, 66]. The locations of the sample points, A, B, C, D, and E, in the $m^2_{H_u}(M_{GUT}) - m^2_{H_d}(M_{GUT})$ plane are listed in Appendix A, and are also indicated in Figs. 4.3 and 4.4. Among the five sample points, A and C have a neutralino relic density

[1] A larger value of E_T^c would be preferable to reduce the large SM backgrounds in the $0\,\ell$ channel. However, the 0ℓ SUSY signal is still easily distinguishable from the large background for the parameter points we consider here.

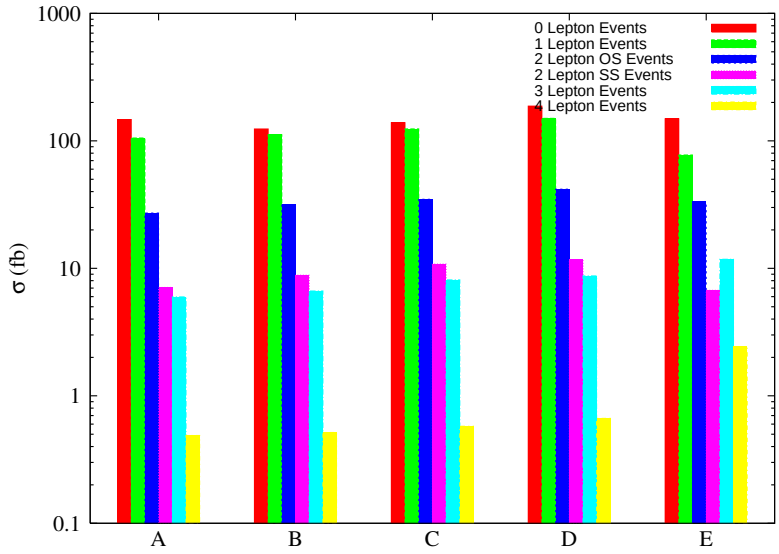

Figure 4.2: Inclusive signal cross-sections after cuts at the LHC for $M_{1/2} = 500$ GeV and $\tan\beta = 10$ for the five sample points described in the text. For comparison, the SM backgrounds are estimated to be about 400 fb, 26 fb, 9 fb, 0.25 fb, 0.1 fb, and 0.002 fb for the 0ℓ, 1ℓ, $2\ell\ OS$, $2\ell\ SS$, 3ℓ and 4ℓ channels respectively [65, 66].

within the WMAP allowed range, while the other points lead to relic densities that are too large (but could be acceptable with a non-standard cosmology). At point E, the μ term is on the same order as $M_2 \simeq 2\,M_1$, but it is greater than 750 GeV at the other sample points. Thus, except for point E, the LSP is a mostly Bino neutralino, while the lightest chargino and the next-to-lightest neutralino are predominantly Wino. At point E where $\mu < M_2$, all the chargino and neutralino states are fairly light and have significant Higgsino components, which, as we shall discuss below, is the reason for the increase in the 3ℓ and 4ℓ rates.

In each of the six search channels, the SUSY signal is easily distinguishable from the background with $10 fb^{-1}$ of luminosity at the LHC. A more challenging task beyond an initial discovery is to distinguish this class of models from other (SUSY) scenarios and to deduce the model parameters. The number of leptonic events relative to the number of $0\,\ell$

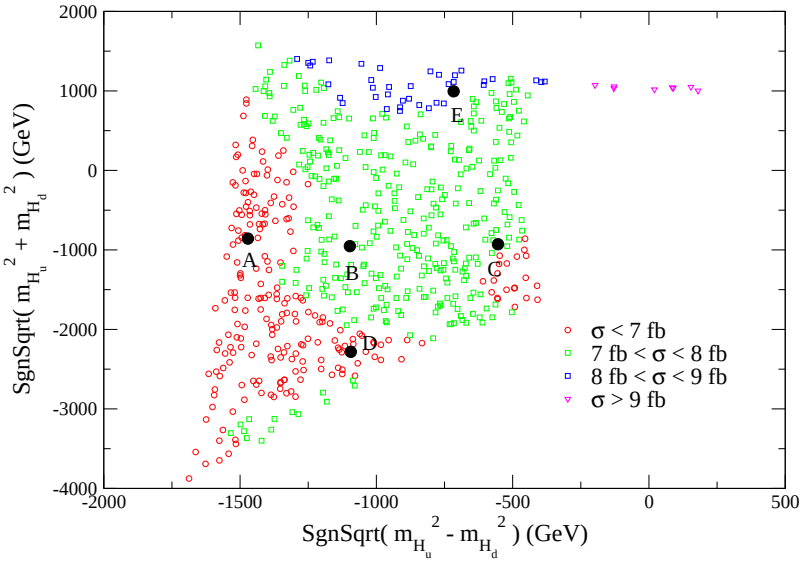

Figure 4.3: 3ℓ cross-sections after cuts at the LHC for $M_{1/2} = 500$ GeV and $\tan\beta = 10$. The estimated background is 0.1 fb.

events is useful in this regard. Compared to a generic mSUGRA input spectrum with $m_0 > 0$, the ratio of $1\,\ell$ events to $0\,\ell$ events is much larger for a given value of $M_{1/2}$. For example, in mSUGRA with $(m_0,\ M_{1/2},\ A_0,\ \tan\beta,\ sgn(\mu)) = (200\ \text{GeV},\ 500\,\text{GeV},\ 0, 10, +)$, the ratio of $0\ \ell$ to $1\,\ell$ events is greater than four, whereas this ratio is close to unity for all five sample points considered. The ratio of the number of $0\,\ell$ events to the number of $2\,\ell$ events is also much larger in a generic mSUGRA framework than it is here. This is the consequence of having left-handed sleptons lighter than the χ_2^0 and $\chi_1^\pm$ states, which are in turn light enough to be generated by squark decays. For example, cascade chains such as $\tilde{q} \to \chi_2^0\, q \to \tilde{\ell}_L^*\, \ell^-\, q \to \chi_1^0\, \ell^+\, \ell^-\, q$ have a significant branching probability, and are a rich source of leptons.

The dependence of the effective 3ℓ cross-section on the input Higgs soft mass parameters is shown in Fig. 4.3. For the most part, this dependence is fairly mild except in the upper right portion of the allowed region. Here, the μ term approaches the Bino mass M_1, and

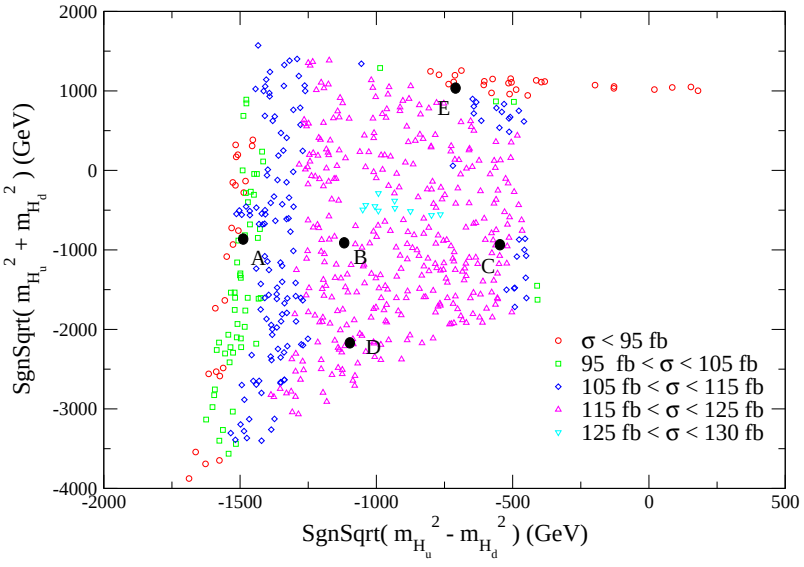

Figure 4.4: 1ℓ cross-sections after cuts at the LHC for $M_{1/2} = 500$ GeV and $\tan\beta = 10$. The estimated background is 26 fb.

in the thin tail extending to the right, μ even falls below M_1. In this region, all the neutralinos and charginos are significantly lighter than the squarks and gluinos. As a result, the decay cascades initiated by the strong superpartners are frequently very long, involving several chargino and neutralino states. At each step in the cascade chain there is a chance of producing a lepton, and thus the total fraction of events containing multiple leptons is very high. For example, the decay chain $\tilde{u}_R \to \chi_3^0 u \to \tilde{\ell}_R^* \ell^- u \to \chi_1^0 \ell^+ \ell^- u$ is kinematically allowed when μ is small, and has a significant branching fraction. The preponderance of leptons can be so high that the number of 0ℓ and 1ℓ events (and even to some extent some 2ℓ events) are significantly suppressed. This can be seen in Fig. 4.4, which shows the 1ℓ effective cross section for $M_{1/2} = 500$ GeV and $\tan\beta = 10$. Note that the small μ region is strongly constrained by direct and indirect searches for dark matter, and will be probed by upcoming experiments, as was discussed above.

In the leftmost portion of the allowed region of Fig. 4.3, there is also a net decrease

in the cross section, which occurs in the other leptonic channels as well. Within this region, leptons typically originate from decays of the mostly Wino χ_2^0 and $\chi_1^\pm$ states into left-handed sleptons and sneutrinos, which subsequently decay into the neutralino LSP. However, these left-handed states are only slightly heavier than the LSP, so the lepton emitted from the slepton decays tends to be soft, making it less likely to pass the lepton p_T cuts.

A particularly distinctive signature of the HENS models are inclusive 4ℓ events. We find effective cross-sections above $0.5\,fb$ for $\tan\beta = 10$ and $M_{1/2} = 500$ GeV, which is sufficient for a $10\,fb^{-1}$ LHC discovery given the SM background of about $0.002\ fb$ [66]. There is a sharp increase in the 4ℓ cross-section in the small μ region at the upper right of the parameter space. The dominant sources of this increase are cascades initiated by right-handed squarks of the type described previously. Furthermore, because the left-handed sleptons are lighter than χ_3^0 but heavier than $\chi_2^\pm$ and χ_4^0 in this region, superpartner cascades such as $\tilde{u}_L \to \chi_2^\pm \to \tilde{\nu} \to \chi_3^0 \to \tilde{\ell}_R \to \chi_1^0$ accompanied by many leptons have a non-trivial branching fraction and can produce three leptons from the single squark parent.[2] As a result, 4ℓ rates greater than $5\,fb$ can occur. We have also investigated the exclusive clean trilepton channel. It does not appear to be as promising as the inclusive channels.

Varying $\tan\beta$ does not qualitatively affect our findings. The cross sections after cuts for $M_{1/2} = 500$ GeV and $\tan\beta = 30$ are given in Fig. 4.5 for five sample points, A', B', C', D', E'. Details of these sample points are given in Appendix A. The cross sections in all six channels are similar to those in Fig. 4.2 with $\tan\beta = 10$. In particular, the ratio of 0ℓ to 1ℓ events is still close to unity, and the 3ℓ and 4ℓ rates are observably large. The main difference that occurs at larger values of $\tan\beta$ is that there is no small μ region.

Since the entire mass spectrum in HENS models scales with $M_{1/2}$, so too do the event

[2] The final lepton in this cascade tends to be quite soft because the mass difference $(m_{\tilde{l}_R} - m_{\chi_1^0})$ is very small in this part of the parameter space. However, the other two leptons in the cascade tend to be quite hard.

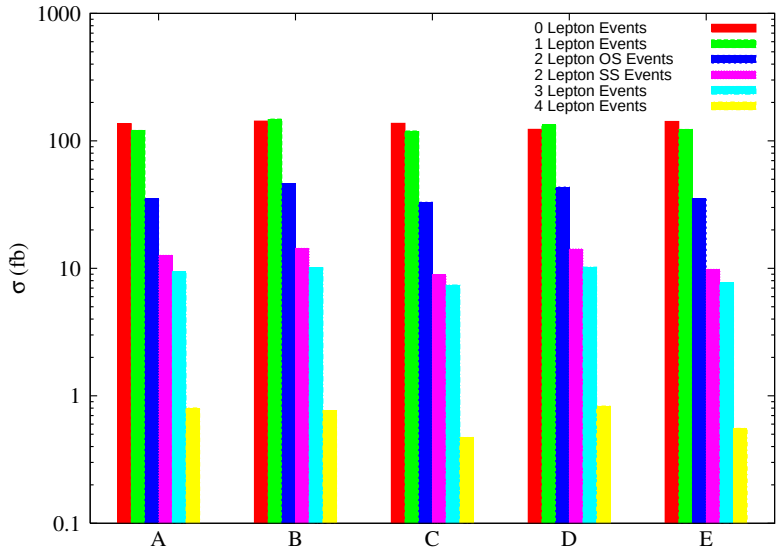

Figure 4.5: Inclusive signal cross-sections after cuts at the LHC for $M_{1/2} = 500$ GeV and $\tan\beta = 30$ for the five sample points described in the text. For comparison, the SM backgrounds are estimated to be about 400 fb, 26 fb, 9 fb, 0.25 fb, 0.1 fb, and 0.002 fb for the 0ℓ, 1ℓ, $2\ell\ OS$, $2\ell\ SS$, 3ℓ and 4ℓ channels respectively [65, 66].

rates. We have checked that for $M_{1/2}$ as large 700 GeV, corresponding to a gluino mass of $m_{\tilde{g}} \simeq 1600\,\mathrm{GeV}$, the inclusive event rates in all channels other than the 0ℓ and 4ℓ are large enough that a discovery with $10 fb^{-1}$ of LHC data is feasible. On the other hand, the event rates become even larger for smaller values of $M_{1/2}$, making discovery even easier.

CHAPTER V

Neutrino Higgs Exempt No-Scale Supersymmetry

While the HENS model is phenomenologically enticing, it does not explain the observation of neutrino oscillations [68]. This shortcoming can be resolved by supplementing the model with three heavy singlet right-handed neutrino chiral superfields, with the superpotential couplings

$$W = W_0 + NY_\nu LH_u + \frac{1}{2}NM_N N, \tag{5.1}$$

where W_0 is the MSSM superpotential, N are the right-handed neutrinos, M_N is their Majorana mass matrix, and Y_ν is the neutrino Yukawa matrix. By taking the singlet neutrino masses M_{N_i} much larger than the electroweak scale, very small masses can be generated for the left-handed neutrinos by the seesaw mechanism [68]. Integrating out the heavy neutrino states yields the effective superpotential coupling

$$W_{eff} = W_0 - \frac{1}{2}(Y_\nu^T M_N^{-1} Y_\nu)_{ij}(L_i H_u)(L_j H_u). \tag{5.2}$$

For $M_N \sim 10^{12}$ GeV, this interaction can generate correct light neutrino masses at the weak scale with the neutrino Yukawa couplings on the order of unity, $Y_\nu \sim 0.1$.

Adding heavy right-handed neutrinos to the HENS scenario also introduces a new flavor-mixing problem to the model. In running the soft parameters in the full theory (Eq. (5.1)) from the input scale M_{GUT} down to the heavy singlet neutrino scale M_N, the neutrino

Yukawa couplings generate non-universal contributions to the soft masses for the charged leptons [69]. Such couplings are dangerous because they are a source of lepton flavor violation (LFV) [69], for which the experimental bounds are extremely strong. This in turn imposes stringent constraints on the heavy neutrino sector.

Although adding right-handed neutrinos to SUSY models can lead to problematic lepton flavor violating (LFV) rates, such extensions also have some attractive collateral features. One of these is the possibility of generating the baryon asymmetry via leptogenesis [70, 71]. The heavy right-handed neutrinos can fulfill the three Sakharov conditions for baryogenesis [74], which can be realized through the mechanism of leptogenesis. Each of these will be discussed below.

Requiring that the neutrino-extended HENS (νHENS) model account for the baryon asymmetry of the universe, while respecting the current bounds on LFV, leads to constraints on the structure of the neutrino Yukawa matrix and the right-handed neutrino masses[75]. Previous studies that combine the requirements for leptogenesis with the bounds from LFV can be found in Refs. [76, 77, 78, 79]. Compared to these previous works, we study the constraints from LFV within the context of a specific model for which the lack of flavor mixing outside the neutrino sector is well-motivated. An interesting result along these lines is that the amount of LFV in the HENS model is largely controlled by the value of $m^2_{H_u}$ at the high input scale. Therefore, the degree to which the neutrino sector parameters are constrained depends strongly on the size of $m^2_{H_u}$.

5.1 LFV in the HENS Model with Heavy Neutrinos

We begin by considering the constraints on the HENS model from LFV induced by the inclusion of heavy right-handed neutrinos. These constraints depend strongly on the parameters in the neutrino sector such as the Majorana masses for the right-handed neutrinos and the neutrino Yukawa matrix. Some of these neutrino sector parameters have been de-

termined by the measurements of the light neutrino mass differences and mixings [80, 81]. In anticipation of computing the LFV constraints, we collect here our notation and assumptions about the neutrino sector.

In terms of the couplings in the full superpotential of Eq. (5.1), the low-energy effective superpotential of Eq. (5.2) implies that the light neutrino mass matrix is given by

$$m_{\nu_{ij}} = \frac{v_u^2}{2}(Y_\nu^T M_N^{-1} Y_\nu)_{ij} \tag{5.3}$$

This matrix can be diagonalized by the unitary PMNS matrix U [82, 83]. Following the standard convention, we will parameterize the PMNS matrix with three real angles and three phases according to

$$U = \mathcal{O}_{23}(\theta_{23})\,\Gamma_\delta \mathcal{O}_{13}(\theta_{13})\,\Gamma_\delta^*\,\mathcal{O}_{12}(\theta_{12})\;\times diag[e^{i\alpha_1/2}, e^{i\alpha_2/2}, 1] \tag{5.4}$$

where $\Gamma_\delta = diag(1, 1, e^{i\delta})$, and $\mathcal{O}_{ij} = [(c_{ij}, s_{ij}), (-s_{ij}, c_{ij})]$ with $c_{ij} = \cos\theta_{ij}$ and $s_{ij} = \sin\theta_{ij}$.

It is convenient to make use of the known structure of the light neutrino mass matrix to parameterize the neutrino Yukawa matrix Y_ν according to [84]

$$Y_\nu = \frac{1}{v_u}\sqrt{M_N}\,R\,\sqrt{m_{\nu_{diag}}}\,U^\dagger \tag{5.5}$$

where R is a *complex orthogonal* matrix, M_N is the diagonal right-handed neutrino mass matrix, and $m_{\nu_{diag}}$ is the diagonalized left-handed neutrino mass matrix. Here, and throughout this paper, we will always work in a field basis such that the right-handed neutrino and charged lepton mass matrices are diagonal. Since the R matrix is complex orthogonal, we can parameterize it in terms of three *complex* angles according to

$$R = diag(\pm 1, \pm 1, \pm 1)\;\mathcal{O}_{12}(\theta_{12R})\,\mathcal{O}_{23}(\theta_{23R})\,\mathcal{O}_{31}(\theta_{31R}). \tag{5.6}$$

with $\mathcal{O}_{ij} = [(c_{ijR}, s_{ijR}), (-s_{ijR}, c_{ijR})]$, where $c_{ijR} = \cos\theta_{ijR}$ and $s_{ijR} = \sin\theta_{ijR}$. Note that since these angles are complex, the components of R are not bounded in magnitude. This

means that some of the entries in the neutrino Yukawa matrix could be quite large, but through cancellations among the see-saw contributions, still give rise to acceptably small light neutrino masses. In order to avoid too much fine-tuning in this regard, we will only consider R matrices with $|R_{ij}| < 10$, which corresponds roughly to a tuning of less than 10% in the light neutrino mass matrix. Our choices for the light neutrino masses and mixings are listed in Appendix B.

5.1.1 Off-Diagonal HENS Soft Terms from RG Running

Without heavy right-handed neutrinos, the HENS model is safe in terms of lepton-flavor violation (LFV). With heavy right-handed neutrinos, lepton-flavor violating couplings can arise among the scalar soft terms in the course of renormalization group (RG) running from the input scale M_{GUT} down to the electroweak scale . The strict experimental limits on LFV will in turn lead to constraints on the neutrino Yukawa couplings and right-handed neutrino masses. Since this new source of flavor changing neutral currents (FCNC) in the HENS model arises from RG running, and not the SUSY breaking mechanism, its amplitude will have a similar form to that found in mSUGRA models.

The dominant contributions to the off-diagonal flavor-mixing components can be approximated by expanding the beta functions about their GUT scale values as

$$\beta(t) = \beta(t_G) + \left(\frac{d}{dt_G}\beta(t_G)\right)(t - t_G) + \cdots . \tag{5.7}$$

As long as the mass of the heavy right-handed neutrinos is not far from the GUT scale, the second term, which is loop suppressed, will be subleading[1]. With the dominant contribution to the beta function being constant, it can easily be integrated. In the case of the HENS model where $m^2_{\tilde{f}} = 0,\ m^2_{H_u},\ m^2_{H_d} \neq 0$, the leading contribution to the off-diagonal

[1]The leading-log approximation breaks down for $M_{1/2} \gtrsim 1000\,\text{GeV}$ and $|m^2_{H_u}| \lesssim (100\text{ GeV})^2$ [85]. To avoid this, we include subleading terms ($m^2_{L_{i\neq j}} - m^2_{L^{(0)}_{i\neq j}} \sim Y_\nu^4 m^2_{H_d}$) in our numerical analysis, where $m^2_{L^{(0)}_{i\neq j}}$ is the leading order contribution.

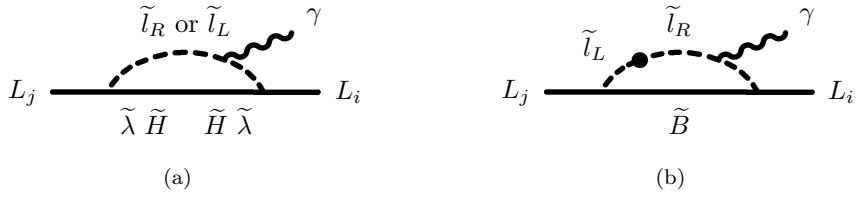

Figure 5.1: All relevant diagrams for the anomalous magnetic moment that do not involve left-right mixing are of this form. The $\widetilde{H}$ can be either the charged or neutral Higgs and $\widetilde{\lambda}$ is either the bino, $\widetilde{B}$, or wino, $\widetilde{W}^{\pm}$. $\widetilde{l}_L$ represents either a sneutrino, $\widetilde{\nu}$ or a left-handed slepton, $\widetilde{e}_L$ and $\widetilde{l}_R$ is a right-handed slepton.

components of the scalar masses is[69, 86]

$$m^2_{\tilde{L}_{i\neq j}} = -\frac{1}{8\pi^2} m^2_{Hu} \sum_k Y^*_{\nu ki} Y_{\nu kj} \ln\left(\frac{M_{GUT}}{M_{N_k}}\right). \tag{5.8}$$

To this order of approximation, the beta functions of the flavor non-diagonal elements in the scalar trilinear soft couplings and the right-handed slepton soft masses vanish. This procedure will also give corrections to the diagonal components of the scalar masses. When the constraints on the neutrino Yukawa couplings from LFV are applied, the corrections to the diagonal components of the scalar masses are numerically very small; less than about 5 GeV in most of the parameter space. However, when these corrections could be relevant we have included them.

5.1.2 HENS LFV

The off-diagonal soft terms introduced by RG running, given in Eq. (5.8), will induce LFV transitions of the type $\ell_i \to \ell_j \gamma$ through loop diagrams containing scalar particles. Because the mass eigenstates are a mixture of different flavors, the scalar particles will change flavor as they propagate. To better understand how this occurs, we will give a simple two flavor example and show how the propagators in the mass eigenstate basis are related to the propagators in the interaction basis (See last Ref. in [2]). A generic propagator in the mass eigenstate basis can be written as

$$B_{ij} = \sum_A \frac{U_{iA} U^*_{Aj}}{q^2 - m_A^2}, \tag{5.9}$$

where m_A are the eigenvalues of the mass matrix

$$\tilde{m}^2 = \begin{pmatrix} \tilde{m}_1^2 & \Delta \\ \Delta & \tilde{m}_2^2 \end{pmatrix}, \tag{5.10}$$

and U_{iA} diagonalizes this matrix. If Δ is small, the eigenvalues of this matrix can be approximated as

$$m_1^2 = \tilde{m}_1^2 - \frac{\Delta^2}{\tilde{m}_2^2 - \tilde{m}_1^2} = \tilde{m}_1^2 - \delta m_1^2, \tag{5.11}$$

$$m_2^2 = \tilde{m}_2^2 + \frac{\Delta^2}{\tilde{m}_2^2 - \tilde{m}_1^2} = \tilde{m}_2^2 + \delta m_1^2. \tag{5.12}$$

Using these expressions for the masses, we expand the propagator about m_1^2, remembering $U_{i1} U^*_{1j} = -U_{i2} U^*_{2j}$. If we keep only term to order Δ^2 we get

$$B_{ij} = \frac{1}{q^2 - \tilde{m}_1^2} \left[U_{i1} U^*_{1j} (m_2^2 - m_1^2) \right] \frac{1}{q^2 - \tilde{m}_2^2} = \frac{1}{q^2 - \tilde{m}_1^2} \delta m_{ij}^2 \frac{1}{q^2 - \tilde{m}_2^2}. \tag{5.13}$$

In this limit of small Δ, the off-diagonal components of U, the matrix that diagonalizes $\tilde{m}^2$, are found to be

$$U_{12} = -U_{21} = \frac{\Delta}{\tilde{m}_2^2 - \tilde{m}_1^2} \simeq \frac{\Delta}{m_2^2 - m_1^2}. \tag{5.14}$$

Combining these relations, we find that the propagator in the mass eigenstate basis is related to the one in the interaction basis as

$$\sum_A \frac{U_{iA} U^*_{Aj}}{q^2 - m_A^2} \simeq \frac{1}{q^2 - \tilde{m}_1^2} \Delta \frac{1}{q^2 - \tilde{m}_2^2}. \tag{5.15}$$

To leading order, the mass eigenstate propagator is equivalent to two interaction eigenstate propagators separated by a mass insertion. This expression explicitly links the flavor violation in the scalar mass matrices to the flavor violation in loop diagrams. It also helps us understand how non-diagonal scalar mass matrices can lead to flavor violation in the SM. Loops composed of these flavor violating propagators will link vertices of different flavors. SM particles attached to the end of this type of propagator can have different flavors.

The non-diagonal scalar masses are most dangerous in the lepton sector. These couplings contributing to LFV are the most dangerous because of the tight experimental constraints on $\ell_i \to \ell_j\,\gamma$. The leading contributions to the branching fractions for these transitions in the HENS model can be written as [86, 87, 88]

$$B(\ell_i \to \ell_j \gamma) = \frac{\alpha}{4\,\Gamma(\ell_i)}\, m_{\ell_i}^5\, |A_L^{(ij)}|^2, \tag{5.16}$$

where $\Gamma(\ell_i)$ is the total decay width of lepton ℓ_i, and the amplitude $A_L^{(ij)}$ has the schematic form [86, 87]

$$A_L^{(ij)} = m^2_{\tilde{L}_{i\neq j}}\, F_L^{(ij)}, \tag{5.17}$$

with $F_L^{(ij)}$ a combination of loop functions that depend on the chargino, neutralino, and slepton masses. These loop functions are such that the dominant contribution to $B(\ell_i \to \ell_j\gamma)$ scales approximately as $m^2_{\tilde{L}_{i\neq j}}\, \tan^2\beta\, M_{1/2}^{-8}$. Note also that in this leading contribution to the LFV branching fractions, the flavor violating term $m^2_{\tilde{L}_{i\neq j}}$ can be factored out. This will allow us to discuss the effects of the neutrino sector and the supersymmetry breaking sector separately.

The differences in the branching fractions of Eq. (5.16) for the HENS model as compared to mSUGRA lie in the form $m^2_{\tilde{L}_{i\neq j}}$ and the low-scale sparticle masses. However, $m^2_{\tilde{L}_{i\neq j}}$ is qualitatively similar in the two theories and will be of the same order of magnitude for

both theories as long as $m_{H_u}^2 \sim m_0^2 + a_0^2$. The loop functions $F_L^{(ij)}$ are also qualitatively similar, but differ in the masses of the gauginos and sleptons running in the loops. From this this functional dependence, there can be a slight enhancement of the LFV rates in HENS relative to mSUGRA because the slepton masses tend to be somewhat lighter in the HENS model. On the other hand, the LFV rates can be reduced in the HENS model relative to mSUGRA by arranging for $m_{H_u}^2$ to vanish, which suppresses the leading source of lepton flavor mixing given in Eq. (5.8). As shown in Ref. [14], it is often possible to obtain a consistent phenomenology with $m_{H_u}^2 \sim 0$, especially for $\tan\beta \lesssim 30$. To obtain a similar suppression in mSUGRA, one would need both m_0 and a_0 to be quite small which can be phenomenologically problematic [89, 90].

5.1.3 Constraints on the HENS Model from LFV

The possibility of inducing LFV places significant constraints on right-handed neutrino extensions of the HENS model. The two strongest bounds on new sources of LFV come from searches for $\mu \to e\gamma$ and $\tau \to \mu\gamma$ transitions:

$$B(\mu \to e\gamma) < 1.2 \times 10^{-11}, \text{ [91]} \tag{5.18}$$

$$B(\tau \to \mu\gamma) < 4.5 \times 10^{-8}, \text{ [92, 93]} \tag{5.19}$$

$$B(\tau \to e\gamma) < 1.1 \times 10^{-7}, \text{ [94]} \tag{5.20}$$

It was shown in Ref. [86] if these bounds are satisfied, the bounds on other experimentally searched-for channels such as $B(\mu \to 3e)$ will generally be satisfied as well.

In Fig. 5.2 we show the dependence of the LFV branching fraction $B(\mu \to e\gamma)$ on the high-scale input values of $m_{H_u}^2$ and $m_{H_d}^2$ in the HENS model with right-handed neutrinos. The other HENS parameters are taken to be $M_{1/2} = 300$ GeV, $\tan\beta = 10$, and $sgn(\mu) = 1$. This value of $M_{1/2}$ is about as small as is possible in the HENS model while still obtaining a sufficiently heavy Higgs boson [14]. The points in this figure cover the region of the HENS

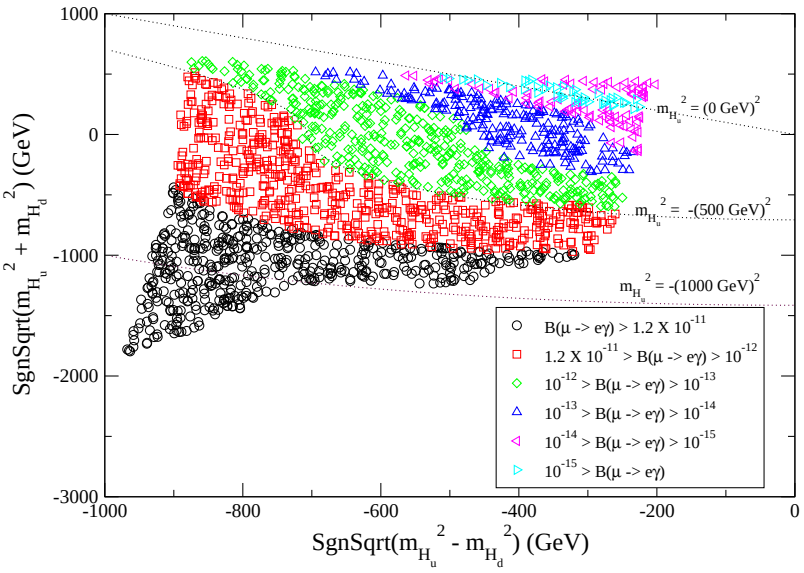

Figure 5.2: $B(\mu \to e\gamma)$ as a function of the HENS model parameters $m^2_{H_u}$ and $m^2_{H_d}$ at the high input scale. The other model parameters are $M_{1/2} = 300\,\text{GeV}$, $\tan\beta = 10$, and $sgn(\mu) = 1$ as well as neutrino-sector parameters $\theta_{12R} = \theta_{13R} = \theta_{23R} = \pi/4 + i\ln(\sqrt{2})$, $M_{N_3} = 10^{12}$ GeV, $M_{N_2} = 10^{11}$ GeV, and $M_{N_1} = 10^{10}$ GeV. All points in this plot are consistent with collider phenomenology constraints and have a neutralino LSP.

parameter space that is consistent with all collider and phenomenological constraints other than from LFV, and that has a neutralino LSP. The neutrino-sector parameters are taken to be $M_{N_3} = 10^{12}$ GeV, $M_{N_2} = 10^{11}$ GeV, $M_{N_1} = 10^{10}$ GeV, the light neutrino masses are as described in Appendix B with $m_3 = 0.05\,\text{eV}$, and the R-matrix angles (see Eq. (5.6)) are equal to $\theta_{12R} = \theta_{13R} = \theta_{23R} = \pi/4 + i\ln(\sqrt{2})$. These particular values of the neutrino sector parameters were chosen for convenience, but we have checked that they lead to typical amounts of LFV. The decreasing trend in $B(\mu \to e\gamma)$ from bottom-left to top-right in this figure corresponds largely to a decreasing value of $m^2_{H_u}$. This is not surprising given Eq. (5.8), which shows that the leading contribution to lepton flavor mixing is proportional to $m^2_{H_u}$.

Fig. 5.3 shows the dependence of the LFV branching fraction $B(\mu \to e\gamma)$ on $m^2_{H_u}$ and $m^2_{H_d}$ for the same neutrino sector parameters as Fig. 5.2, but now with $M_{1/2} =$

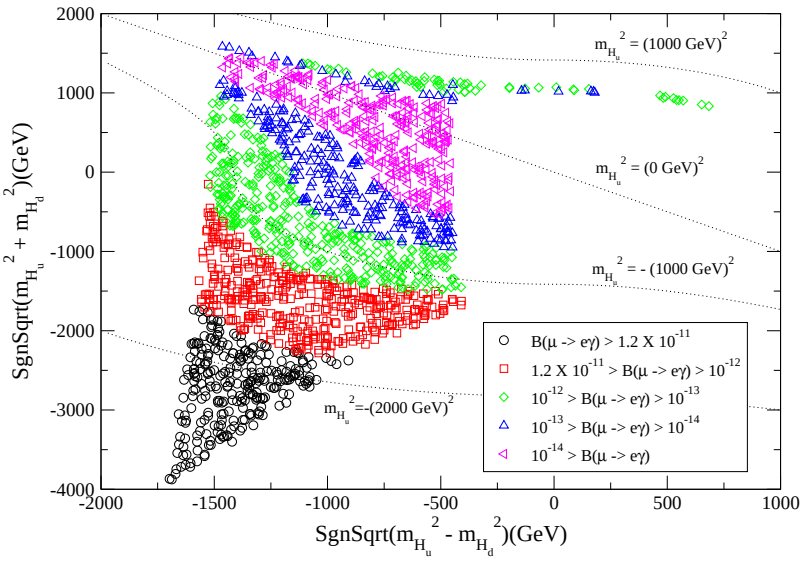

Figure 5.3: $B(\mu \to e\gamma)$ as a function of the HENS model parameters $m^2_{H_u}$ and $m^2_{H_d}$. The other model parameters are $M_{1/2} = 500\,\text{GeV}$ and $\tan\beta = 10$, as well as neutrino-sector parameters $\theta_{12R} = \theta_{13R} = \theta_{23R} = \pi/4 + i\ln(\sqrt{2})$, $M_{N_3} = 10^{12}$ GeV, $M_{N_2} = 10^{11}$ GeV, and $M_{N_1} = 10^{10}$. All points in this plot are consistent with collider phenomenology constraints and have a neutralino LSP.

500 GeV. Also as before, $\tan\beta = 10$, $sgn(\mu) = 1$, and all points shown are consistent with collider constraints and have a neutralino LSP. Compared to Fig. 5.2, the LFV rates are considerably lower. This can be understood in terms of the general scaling of all the superpartner masses with $M_{1/2}$, and the fact that larger superpartner masses suppress the loop functions appearing in Eq. (5.17). Aside from this scaling, the shapes of the contours in the two figures are very similar, with the dominant variation in the branching fraction due to the changing input value of $m^2_{H_u}$.

In Fig. 5.4 we illustrate the dependence of the LFV branching ratio $B(\mu \to e\gamma)$ on $m^2_{H_u}$ and $m^2_{H_d}$ for $\tan\beta = 30$, $M_{1/2} = 500$ GeV, and $sgn(\mu) = 1$ over the allowed parameter space in the HENS model. All points in the plot satisfy collider phenomenology constraints and have a neutralino LSP. The values of the neutrino sector parameters are the same as in Figs. 5.2 and 5.3. The variation of $B(\mu \to e\gamma)$ in this plot again tracks the value of

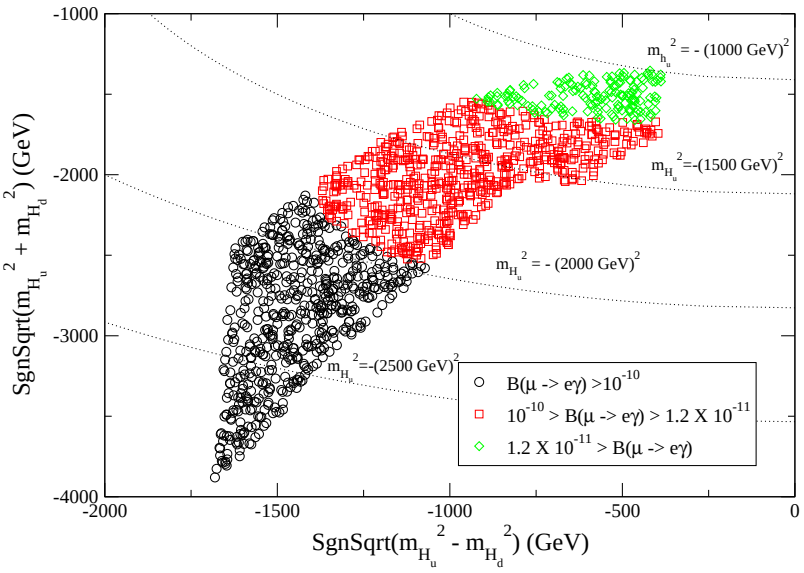

Figure 5.4: $B(\mu \to e\gamma)$ as a function of the HENS model parameters $m^2_{H_u}$ and $m^2_{H_d}$. The other model parameters are $M_{1/2} = 500\,\text{GeV}$ and $\tan\beta = 30$, as well as neutrino-sector parameters $\theta_{12R} = \theta_{13R} = \theta_{23R} = \pi/4 + i\ln(\sqrt{2})$, $M_{N_3} = 10^{12}$ GeV, $M_{N_2} = 10^{11}$ GeV, and $M_{N_1} = 10^{10}$. All points in this plot are consistent with collider phenomenology constraints and have a neutralino LSP.

$m^2_{H_u}$. However, the overall values of the LFV branching ratio $B(\mu \to e\gamma)$ are larger than in the previous figures. There are two reasons for this. The first is that the expression for $B(\mu \to e\gamma)$ scales like $\tan^2\beta$. The second reason for the relative enhancement in the LFV rates is that larger values of $\tan\beta$ also enhance the τ Yukawa coupling, making it more likely to obtain a stau LSP. To obtain a neutralino LSP, which we demand as a phenomenological constraint, $m^2_{H_u}$ must be large in magnitude and negative in sign. This limits the suppression of $B(\mu \to e\gamma)$ that occurs in the HENS model as $m^2_{H_u}$ becomes small. With these two sources of relative enhancement at larger values of $\tan\beta$, we see that in the present example there are very few parameter points consistent with the bound on $B(\mu \to e\gamma)$ listed in Eq. (5.18).

In the plots discussed above, the LFV rates depend most sensitively on the parameter $m^2_{H_u}$. To better illustrate this relationship, we plot in Fig. 5.5 the same sets of points as in

Figs. 5.2, 5.3, and 5.4 in terms of $B(\mu \to e\gamma)$ as a function of $m^2_{H_u}$. These sets correspond to $\tan\beta = 10$ and $M_{1/2} = 300$ GeV, $\tan\beta = 10$ and $M_{1/2} = 500$ GeV, and $\tan\beta = 30$ and $M_{1/2} = 500$ GeV respectively, with $m^2_{H_d}$ scanned over. The values of the neutrino sector parameters are the same as in the previous plots. As expected from Eq. (5.8), the LFV rates drop precipitously as $m^2_{H_u} \to 0$. When this occurs, only the much smaller terms beyond the leading order term given in Eq. (5.8) contribute to lepton flavor mixing. These subleading terms scale like $M_{1/2}$, and can not be zeroed out due to the phenomenological lower bounds on $M_{1/2}$. Fig. 5.5 also illustrates the scaling of $B(\mu \to e\gamma)$ with $M_{1/2}$, which we expect to go like $M^{-8}_{1/2}$, as well as the enhancement of the LFV rates for larger values of $\tan\beta$. There is a dip in the branching fraction at $m^2_{H_u} \simeq (700)^2\,\mathrm{GeV}^2$. This corresponds to $M_1 \simeq \mu$, leading to a large mixing among the neutralinos and a cancellation between contributions to the amplitude.

We have concentrated so far on the specific branching fraction $B(\mu \to e\gamma)$. The related branching fractions $B(\tau \to \mu\gamma)$ and $B(\tau \to e\gamma)$ both have a very similar dependence on the HENS model parameters. Plots of these branching fractions as a function of $m^2_{H_u}$ are nearly identical in both shape and overall normalization to those in Fig. 5.5. However, since the experimental upper bounds on the branching fractions of these τ modes are more than a couple of orders of magnitude larger than the μ mode, they provide much weaker constraints on the neutrino-enhanced HENS parameter space. We will therefore concentrate most strongly on the $\mu \to e\gamma$ mode in the present work, but will briefly mention when the τ modes can be relevant.

Having studied the dependence of the LFV rates on the HENS model parameters for a particular (but typical) set of neutrino sector parameters, let us next examine the dependence of the LFV rates on the details of the neutrino sector. In Fig. 5.6 we show the branching fraction $B(\mu \to e\gamma)$ as a function of the heaviest right-handed neutrino mass

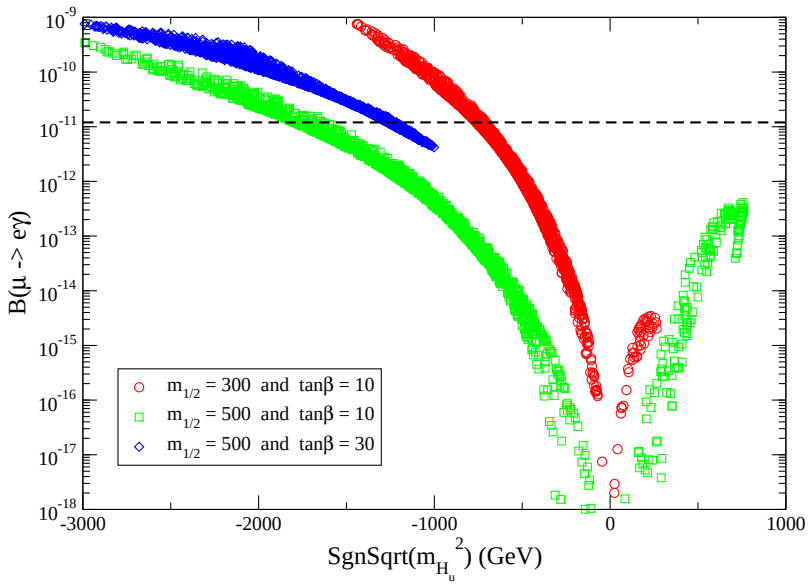

Figure 5.5: $B(\mu \to e\gamma)$ as a function of $m^2_{H_u}$ at the high input scale for several values of $M_{1/2}$ and $\tan\beta$. Values of $m^2_{H_d}$ were scanned over, and all points are consistent with collider phenomenology constraints and have a neutralino LSP. The neutrino sector parameters are given by $\theta_{12R} = \theta_{13R} = \theta_{23R} = \pi/4 + i\ln(\sqrt{2})$, $M_{N_3} = 10^{12}$ GeV, $M_{N_2} = 10^{11}$ GeV, and $M_{N_1} = 10^{10}$ GeV. The dashed line in this figure corresponds to the experimental LFV bound $B(\mu \to e\gamma) < 1.2 \times 10^{-11}$.

M_{N_3}. Of the heavy neutrino masses, this one usually plays the most important role in determining the amount of LFV. The HENS model parameters for this plot are $\tan\beta = 10$, $M_{1/2} = 300$ GeV, $m^2_{H_u} = -(511\text{ GeV})^2$ and $m^2_{H_d} = -(668\text{ GeV})^2$. These values produce a phenomenologically consistent spectrum, which we list in Appendix C, and are not unusual in terms of LFV. The light neutrino masses are as described in Appendix B. The remaining neutrino sector parameters were scanned over: heavy neutrino masses lie in the range $M_N \in [10^7, 10^{14}]$ GeV with no particular hierarchy between them, and the R matrix angles range over $\mathbf{Re}(\theta) \in [0, 2\pi]$ and $\mathbf{Im}(\theta) \in [-2, 2]$. Within the plot, the blue circles, green squares, and red diamonds correspond to $Max\{|R|\} \in [0, 2]$, $Max\{|R|\} \in [2, 5]$, and $Max\{|R|\} \in [5, 10]$. Recall that since R is a complex orthogonal matrix, its components are unbounded, although large components require a fine-tuning to obtain small neutrino masses.

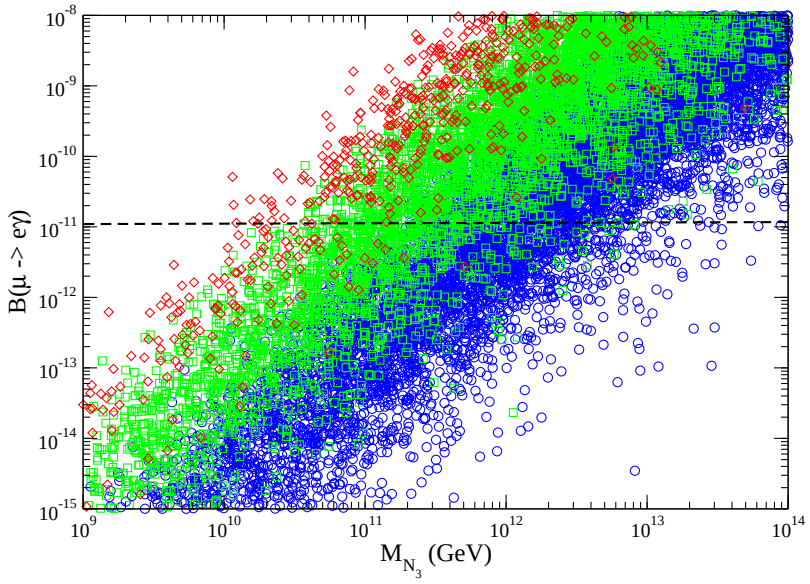

Figure 5.6: $B(\mu \to e\gamma)$ as a function of the heaviest right-handed neutrino mass M_{N_3} for the HENS parameters $m^2_{H_u} = -(668)^2\,\mathrm{GeV}^2$, $m^2_{H_d} = -(511)^2\,\mathrm{GeV}^2$, $\tan\beta = 10$, and $M_{1/2} = 300$ GeV. The blue circles, green squares, and red diamonds correspond to $Max\{|R|\} < 2$, $2 < Max\{|R|\} < 5$, and $5 < Max\{|R|\} < 10$, respectively. The dashed line represents the experimental bound of $B(\mu \to e\gamma) < 1.2 \times 10^{-11}$.

The two most important neutrino sector quantities for $B(\mu \to e\gamma)$ are the structure of the R matrix and the value of M_{N_3}. The importance of both quantities can be seen in Fig. 5.6. In general, smaller neutrino Yukawa couplings lead to less lepton flavor mixing which is apparent from examining Eq. (5.8). In fact, the branching fraction will scale as $Y_\nu^4 \sim M_{N_3}^2$. Thus, given Eq. (5.5), it is not surprising that smaller components in the R matrix, and lower values of M_{N_3} lead to lower values of $B(\mu \to e\gamma)$. What is more interesting is the wide range of values of this branching fraction for a given fixed value of M_{N_3}. This indicates that certain textures of the neutrino Yukawa matrix can greatly reduce the amount of LFV. On account of these various sensitivities, it is difficult to demarcate a region of parameter space consistent with the LFV bounds other than by what we have illustrated in Fig. 5.6. Certain challenging sets of neutrino sector parameters require $M_{N_3} < 10^{10}$ GeV, while for other neutrino parameters the requirement can be weakened

to $M_{N_3} < 10^{13}$ GeV. More concrete constraints can be derived in certain limits, such as when the right-handed neutrinos are strongly hierarchical.

5.2 νHENS Leptogenesis with LFV Constraints

The primary motivation for heavy right-handed neutrinos is to explain the findings of neutrino oscillation experiments. However, heavy neutrinos also provide a mechanism to account for the baryon asymmetry, which is measured to be [95]

$$Y_B = \frac{n_B - n_{\overline{B}}}{s} = (8.7 \pm 0.3) \times 10^{-11}. \tag{5.21}$$

With heavy right-handed neutrinos, this baryon asymmetry can be generated through the process of leptogenesis [70, 71].

In the present section we investigate whether the HENS model with heavy right-handed neutrinos can explain the baryon asymmetry through *thermal* leptogenesis while still satisfying the constraints on the model from LFV discussed above. To be concrete, we focus on two particular points in the HENS parameter space. For these points, we study many different structures of the neutrino sector, with the one simplifying assumption of slightly hierarchical right-handed neutrino masses with $M_{N_1} \lesssim M_{N_{2,3}}/3$. We will refer to the two HENS model parameter sets as points A and B. Both points have $\tan\beta = 10$, $M_{1/2} = 300$ GeV, and $sgn(\mu) > 0$. For point A, the Higgs sector parameters at the input scale are $m^2_{H_u} = -(668)^2\,\text{GeV}^2$ and $m^2_{H_d} = -(511)^2\,\text{GeV}^2$. The corresponding input values for point B are $m^2_{H_u} = -(100)^2\,\text{GeV}^2$, $m^2_{H_d} = -(359)^2\,\text{GeV}^2$. The resulting low-energy spectra for these two points are phenomenologically consistent, aside from LFV constraints. We list their mass spectra in Appendix C. The crucial difference between the two parameter points is that the input value of $m^2_{H_u}$ is much larger for point A than for point B.

5.2.1 The Three Conditions for Baryogenesis

There are three necessary conditions for baryogenesis known as the Sakharov conditions [74, 96]. The first, and most obvious, is that there must be baryon number violation $\Delta B \neq 0$. Without baryon number violating interactions, it is impossible for the universe to start with $B = 0$ and evolve to a state with $B \neq 0$.

A second condition for baryogenesis is C (charge) and CP (charge parity) violation. Because the baryon asymmetry is contained mostly in protons which are charged, the universe was either initially charged or C is not conserved. An initially charged universe could accommodate but never fully explain the baryon asymmetry. Thus, it is usually assumed, and we will assume it here, that the universe was initially neutral and through charge violating interactions became charged. Otherwise, the universe which was originally neutral could never evolve to a state with an excess of protons. If the CP symmetry was not broken, matter and anti-matter would couple identically. If they couple identically, the evolution of the universe would be symmetrical in matter and anti-matter, producing no baryon asymmetry. Explicitly what this means is that the time evolution operator of the universe does not commute with the C and CP operators. The evolution of the state vector of the universe is as follows

$$|\phi(t)\rangle = e^{iHt}|\phi_0\rangle. \tag{5.22}$$

If $[C, H] = [CP, H] = 0$, the universe would still be an eigenstate of C and CP and no baryon asymmetry would exist.

The last needed condition is non-equilibrium. If the universe remains in equilibrium, chemical and thermal, all chemical potentials will be zero throughout the evolution of the universe. The difference in the number density of particles and their anti-particle, when in thermal equilibrium, can be written as[96]

$$n_X - n_{\bar{X}} = \begin{cases} \frac{g_X T^3}{6\pi^2}\left[\pi^2\left(\frac{\mu_X}{T}\right) + \left(\frac{\mu}{T}\right)^3\right] & (T \gg m_X) \\ 2g_X\left(\frac{m_X T}{2\pi}\right)^2 \sinh\left(\frac{\mu_X}{T}\right)\exp\left(-\frac{m_X}{T}\right) & (T \ll m_X) \end{cases} . \tag{5.23}$$

From this equation, it is clear that if the universe remains in chemical equilibrium, $\mu_X = 0$, no particle anti-particle asymmetry can be produced.

5.2.2 Baryogenesis from Leptogenesis

By introducing right-handed neutrinos to the SM, all the necessary elements for baryogenesis are present. The decay of right handed neutrinos violate C and CP, and the expanding universe produces non-equilibrium. The baryon violation is through the sphaleron which converts leptons into baryons. To get a better understanding of these features of leptogenesis, we will include further explanation.

The $U(1)$ global symmetries of the SM are baryon and lepton number conservation. It is the anomalous behavior of these global symmetries that lead to baryon number violation. These $U(1)$ transformations lead to a non-trivial Jacobian in the functional integral. Unless the sum of all the anomalies cancel, these symmetries will not be conserved. Because the anomalies of the combination $B - L$ cancel, baryon number and lepton number can only be violated in the combination $B + L$. To understand this symmetry violation better[96], we consider the effect of a general chiral transformation

$$\psi \to e^{(a+b\gamma_5)\theta(x)}\psi. \tag{5.24}$$

Under this transformation, the variation of the action for a free massless fermion is

$$\delta S_0 = \int d^4x \left[\bar{\psi}\gamma^\mu(a + b\gamma_5)\psi\partial_\mu\theta(x)\right] = \int d^4x\theta(x)\partial_\mu\left(\bar{\psi}\gamma^\mu(a + b\gamma_5)\psi\right]. \tag{5.25}$$

If no other terms proportional to $\theta(x)$ were produced, the current ($J_\mu = \bar{\psi}\gamma_\mu\psi$) would be conserved and $\partial_\mu J^\mu = 0$. However, this rotation also produces a nontrivial Jacobian

that will contribute to the variation of the action. For vector like particles, the anomalous contribution to the action is

$$\delta S_{anomaly} = \int -\alpha(x)\frac{g^2}{16\pi}\epsilon^{\alpha\beta\mu\nu}F^{\alpha\beta}F_{\mu\nu}. \tag{5.26}$$

This anomalous contribution arises from the field transformation

$$\psi \rightarrow e^{i\alpha(x)\gamma_5}\psi = (1 + i\alpha(x)\gamma_5)\psi. \tag{5.27}$$

For chiral fields, this transformation is equivalent to the general transformation found in Eq. (5.24). This can be seen by considering the infinitesimal form of the transformation in Eq. (5.24)

$$e^{ia}(1+\gamma_5) = (1+a)(1+\gamma_5) = (1+a\gamma_5)(1+\gamma_5) = e^{ia\gamma_5}(1+\gamma_5), \tag{5.28}$$

$$e^{ia}(1-\gamma_5) = (1+a)(1-\gamma_5) = (1-a\gamma_5)(1-\gamma_5) = e^{-ia\gamma_5}(1-\gamma_5). \tag{5.29}$$

The generalized transformation in Eq. (5.24) becomes

$$\begin{aligned} \psi_L &\rightarrow e^{-(a-b)\gamma_5\theta(x)}\psi_L, \\ \psi_R &\rightarrow e^{(a+b)\gamma_5\theta(x)}\psi_R. \end{aligned} \tag{5.30}$$

Because this generalized transformation on chiral fields is equivalent to the transformation in Eq. (5.27) for vector fields, the anomaly for each chiral field will be equivalent to that for the vector field with the modification to the coefficients as found in Eq. (5.30). The anomalous contribution to the action from the transformation in Eq. (5.24) is then

$$\begin{aligned} \delta S_{anomaly} = \int d^4x\theta(x)\frac{1}{16\pi^2}[&(a+b)(g_1^2Y^2\epsilon^{\alpha\beta\mu\nu}F^{hy}_{\alpha\beta}F^{hy}_{\mu\nu}) \\ &-(a-b)(g_1^2Y^2\epsilon^{\alpha\beta\mu\nu}F^{hy}_{\alpha\beta}F^{hy}_{\mu\nu} + \epsilon^{\alpha\beta\mu\nu}F^{weak}_{\alpha\beta}F^{weak}_{\mu\nu})]. \end{aligned} \tag{5.31}$$

To have a stationary action, the coefficient of $\theta(x)$ must vanish. This gives the equation of current conservation

$$\partial_\mu\left(\bar{\psi}\gamma^\mu(a+b\gamma_5)\psi\right) = \frac{a-b}{8\pi^2}Tr\widetilde{F}^{(L)\mu\nu}F^{(L)}_{\mu\nu} + \frac{a+b}{8\pi^2}Tr\widetilde{F}^{(R)\mu\nu}F^{(R)}_{\mu\nu}, \tag{5.32}$$

where the gauge coupling has been absorbed into the definition of $F_{\mu\nu}$ and $\widetilde{F}^{\mu\nu} = 1/2\epsilon^{\mu\nu\alpha\beta}F_{\alpha\beta}$. To identify these symmetry transformations with baryon number or lepton number violation, we can chose a and b accordingly. Substituting $a = 1/3$ into the previous expression, it corresponds to a baryon number violation. This gives the following relation for the baryonic current, $J_B^\mu = 1/3\sum \bar{q}\gamma^\mu q$,

$$\partial_\mu J_B^\mu = i\frac{N_f}{32\pi^2}(-g_2^2 F^{a\mu\nu}\tilde{F}^a_{\mu\nu} + g_1^2 f^{\mu\nu}\tilde{f}_{\mu\nu}). \tag{5.33}$$

If $a = 1$, we have the equation for the lepton number anomalous current, $J_L = \sum(\bar{l}\gamma^\mu l + \bar{\nu}\gamma^\mu\nu)$, which is related to the baryonic current as follows

$$\partial_\mu J_B^\mu = \partial_\mu J_L^\mu. \tag{5.34}$$

This relation is the reason that all the anomalies of the SM cancel. This equivalence also preserves the $B - L$ symmetry in the SM, but says nothing about the $B + L$ symmetry. If these equations have a background field solution with a non-zero value of $\int d^4x\partial_\mu J^\mu_{B,L}$, baryon number and lepton number will be violated while the combination $B - L$ will be preserved. Manipulating the right side of Eq. (5.33) [96], we find

$$\partial_\mu J_B^\mu = i\frac{N_f}{32\pi^2}(-g_2^2\partial_\mu K^\mu + -g_1^2\partial_\mu k^\mu) \tag{5.35}$$

where

$$K^\mu = 2\epsilon^{\mu\nu\alpha\beta}(\partial_\nu A^a_\alpha A^a_\beta - \frac{1}{3}g_2\epsilon_{abc}A^a_\nu A^c_\alpha A^c_\beta) \tag{5.36}$$

$$k^\mu = 2\epsilon^{\mu\nu\alpha\beta}(\partial_\nu B_\alpha B_\beta). \tag{5.37}$$

If either of these fields, k^μ or K^μ, have non-zero surface terms $\int dx^4\partial_\mu J^\mu_{B,L} \neq 0$, there will be baryon number and lepton number violation. The operator that arises from this non-perturbative effect is[97]

$$O_{B+L} = \prod_{i=1}^{3} q_{L_i}q_{L_i}q_{L_i}l_{L_i}, \tag{5.38}$$

and leads to interactions that can convert leptons to baryons and give the baryon asymmetry.

To take advantage of the the sphaleron which converts leptons to baryons, we need to create an excess of leptons. This can be done when right handed neutrinos are introduced to the SM. Because the right-handed neutrinos are singlets under the gauge groups of the SM, they can have a Majorana mass term. With this Majorana mass term, a fairly generic neutrino sector can be written as

$$W_N = NY_\nu LH_u + \frac{1}{2}NM_N N. \tag{5.39}$$

The Majorana mass matrix can be diagonalized by a field redefinition of N. The neutrino Yukawa coupling, on the other hand, can only be simplified by the neutrino fields absorbing three phases. This leaves 9 real parameters and 6 phases in the Yukawa matrices. These phases will lead to a difference in the interactions of neutrinos and anti-neutrinos. This can be seen from considering a simple Lagrangian,

$$\mathcal{L} = y\phi\bar{\phi}_1\phi_2 + y^*\phi^*\bar{\phi}_2\phi_1, \tag{5.40}$$

where the first operator is an interaction for particles and the second is for anti-particles. The CP operation on the above Lagrangian essentially interchanges the two operators but not the couplings. In order for the Lagrangian to be CP invariant, the coupling y must be real. If CP is violated and y is complex, the coupling of the fermions and anti-fermions are different. The phases in the Yukawa matrix, which controls how large the complex part is, give different couplings for neutrinos and anti-neutrinos. These different couplings make it possible to produce a lepton asymmetry.

Thermal non-equilibrium is a consequence of the expanding universe. To maintain

equilibrium, the particles must be able to react faster than the expansion of the universe moves them away from each other. From this it may not seem to be difficult to maintain equilibrium, but the expanding universe also affects the number density. When the temperature drops below the mass of a given particle, the equilibrium number density becomes exponentially suppressed as follows

$$n_X^{EQ} = g_X \left(\frac{m_X T}{2\pi}\right)^{\frac{3}{2}} \exp\left(-\frac{m_X}{T}\right). \tag{5.41}$$

In order for particle X to maintain equilibrium, the number density of a particle X must decrease very quickly in order to keep up with the exponentially decreasing equilibrium number density. Because the reactions of the particles are unable to do this, the universe departs from equilibrium.

5.2.3 νHENS Leptongenesis

We use the results of Ref. [98] to compute the baryon density due to thermal leptogenesis in the HENS model, which does not differ significantly from the story for other supersymmetric models. In our analysis, we take into account *flavor effects* [98, 99, 100, 101, 102] arising from interactions of the charged Yukawa couplings. In the calculation of the baryon asymmetry produced from the N_1 decay, there are two important parameters: the CP and L asymmetry ϵ_α and the effective neutrino mass $\tilde{m}_\alpha$ for each lepton flavor $\alpha = e, \mu, \tau$. In the limit of $M_{N_1} \ll M_{N_{2,3}}$, they are given by

$$\epsilon_\alpha \simeq -\frac{3M_{N_1}}{16\pi v_u^2} \frac{\mathbf{Im}\left[\sum_{i,j} m_i^{1/2} m_j^{3/2} U_{\alpha i}^* U_{\alpha j} R_{1i} R_{1j}\right]}{\sum_k m_k |R_{1k}|^2}, \tag{5.42}$$

$$\widetilde{m}_\alpha \equiv \frac{|Y_{\nu 1\alpha}|^2 v_u^2}{M_{N_1}} = \left|\sum_k R_{1k} m_k^{1/2} U_{\alpha k}^*\right|^2. \tag{5.43}$$

Now for $(1+\tan^2\beta)\,10^9\,\mathrm{GeV} \lesssim M_{N_1} \lesssim (1+\tan^2\beta)\,10^{12}\,\mathrm{GeV}$, the two-lepton flavor approximation is appropriate and the resulting baryon density is [98]

$$Y_B \simeq -\frac{10}{31 g_*}\left[\epsilon_2\eta\left(\frac{541}{761}\widetilde{m}_2\right)+\epsilon_\tau\eta\left(\frac{494}{761}\widetilde{m}_\tau\right)\right]. \tag{5.44}$$

In this expression, g_* is the usual number of relativistic degrees of freedom, and $\widetilde{m}_2 \equiv \widetilde{m}_e + \widetilde{m}_\mu$ and $\epsilon_2 \equiv \epsilon_e + \epsilon_\mu$.

For lighter right-handed neutrino states, in the range $(1+\tan^2\beta)10^5 \lesssim M_{N_1} \lesssim (1+\tan^2\beta)10^9$, we must account for all three lepton flavors. The appropriate expression for the final baryon asymmetry in this case is

$$Y_B \simeq -\frac{10}{31 g_*}\left[\epsilon_e\eta\left(\frac{93}{110}\widetilde{m}_e\right)+\epsilon_\mu\eta\left(\frac{19}{30}\widetilde{m}_\mu\right)+\epsilon_\tau\eta\left(\frac{19}{30}\widetilde{m}_\tau\right)\right]. \tag{5.45}$$

In the above equations, the parameter η is the *washout parameter* which is given by

$$\eta(\widetilde{m}_l) = \left[\left(\frac{\widetilde{m}_l}{8.25\times10^{-3}eV}\right)^{-1}+\left(\frac{0.2\times10^{-3}eV}{\widetilde{m}_l}\right)^{-1.16}\right]^{-1}. \tag{5.46}$$

Motivated both by the apparent hierarchy of light neutrino masses and the desire to reduce the amount of washout of the lepton asymmetry generated by heavy neutrino decays, we will focus on mildly hierarchical right-handed neutrino masses, with $M_{N_1} < M_{N_{2,3}}/3$. Within this mild hierarchy, the washout of $M_{N_{2,3}}$ have no effect on the asymmetry produced from N_1 interactions. It also allows us to use the well accepted N_1 dominated scenario of leptogenesis, even in the flavored case. Recently, this scheme was called into question by [103]. In this work they considered flavor dependent leptogenesis, but only considered decays and $\Delta L = 2$ scattering. With this scenario, the washout of the lepton asymmetry produced by N_2 from inverse decays of N_1 is suppressed by a projection operator $P_{i\alpha} = \Gamma_{i\alpha}/\Gamma_i = |Y_{\nu i\alpha}|^2/(Y_\nu Y_\nu^\dagger)_{ii}$. Because of this projection operator, the asymmetry in N_2 is not always completely washed out like it is in the single flavor case. However, the washout from interactions like $Q_t t \leftrightarrow \ell_\alpha N_1$ on the asymmetry produced by N_2 was never considered. In

the regime of $M_{N_2} > 3M_{N_1}$ this washout can have a significant effect on lepton asymmetry making it difficult for any asymmetry produced by N_2 to survive. However, we have also checked that using the approximation found in [103] still gives nearly identical result as we have here. The reason for this is that the important interplay here is between the lower mass bound set by leptogenesis and the upper bound set by FCNC. Even if N_2 decays completely account for the baryon asymmetry, they can only do so if they have a large enough mass. In [103] they found that $M_{N_2} \gtrsim 10^{11}\,\text{GeV}$. Including $Q_t t \leftrightarrow \ell_\alpha N_1$ can only push up this lower bound on mass scale. With the mild hierarchy we have chosen, M_{N_2} can be pushed below this lower bound with the BAU coming from N_1 interactions. In this N_1 dominated scenario, the lower bound on M_{N_2} comes from the leptogenesis bounds on $M_{N_1} \gtrsim 10^{10}$ which gives $M_{N_2} \gtrsim 3 \times 10^{10}$. With or without N_2 interactions being relevant, the smallest M_{N_2} that will give an acceptable BAU comes from N_1 dominated scenario.

In Fig. 5.7 we show the baryon density due to leptogenesis in the HENS model with heavy right-handed neutrinos as a function of the lightest heavy neutrino mass M_{N_1}. The neutrino sector parameters were scanned over, with the blue circles, green squares, and red diamonds corresponding to $Max\{|R|\} < 2$, $2 < Max\{|R|\} < 5$, and $5 < Max\{|R|\} < 10$, respectively. The HENS model parameters were set to $M_{1/2} = 300$ GeV, $\tan\beta = 10$, $m^2_{H_u} = -(668\text{ GeV})^2$, and $m^2_{H_d} = -(511\text{ GeV})^2$, although the resulting baryon asymmetry is fairly independent of these values. The corresponding superpartner spectrum is phenomenologically acceptable aside from LFV constraints. We will impose these constraints in the next section.

Fig. 5.7 illustrates the well-known lower bound on M_{N_1} if thermal leptogenesis is to be the source of the baryon asymmetry of the universe. The minimal value of M_{N_1} that works is on the order of 10^{10} GeV, which is consistent with the results of Refs. [104, 105, 106]. This plot also shows that the final baryon asymmetry is reduced as the magnitudes of the

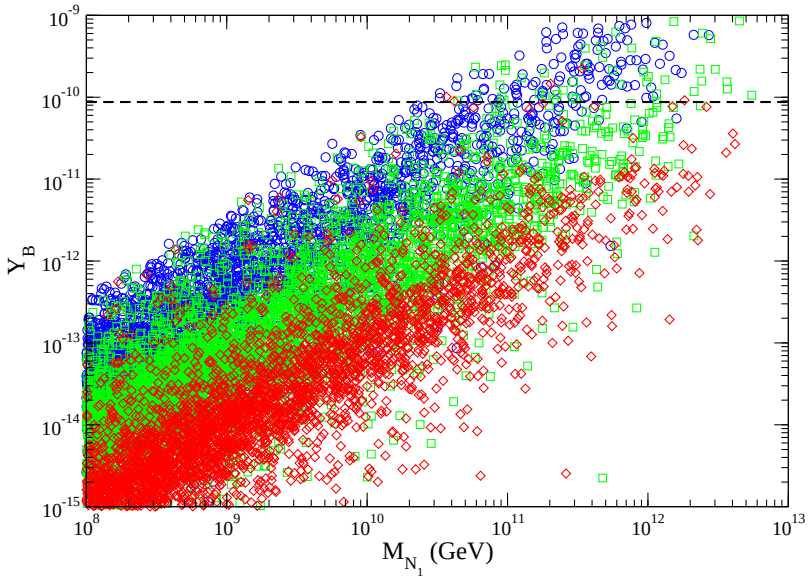

Figure 5.7: Baryon density due to leptogenesis in the HENS model as a function of M_{N_1}. The HENS model parameter were set to $m^2_{H_u} = -(668)^2\,\mathrm{GeV}^2$, $m^2_{H_d} = -(511)^2\,\mathrm{GeV}^2$, $\tan\beta = 10$, and $M_{1/2} = 300$ GeV, and the neutrino sector parameters were scanned over. The blue circles, green squares, and red diamonds correspond to $Max\{|R|\} < 2$, $2 < Max\{|R|\} < 5$, and $5 < Max\{|R|\} < 10$, respectively. The dashed line represents the measured baryon density $Y_B = (8.7 \pm 0.3) \times 10^{-11}$.

entries in the R matrix become larger. The reason for this is that larger values of $|R_{ij}|$ increase the amount of washout. In the strong washout regime, which we find to be the case throughout much of the relevant parameter space, the lepton asymmetry produced in right-handed neutrino decays is thereby greatly diluted. To obtain a sufficiently large lepton asymmetry to explain the baryon excess in this regime, M_{N_1} must be larger than about 10^{10} GeV. This can make it difficult to avoid the experimental constraints on LFV, as we will discuss later.

Let us also make note of the fact that the lower bound on M_{N_1} of about 10^{10} GeV suggests that the reheating temperature after inflation was larger than this if thermal leptogenesis is to explain the baryon asymmetry. In supersymmetric models, such large reheating temperatures lead to the overproduction of gravitinos [107]. Within the HENS

model with an input scale on the order of M_{GUT} and an underlying gravity or gaugino mediation of supersymmetry breaking, we expect gravitino masses on the order of the weak scale [108]. Gravitinos of this mass decay during nucleosynthesis, and can ruin the ratios of the light element abundances for $T_{RH} \gtrsim 10^{7\pm1}$ GeV [109]. A couple of possible approaches to this problem are resonant enhancements of the lepton asymmetry as the heavy neutrinos become nearly degenerate that allow M_{N_1} to be lowered further [110, 111, 112, 113, 114], or the non-thermal production of heavy right-handed neutrinos after inflation [115, 116].

5.2.4 Simultaneous Constraints

In Section 5.1 we found that LFV constraints favor smaller values of M_{N_3}. On the other hand, thermal leptogenesis prefers larger values of $M_{N_1} < M_{N_3}$. The tension between these two requirements is illustrated in Fig. 5.8, where we plot points in the M_{N_3}-M_{N_1} plane that are consistent with LFV constraints, that generate enough of a baryon asymmetry through thermal leptogenesis, or that satisfy both conditions. The left-hand panel of this figure corresponds to point A described above, while the right-hand panel corresponds to point B. In both panels, we have scanned over heavy neutrino masses M_{N_i}, as well as the light neutrino masses and the values of the U and R mixing matrices subject to the constraints listed in Appendix B. The blue squares in the figure are points that obey the LFV constraints, the red circles are points that generate enough of a baryon excess, and the green diamonds satisfy both requirements.

Only a very small subset of the points in Fig. 5.8 for set A are consistent with both the LFV constraints and leptogenesis. This is primarily the result of the large value of $m^2_{H_u}$ for this parameter set, which leads to large LFV rates unless M_{N_3} is very small. This in turn pushes down the possible range of values of M_{N_1}, making leptogenesis less effective. Only for a small and special subset of the neutrino sector parameters can both requirements be met. We will discuss these requirements in more detail below. In contrast, there are many

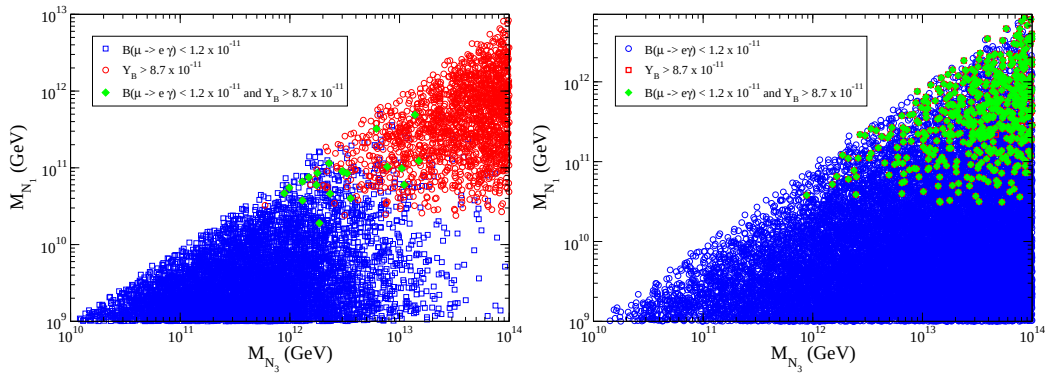

Figure 5.8: HENS parameter points in the M_{N_3}-M_{N_1} plane consistent with LFV constraints (blue squares), baryogenesis through thermal leptogenesis (red circles), or both simultaneously (green diamonds). The panel on the left (a) is for HENS parameter set A, with $M_{1/2} = 300\,\text{GeV}$, $\tan\beta = 10$, $m^2_{H_u} = -(668)^2\,\text{GeV}^2$, and $m^2_{H_d} = -(511)^2\,\text{GeV}^2$. The panel on the right (b) is for HENS parameter set B, with $M_{1/2} = 300\,\text{GeV}$, $\tan\beta = 10$, $m^2_{H_u} = -(100)^2\,\text{GeV}^2$, and $m^2_{H_d} = -(359)^2\,\text{GeV}^2$. In both plots we have scanned over neutrino sector parameters.

points for parameter set B for which both the LFV and leptogenesis constraints are met. Indeed, very few of the points that are consistent with generating the baryon asymmetry through leptogenesis do not satisfy the LFV constraints. This is due to the LFV constraints being very weak given the relatively small value of $m^2_{H_u}$ for this parameter set.

5.2.5 Neutrino Yukawa Matrix Structures

We found above that only a small subset of the neutrino sector parameters allowed for the HENS parameter set A to be consistent with the constraints from LFV while generating the baryon asymmetry via thermal leptogenesis. The combination of these two requirements selects a particular structure for the neutrino Yukawa matrix which we describe here. Due to the assumed hierarchy among the right-handed neutrinos, the Yukawa matrix will generally decrease in size from row three to row one. Thus, the leading contributions to the off-diagonal components of $m^2_{L_{ij}}$ responsible for LFV are typically

$$m^2_{\tilde{L}_{ij}} = -\frac{m^2_{H_u}}{8\pi^2}\left(Y^*_{\nu 3i} Y_{\nu 3j}\, t_3 + Y^*_{\nu 2i} Y_{\nu 2j}\, t_2\right), \tag{5.47}$$

where $t_i = \ln(M_{GUT}/M_{N_i})$. This feature selects out the $Y_{\nu 3i}$ and $Y_{\nu 2i}$ components of the neutrino Yukawa matrix as being particularly important.

In Fig. 5.9 we show the dependence of the LFV branching fraction $B(\mu \to e\gamma)$ on the $Y_{\nu 3i}$ and $Y_{\nu 2i}$ components of the neutrino Yukawa matrix for the HENS model parameter set A described above and in Appendix C. The points in this plot correspond to different values of the R and U matrix elements, and (hierarchical) right-handed neutrino masses. With the spectrum of parameter set A, the $\mu \to e\gamma$ branching fraction can be written as

$$B(\mu \to e\gamma) = (1400 \text{ GeV})^{-4} \, |m^2_{\tilde{L}_{21}}|^2. \tag{5.48}$$

With $M_{N_3} = 10^{11}\,\text{GeV}$, for example, this translates into a constraint on the Yukawa couplings of

$$Y^*_{\nu 32} Y_{\nu 31} + Y^*_{\nu 22} Y_{\nu 21} \frac{t_2}{t_3} < 9.6 \times 10^{-5} \tag{5.49}$$

where $t_i = \ln(M_{GUT}/M_{N_i})$. This constraint can be met in two different ways: both $|Y_{\nu 32}||Y_{\nu 31}|$ and $|Y_{\nu 22}||Y_{\nu 21}|$ can be separately very small, or $Y^*_{\nu 32} Y_{\nu 31}$ and $Y^*_{\nu 22} Y_{\nu 21}$ can cancel against each other. It is this cancellation that leads to the pointed structure in Fig. 5.9.

The constraints on the neutrino Yukawa couplings become even stronger when we demand successful leptogenesis as well. In Fig. 5.10 we show the equivalent plot to Fig. 5.9 for HENS parameter set A, but now restricted to points that are consistent with thermal leptogenesis. Clearly, larger values of the Yukawa couplings are required for successful leptogenesis. For these points to also be consistent with LFV constraints, there must be a significant cancellation between $Y^*_{\nu 32} Y_{\nu 31}$ and $Y^*_{\nu 22} Y_{\nu 21}$ to suppress $B(\mu \to e\gamma)$, as suggested by Eq. (5.49).

With the present sensitivities, the bounds on LFV in τ decays do not significantly constrain the allowed parameter space in this example. However, improved sensitivities

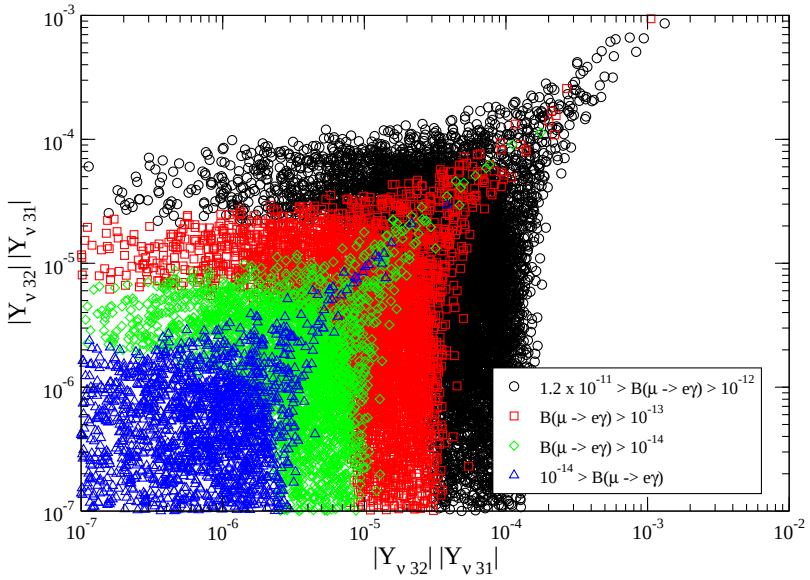

Figure 5.9: $B(\mu \to e\gamma)$ in the plane of $|Y_{\nu 32}||Y_{\nu 31}|$ and $|Y_{\nu 22}||Y_{\nu 21}|$ for the mass spectrum A in Appendix C, corresponding to HENS parameters $m^2_{H_u} = -(668)^2\,\mathrm{GeV}^2$, $m^2_{H_d} = -(511)^2\,\mathrm{GeV}^2$, $\tan\beta = 10$, and $M_{1/2} = 300\,\mathrm{GeV}$.

from current and future experiments could change this. To illustrate the effects of improved experimental bounds, we also draw a dashed contour in Fig. 5.10 corresponding to the parameter region that would be allowed with the stronger constraint $B(\tau \to \mu\gamma) < 10^{-10}$. The stronger bound on τ decays cuts of this pointed structure by placing an upper bound on the overall size of the neutrino Yukawa couplings. This can be understand by examining the off-diagonal component of the slepton mass matrix that governs these decays which correspond to taking $i = 3$ and $j = 2, 1$ in Eq. (5.47). Each one of these contains a linearly independent set of the neutrino Yukawa couplings. However, each component of the scalar mass matrices depends on a neutrino Yukawa coupling that is in the other components. Unless there is a miraculous tuning among the neutrino Yukawa couplings that suppresses more than one of the components of $m^2_{\tilde{L}_{ij}}$, a strong constraint on τ decays will place an upper bound on the size of the the neutrino Yukawa couplings. The points with large neutrino Yukawa coupling in Fig. 5.10 are then excluded. Such a level of sensitivity on τ

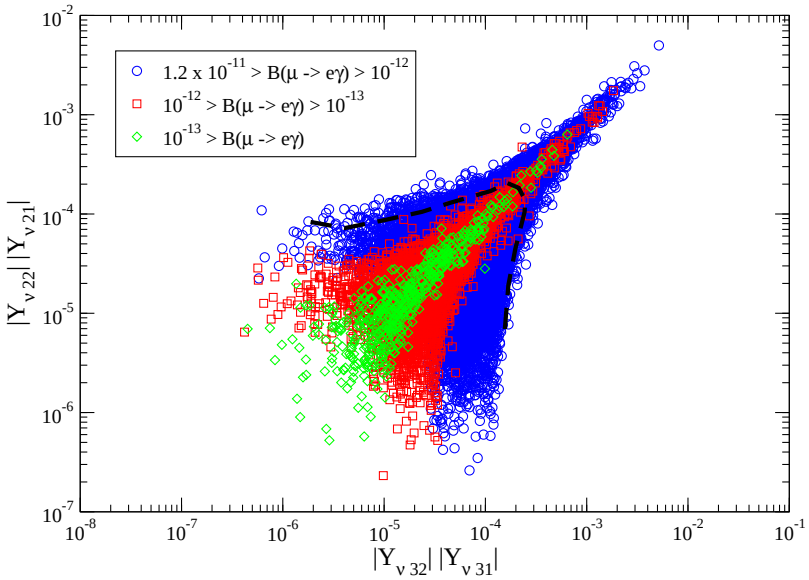

Figure 5.10: $B(\mu \to e\gamma)$ in the plane of $|Y_{\nu 32}||Y_{\nu 31}|$ and $|Y_{\nu 22}||Y_{\nu 21}|$ for the mass spectrum A in Appendix C. All points in this figure can account for the baryon asymmetry through thermal leptogenesis. The dashed line corresponds to the region that would still be allowed if the bound on $\tau \to \mu\gamma$ decay were improved to $B(\tau \to \mu\gamma) < 10^{-10}$.

decays could potentially be achieved by super B factories [118]. Improving $B(\mu \to e\gamma)$, on the other hand, forces more fine tuning among the different neutrino Yukawa matrix elements.

In Fig. 5.11 we show the allowed regions in the $|Y_{\nu\,32}||Y_{\nu\,31}|$ and $M_{N_{1,3}}$ planes for HENS parameter set A points requiring both consistency with the current LFV bounds as well as successful thermal leptogenesis. We have scanned over the neutrino sector parameters in the same way as in Fig. 5.10. In this plot we also show the regions of the parameter space that would be allowed if the bounds on LFV were improved to $B(\mu \to e\gamma) < 10^{-13}$ and $B(\tau \to \mu\gamma) < 10^{-10}$. As discussed above, strengthening the LFV bounds tends to push the allowed range of M_{N_3} to lower values making leptogenesis less effective.

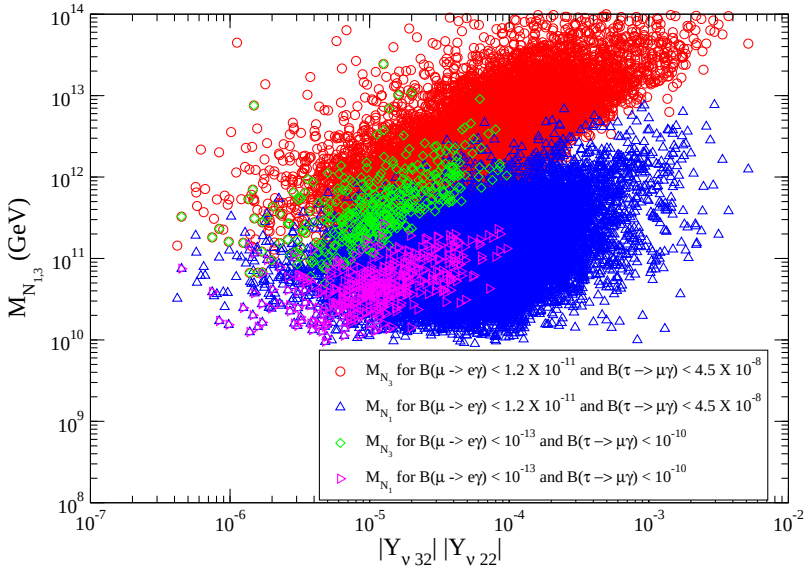

Figure 5.11: Allowed points subject to the constraints of LFV and thermal leptogenesis for the HENS model parameter set A. The points are plotted as $|Y_{\nu\,32}||Y_{\nu 31}|$ against either M_{N_1} or M_{N_3}, with the neutrino sector parameters scanned over.

CHAPTER VI

Vacuum Stability

While these HENS models are compelling, the tachyonic Higgs soft masses at the boundary scale lead to concerningly large tachyonic low-scale Higgs soft masses. These, combined with the small (but positive) slepton soft masses, suggest that the true vacuum of the theory might be a charge-and-color-breaking (CCB) minimum, or there may exist unbounded-from-below (UFB) directions that are only stabilized far out in field space by higher-dimensional operators [7, 8, 9, 10, 11, 12]. The presence of such features need not exclude these regions of the parameter space provided our SM electroweak vacuum is metastable and long-lived relative to the age of the universe.

In this section we study the vacuum structure of HENS models, and compute the lifetime of the SM vacuum state when it turns out to be metastable. We concentrate on the stability of the SM vacuum at zero temperature with respect to vacuum tunneling. Thermal effects in the early universe can also potentially induce thermal transitions between different vacua, and modify the shape of the potential itself. However, these thermal effects tend to stabilize the origin of the field space to which the SM vacuum is connected, favoring this vacuum over others that lie further out in the field space [120]. Thermal effects are especially effective in delaying the formation of vacua that break color due to the large thermal corrections from the strong gauge and top quark Yukawa couplings [11, 120, 121]. Scalar field evolution during and after inflation may also populate non-standard vacua,

although the precise result depends on the details of inflation and lies beyond the scope of this paper [12, 11]. By focusing solely on the $T = 0$ constraints we obtain conservative and unambiguous bounds on the HENS parameter space that do not depend on the cosmological history.

6.1 UFB Directions and CCB Minima in the HENS Model

With the HENS model input parameters of Eq. (1.10), relatively small slepton soft masses as well as large tachyonic Higgs soft masses obtain near the electroweak scale in much of the phenomenologically allowed parameter space [14]. This spectrum of soft parameters frequently implies the existence of UFB directions and CCB minima that are much deeper than the standard electroweak vacuum. Indeed, we find that nearly the entire allowed parameter space in the HENS model (before imposing vacuum stability constraints) has at least one UFB direction. We investigate the existence and nature of such potentially dangerous vacuum features in the present section.

Given the soft breaking spectrum that arises in the HENS scenario, the results of Ref. [9] suggest that the most dangerous vacuum feature will be a sleptonic UFB-3[9] direction. This direction has $H_d = 0$, with $\tilde{\tau}_L$, $\tilde{\tau}_R$, $\tilde{\nu}_{L_{i\neq 3}}$, and H_u^0 all non-zero. Turning on expectation values for these fields, there exists a D- and F-flat direction that is only lifted by quadratic supersymmetry breaking operators. To obtain F-flatness, only the F-term of H_d must be cancelled. This can be arranged by taking

$$|\tilde{\tau}| = |\tilde{\tau}_L| = |\tilde{\tau}_R| = \sqrt{\left|\frac{\mu}{y_\tau} H_u^0\right|}, \tag{6.1}$$

with the relative phase of $\tilde{\tau}_L$ and $\tilde{\tau}_R$ chosen appropriately. D-flatness is then obtained by setting

$$|\tilde{\nu}_{L_{i\neq 3}}|^2 = -\left(\frac{4\, m_{L_i}^2}{g^2 + g'^2}\right) + |\tilde{\tau}|^2 + |H_u^0|^2, \tag{6.2}$$

and represents the lowest-energy F-flat field configuration provided

$$|H_u^0| > \sqrt{\left|\frac{\mu}{2y_\tau}\right|^2 + \frac{4m_{L_i}^2}{(g^2+g'^2)}} - \left|\frac{\mu}{2y_\tau}\right|. \tag{6.3}$$

The scalar potential along this direction in field space then becomes [9]

$$V_{UFB-3} = (m_{H_u}^2 + m_{L_i}^2)|H_u^0|^2 + \left|\frac{\mu}{y_\tau}\right| (m_{L_3}^2 + m_{E_3}^2 + m_{L_i}^2)\,|H_u^0| - \frac{2m_{L_i}^4}{g^2+g'^2}. \tag{6.4}$$

When $(m_{H_u}^2 + m_{L_i}^2)$ is negative, the potential becomes unbounded in the limit $|H_u^0| \to \infty$. It will ultimately be stabilized by loop corrections or higher-dimensional operators (that we have not included in Eq. (6.4)) at a location that is very deep and far out in field space relative to the electroweak vacuum.

This sleptonic UFB-3 direction is particularly dangerous in the HENS models on account of the large and negative values of $m_{H_u}^2$ and the smaller values of $m_{L_i}^2$ and $m_{E_i}^2$ that emerge in the low-energy spectrum. These properties imply that the barrier against tunneling from the electroweak vacuum near the origin out to the deeper UFB-3 direction, arising from the linear term in $|H_u^0|$ in Eq. (6.4), will not be especially large. The barrier will be further weakened by larger values of $\tan\beta$ which enhance the coupling $y_\tau = m_\tau/v\cos\beta$. Other similar UFB-3 directions may be present in the theory, but they will generally have larger barriers due to the larger values of the squark soft masses or the smaller values of the first- and second-generation lepton Yukawa couplings.

When $|H_u^0|$ does not satisfy the bound given in Eq. (6.3), the lowest-energy F-flat direction in the potential has $|\tilde{\nu}_{L_i\neq 3}| = 0$, and is given by [9]

$$V_{UFB-3} = m_{H_u}^2|H_u^0|^2 + \left|\frac{\mu}{y_\tau}\right| (m_{\tilde{\tau}_L}^2 + m_{\tilde{\tau}_R}^2)|H_u^0| + \frac{1}{8}(g_1^2+g_2^2)\,\left(|H_u^0|^2 + \left|\frac{\mu}{y_\tau}\right| |H_u^0|\right)^2. \tag{6.5}$$

This potential is no longer D-flat, and is stabilized at a finite value of $|H_u^0|$. If this point occurs with $|H_u^0|$ less than the bound of Eq. (6.3), it is a constrained local CCB minimum. On the other hand, when this constrained local extremum has $|H_u^0|$ larger than the bound

of Eq. (6.3), it represents a saddle point that is unstable under flowing to a non-zero value of $|\tilde{\nu}_{L_{i\neq 3}}|$.

In practice, we find that for smaller values of $|H_u^0|$ the potential can be reduced further by relaxing the F-flatness constraint of Eq. (6.1). The effect of dropping the F-flatness constraint is that the minimal potential for a given value of $|H_u^0|$ is deformed slightly away from the precise UFB-3 form of Eqs. (6.4,6.5), but that the same qualitative features remain. In particular, there usually remains a local extremum at $|H_u^0| \neq 0$ and $|\tilde{\nu}_{L_{i\neq 3}}| = 0$. We shall designate this local extremum as CCB-4. If this extremum occurs at smaller values of $|H_u^0|$, on the order of the electroweak scale, it can be a local CCB minimum. When the CCB-4 extremum occurs with a value of $|H_u^0|$ much larger than the electroweak scale, it is generally a saddle point that flows in the $\tilde{\nu}_{L_{i\neq 3}}$ direction to a genuine UFB-3 direction of the form given in Eq. (6.4). Even when it is only a saddle, the CCB-4 point plays an important role in determining the tunneling rate from the electroweak minimum to the UFB-3 direction, as we will discuss below.

A stable CCB-4 minimum with stops can also arise for smaller values of $\tan\beta$ and a correspondingly larger y_t Yukawa coupling. In this case we have $H_u = 0$ while $|\tilde{t}_L| = |\tilde{t}_R| = |\tilde{t}|$ and H_d^0 are all non-zero. The relevant potential is

$$V_D = m_{H_d}^2 |H_d^0|^2 + (m_{\tilde{t}_L}^2 + m_{\tilde{t}_R}^2)|\tilde{t}|^2 + |\mu\, H_d - y_t \tilde{t}^2|^2 + \frac{g^2 + g'^2}{8}\left(|H_d|^2 + |\tilde{t}|^2\right)^2 . \tag{6.6}$$

This potential is generally stable against excursions in the $|\tilde{d}| = |\tilde{d}_{L_{i\neq 3}}| = |\tilde{d}_{R_{i\neq 3}}|$ direction on account of the larger squark soft masses that arise in the HENS model. With $m_{H_d}^2 < 0$ at the low scale, this potential often has a CCB-4 minimum with both $|H_d^0|$ and $|\tilde{t}|$ non-zero. However, as we show below, the barrier to tunneling to this minimum from the standard electroweak minimum to this CCB-4 minimum is usually safely large, again on account of the larger values of the squark soft masses as well as the less negative values of $m_{H_d}^2$. For similar reasons, we expect that the rate for tunneling to the other potential CCB minima

discussed in Ref. [9] will typically be less constraining than the rate to tunnel to a stau UFB-3 direction.

6.2 Computing the Vacuum tunneling Rate

The existence of vacua deeper than the standard electroweak minimum in HENS models implies there is a danger of tunneling into one of these phenomenologically unacceptable states. At the very least, the lifetime for this tunneling must be greater than the age of the universe. The vacuum-to-vacuum transition rate associated with tunneling can be calculated using path integral methods [127, 128]. In the semiclassical approximation, the lifetime of the vacuum is found to be

$$\frac{1}{\tau V} = \Gamma/V = Ae^{-S_b[\bar{\phi}]} \tag{6.7}$$

where A is a dimension-four prefactor to be discussed below, $\bar{\phi}_i$ denotes the *bounce solution* for the *i-th* field, and S_b is the Euclidean action,

$$S_b[\bar{\phi}] = \int d^4x_E \left(\left|\nabla\bar{\phi}_i\right|^2 + U(\bar{\phi}_1, ..., \bar{\phi}_i) \right) = T[\bar{\phi}_i] + V[\bar{\phi}_i]. \tag{6.8}$$

The *bounce solution* for the fields $\bar{\phi}_i$ is the extremum of the Euclidean action that is $O(4)$-symmetric and obeys the the following boundary conditions:

$$\frac{d\bar{\phi}_i(0)}{d\rho} = 0 \tag{6.9}$$

$$\lim_{\rho\to\infty} \bar{\phi}_i(\rho) = \phi_i^{SM} \tag{6.10}$$

where $\rho = (\vec{x}^2 + t_E^2)^{1/2}$ is the Euclidean distance. These boundary conditions correspond to a field that begins in a metastable vacuum and tunnels through a barrier separating it from a deeper vacuum state, emerging with zero kinetic energy. We focus on $O(4)$ symmetric solutions because these are expected to have the least action, and therefore dominate the tunneling probability [129].

Even with the simplification of an $O(4)$ symmetry, the equation of motion for the bounce cannot in general be solved analytically. We compute the bounce solution numerically using the *improved action method* [130]. The details of this method will be discussed below. Even more difficult to compute is the non-exponential pre-factor A in Eq. (6.7) [128]. On general grounds, we expect it to be on the order of the mass scale setting the size of the potential barrier. In low-energy supersymmetry, a good estimate for this number is $(100\,\mathrm{GeV})^4$, which we take to be the case throughout the rest of this article. The precise value of this pre-factor is unlikely to affect our qualitative conclusions as the multiplicative uncertainty in its value is much more slowly-varying than the exponentiated large values of the action that lead to acceptable lifetimes. Our choice for the pre-factor is also conservative, in that choosing a larger number here would only exclude more points. With this pre-factor, it is found that the lifetime of the SM vacuum will be greater than the age of the universe, $1/(\Gamma/V) \gtrsim t_0^4$, provided $S_b[\bar{\phi}] > 400$.

The value of the bounce action for tunneling between a pair of local vacua depends on the relative depth of the minima, the number of distinct minima, the height of the barriers between them, and the relative size of the field values within them. In general, the bounce solution represents a configuration of fields that simultaneously minimizes these opposing contributions, with the kinetic term favoring slowly varying fields, and the potential term preferring to reach the deepest minimum as quickly as possible.

As expected, our analytic tunneling solution shows that the bounce action increases with the size of the barrier. This solution also implies that the depth of the minimum to which one is tunneling to ceases to matter once it becomes very deep. Thus, we can safely compute the rate to tunnel into a UFB-3 direction without knowing where it is ultimately stabilized provided the corresponding minimum is very deep relative to the height of the barrier. On the other hand, the relative depth of the minima is relevant to the tunneling rate

when they are nearly degenerate, as can be seen from the analytic *thin-wall* approximate solution that can be safely applied in this case [127]. One important feature not captured by our one-dimensional analytic tunneling solution is that the bounce action tends to also increase when there are more independent fields involved in the tunneling process, as each one of them contributes non-negatively to the kinetic portion of the bounce action. For these reasons, numerical solutions are used to get the details correct.

6.2.1 The Improved Action Method

The bounce action is a stationary point of the Euclidean action given in Eq. (6.8) subject to the boundary conditions of Eqs. (6.9,6.10). The corresponding equations of motion for the $O(4)$ symmetric solution are

$$\frac{d^2\bar{\phi}_i}{d\rho^2} + \frac{3}{\rho}\frac{d\bar{\phi}_i}{d\rho} = \frac{\partial}{\partial\bar{\phi}_i}U(\bar{\phi}_i). \tag{6.11}$$

where i runs over the independent fields. These equations are a set of non-linear coupled differential equations with an *a priori* unknown starting point. These conditions together make it a very difficult problem to solve and require numerical techniques [8, 130, 131].

The technique we use in the present work is called the *improved action method* [130]. In this method, additional terms are added to the action that are identically zero for the bounce solution. The advantage of adding these terms is that they make the bounce solution a minimum of this modified action and not just an extremum. The term that does this is found by making the change of variable $x \to \sigma x$ in Eq. (6.8). Because the bounce is the extremum of the action, the first derivative of the scaled action with respect to σ will be zero for $\sigma = 1$. This gives the following condition:

$$\left(\sigma^2 T[\bar{\phi}_i] + 2\sigma^4 U[\bar{\phi}_i]\right)|_{\sigma=1} = 0 \tag{6.12}$$

This relation illustrates that the potential term must be negative. The kinetic term cannot be negative because it is the integral of a sum of squares. Since the potential term scales

as σ^4 and the kinetic term scales as σ^2, Eq. (6.12) defines a maximum. Thus, we have determined the maximal direction of the saddle point. By adding to the action the absolute value of this quantity to a positive power, the saddle point of the action can be turned into a minimum. In this case the improved action is

$$S[\bar{\phi}_i] = T[\bar{\phi}_i] + U[\bar{\phi}_i] + \lambda \left| T[\bar{\phi}_i] + 2U[\bar{\phi}_i] \right|^n \tag{6.13}$$

where λ and n are positive constants.

To solve for the bounce with this improved action, we take an initial profile for the vevs ϕ_i with the kinetic and potential terms

$$T[\phi_i] = 2\pi^2 \Delta^4 \sum_{m=1}^{L-1} (\rho_{m+1} - \rho_m) \rho_m^3 \left[\sum_i^n \frac{(\phi_i^{m+1} - \phi_i^m)^2}{2(\rho_{m+1} - \rho_m)^2 \Delta^2} \right] \tag{6.14}$$

$$U[\phi_i] = 2\pi^2 \Delta^4 \sum_{m=1}^{L-1} (\rho_{m+1} - \rho_m) \rho_m^3 U(\phi_1^m, ..., \phi_n^m). \tag{6.15}$$

Δ is a parameter determined by Eq. (6.12). Inspired by the thin-wall approximation, we take the following initial guess for the bounce solution

$$\phi(\rho) = a \tanh(b(\rho - \rho_0)) + c. \tag{6.16}$$

The coefficients a and c can be solved for by applying the boundary conditions $\phi(0) = \phi_e$ and $\phi(\infty) = \phi_f$, where ϕ_f are the field values in the SM minimum and ϕ_e are the values in the vacuum to which the tunneling connects. Since ϕ_e is *a priori* unknown, this leaves ϕ_e, b, and ρ_0 as free parameters. These parameters are determined by first substituting the field profile in Eq. (6.16) into the modified action for each ϕ_i.

The ϕ_e will not in general be the field configuration of the minima, but rather some field points inside the well. In the case of a UFB-3 direction there is no minimum, and ϕ_e will be some point on the runaway downslope with a potential energy less than that at SM minimum. The exact value of ϕ_e as well as b and ρ_0 are determined using a minimization routine that finds the coefficients that minimize the modified action. In Ref. [11] the

authors used the thick-wall approximation as an initial guess. In our case, the guess given in Eq. (6.12) works better numerically because it is adaptable to both thick- and thin-wall potential profiles. Once the initial profile, coefficients and all, is determined, we randomly vary each lattice site. The variations are stopped when further iterations do not reduce the modified action. To ensure that we arrive at the bounce solution, we choose a value of λ that ensures $0.999 < (-T[\phi_i]/2/V[\phi_i])^{1/2} < 1.001$. The smallest value of λ able to maintain this condition and used to optimize the code was close to 0.5 with $n = 1$.

6.3 Vacuum Stability Bounds on the HENS Parameters

The possibility of tunneling from the SM vacuum to a phenomenologically unacceptable vacuum places strong constraints on the parameter space of the HENS model. To investigate these constraints, we have calculated the bounce action for tunneling to a CCB-4 minimum or a UFB-3 direction for a series of representative HENS parameter sets. Our strategy is to fix $m_{1/2}$ and $\tan\beta$, and scan over the input values of $m^2_{H_u}(M_c)$ and $m^2_{H_d}(M_c)$ that lead to an acceptable low energy spectrum. We focus on the values $m_{1/2} = 500, 1000\,\text{GeV}$ for $\tan\beta = 30$ and $m_{1/2} = 300, 500\,\text{GeV}$ for $\tan\beta = 10$. In each of these scans we have consider points that meet the phenomenological constraints laid out in Ref. [14], including the current LEP lower bounds on the lightest Higgs boson. We also keep the points with a charged slepton as the lightest MSSM superpartner found in Ref. [14], noting that they would require a more complicated cosmology and likely R-parity violation or a gravitino LSP [126]. By keeping such points, our results are also applicable to minimal gaugino mediation subject to our assumptions about the gaugino masses and the input (compactification) scale.

We first consider the cases with $\tan\beta = 30$, where the tau Yukawa coupling is enhanced. This has the effect of opening up a CCB-4 minimum or CCB-4-like saddle point that flows to a UFB-3 direction. In Fig. 6.1 we show ranges of the bounce action for tunneling out

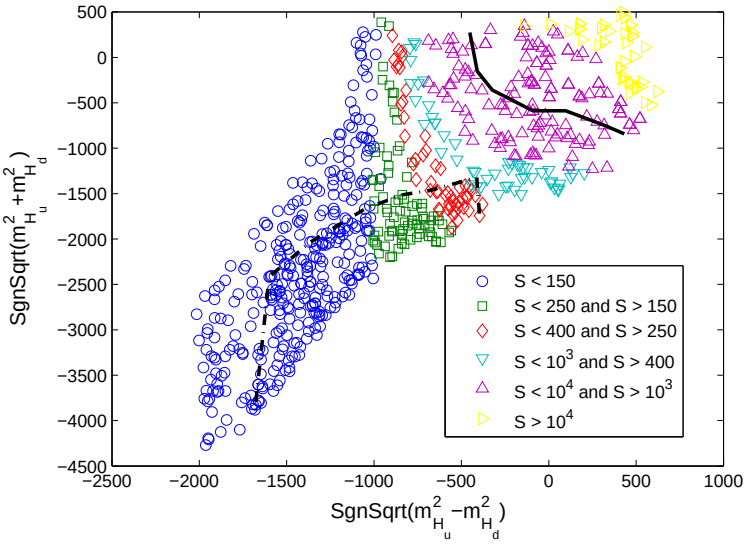

Figure 6.1: The bounce action for tunneling to a stau UFB-3 direction or a CCB-4 minimum as a function of the HENS model high scale input parameters $m^2_{H_u}(M_c)$ and $m^2_{H_d}(M_c)$ for $m_{1/2} = 500$ GeV and $\tan\beta = 30$. All points shown are consistent with collider phenomenology. The points enclosed below by the dash-dot line have a neutralino LSP. The solid line separates the region with a CCB-4 minimum or saddle point (left) from that which only has a UFB-3 (right). $S > 400$ is cosmologically safe.

of the SM vacuum to a CCB-4 minimum or a UFB-3 direction for $m_{1/2} = 500$ GeV as a function of the input values of $m^2_{H_u}(M_c)$ and $m^2_{H_d}(M_c)$. All points to the left of the solid line in this figure have either a CCB-4 minimum or saddle point. The points to the right have either a stable SM vacuum or a UFB-3 direction with no CCB-4 stationary point. To the left and the right of the solid line we show the bounce action for tunneling along the direction leading to the CCB-4 stationary point or to the UFB-3 direction, whichever is smaller.[1] We emphasize the CCB-4 stationary point here, even when it is only a saddle point, because we find that the most dangerous lowest-action tunneling path from the electroweak minimum is typically one that passes near this point with $\tilde{\nu}_{L_{i\neq 3}} = 0$. The dot-dashed line in Fig. 6.1 indicates the upper border of the portion of parameter space in which the LSP is the lightest neutralino. (See Ref. [14] for more details.). In Fig. 6.2 we

[1]Except for those points very near the solid line, the CCB-4 extremum is a saddle point flowing to the UFB-3 direction.

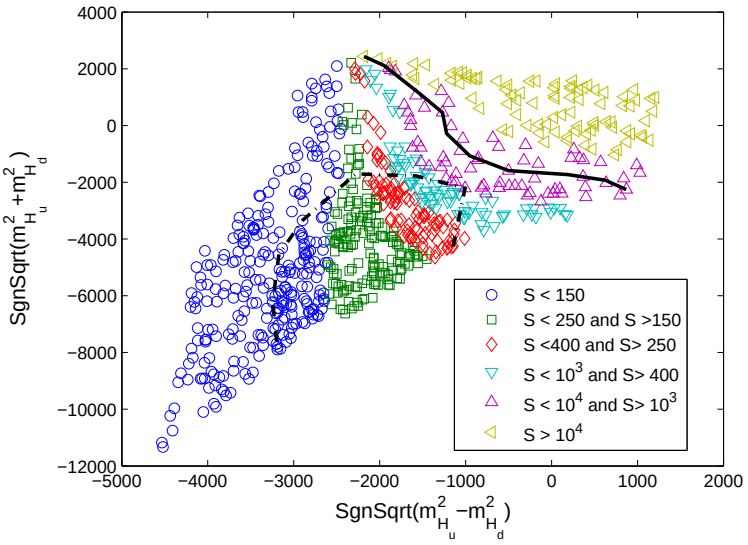

Figure 6.2: The bounce action for tunneling to a stau UFB-3 direction or a CCB-4 minimum as a function of the high-scale HENS model input parameters $m^2_{H_u}(M_c)$ and $m^2_{H_d}(M_c)$ for $m_{1/2} = 1000\,\text{GeV}$, $\tan\beta = 30$ and $sgn(\mu) = 1$. All points shown are consistent with collider phenomenology. The points enclosed below by the dash-dot line have a neutralino LSP. The solid line separates the region with a CCB-4 minimum or saddle point (left) from that which only has a UFB-3 direction. $S > 400$ is cosmologically safe.

show the same quantities as in Fig. 6.1 for $m_{1/2} = 1000$ GeV.

Both Fig. 6.1 and Fig. 6.2 show that for $\tan\beta = 30$ the lifetime for tunneling to a stau UFB-3 direction or CCB-4 minimum is shorter than the age of the universe, corresponding to $S_b < 400$, over a large portion of the otherwise acceptable parameter space. As expected, the newly disallowed regions are those with large and negative values of $m^2_{H_u}$ and $m^2_{H_d}$ at the input scale M_c. Of these two soft masses, only $m^2_{H_u}$ appears in the potential relevant for the UFB-3 direction or the CCB-4 minimum, and it has the stronger effect. Indeed, the isocontours of S_b coincide roughly with lines of constant $m^2_{H_u}$ for smaller values of $m^2_{H_d}$. For smaller values of $m^2_{H_u}$ the SM vacuum becomes sufficiently long-lived to describe our universe. The bounce action for these points is much larger simply because the effective width of the barrier is larger. Note that this stable region includes the minimal gaugino mediation point, $m^2_{H_u} = m^2_{H_d} = 0$ at M_c.

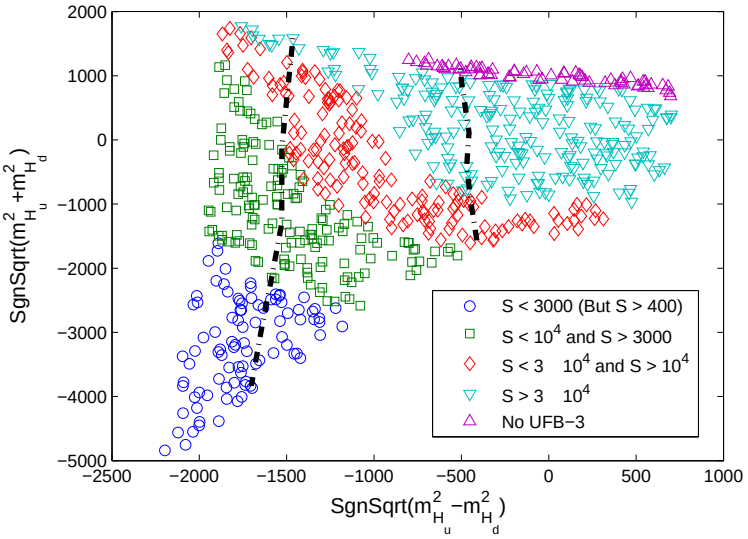

Figure 6.3: The bounce action for tunneling to a stau UFB-3 direction as a function of the HENS model parameters $m^2_{H_u}$ and $m^2_{H_d}$. The other HENS parameters have been fixed to be $m_{1/2} = 500\,\text{GeV}$, $\tan\beta = 10$, and $sgn(\mu) = 1$. All points shown are consistent with collider phenomenology. The points between the two dash-dotted lines have a neutralino LSP. $S > 400$ is cosmologically safe.

Comparing the plots for $m_{1/2} = 500$ GeV and $m_{1/2} = 1000$ GeV, we see that larger $m_{1/2}$ tends to yield a slightly more stable SM vacuum. This arises simply because increasing the input gaugino masses also increases the low-scale slepton soft masses through RG running. On the other hand, larger gaugino masses also permit more negative values of $m^2_{H_u}$, so there remain significant parameter regions in which the tunneling rate is too fast. From Fig. 6.1, where $m_{1/2} = 500$ GeV, we see that nearly the entire region in which the lightest superpartner is a neutralino is ruled out by our vacuum stability considerations. For $m_{1/2} = 1000$ GeV, there is a small region in which the lightest superpartner is a neutralino and the electroweak vacuum is sufficiently long-lived.

We turn next to the cases with $\tan\beta = 10$, for which the tau Yukawa coupling is smaller. In Figs. 6.3 and 6.4 we show ranges of the bounce action for tunneling from the SM vacuum to the UFB-3 direction for $\tan\beta = 10$ and $M_{1/2} = 500$, 300 GeV as a function

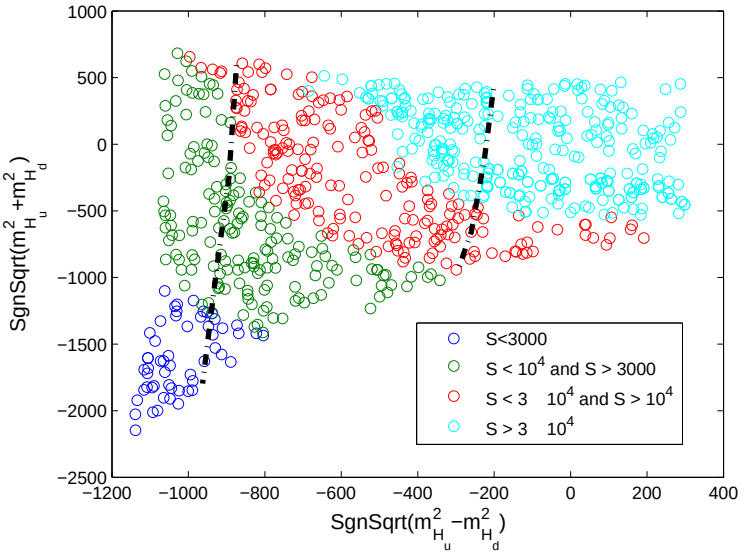

Figure 6.4: The bounce action for tunneling to a stau UFB-3 direction as a function of the HENS model parameters $m^2_{H_u}$ and $m^2_{H_d}$. The other HENS parameters have been fixed to be $m_{1/2} = 300\,\text{GeV}$, $\tan\beta = 10$, and $sgn(\mu) = 1$. All points shown are consistent with collider phenomenology. The points between the two dash-dot lines have a neutralino LSP. $S > 400$ is cosmologically safe.

of the input values of $m^2_{H_u}$ and $m^2_{H_d}$ at M_c. No CCB-4 local extremum is found for any of the points scanned over since the deviation from F-flatness is a sizeable effect in this case. The dot-dashed lines in these plots enclose the portion of parameter space in which the LSP is the lightest neutralino. (See Ref. [14] for more details.) From these plots we see that the lifetime of the standard electroweak vacuum against tunneling to a UFB-3 direction is safely large for both $m_{1/2} = 500$, 300 GeV. This is the result of the smaller value of the tau Yukawa coupling y_τ, which gives rise to a larger barrier against tunneling, Eq. (6.4). As before, with all else equal S_b increases with $m_{1/2}$ and so higher values of $m_{1/2}$ remain safe.

At smaller values of $\tan\beta$ the top quark Yukawa coupling grows larger, and we should check that the tunneling rate to CCB-4 minima associated with the stops is adequately small. As was previously discussed, this direction will only occur if $m^2_{H_d}$ is large and

negative. In Fig. 6.5 we show contours of the bounce action for tunneling to the stop CCB-4 minimum, as well as the regions in which the SM minimum is the true minimum. Only a very few points at the largest and most negative values of $m^2_{H_d}$ are excluded, while in the great majority of the parameter space the SM vacuum is the true minimum. We find a similar result for $m_{1/2} = 300$ GeV.

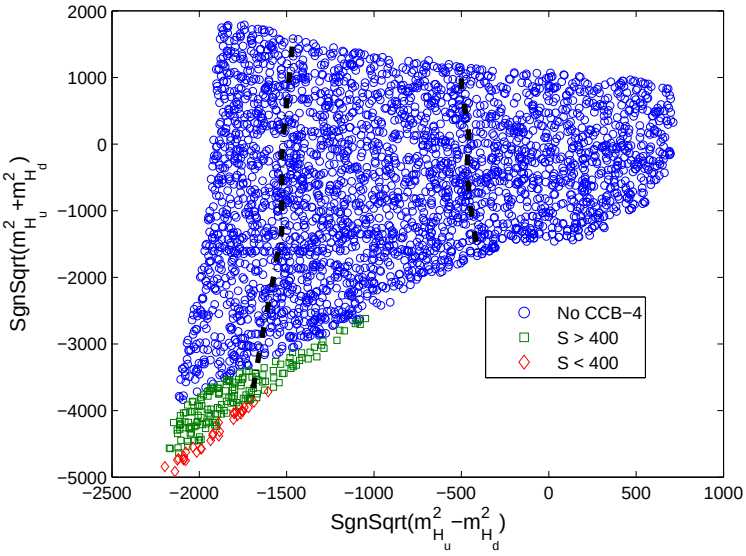

Figure 6.5: The bounce action for tunneling to a stop CCB-4 minimum as a function of the HENS model parameters $m^2_{H_u}$ and $m^2_{H_d}$. The other HENS parameters are $m_{1/2} = 500\,\text{GeV}$, $\tan\beta = 10$ and $sgn(\mu) = 1$. All these points are consistent with collider phenomenology. The points between the two dash-dot lines have a neutralino LSP. $S > 400$ is cosmologically safe.

CHAPTER VII

Conclusions

Supersymmetry has been recognized as a viable theory of physics beyond the Standard Model for many years now. It was quickly realized that it was not only viable, but also potentially useful in the quest to understand stability of the electroweak potential, radiative electroweak symmetry breaking, grand unification, dark matter, and baryogenesis. In subsequent years, there has been much effort devoted to understanding how supersymmetry breaking is to be achieved without creating additional phenomenological problems, such as large amounts of FCNC.

There are two particularly simple alternatives that keep the good features of supersymmetry while (mostly) dismissing the bad features. One approach is to raise the scalar masses significantly higher than the supersymmetric fermion masses. This is the idea of Split Supersymmetry discussed in the introduction. One drawback of this scenario is the apparent finetuning in the electroweak sector.

The approach we pursue in this article is in some sense the opposite of Split Supersymmetry. Here, rather than introduce a huge hierarchy of scalar masses over fermion masses, we wish to zero out the superpartner scalar masses at some scale (i.e., "Splat Supersymmetry"). The simplest model of all scalar masses having a zero boundary condition does not work. However, applying a small alteration to the most minimal idea, namely that the Higgs bosons are exempt from zero boundary condition requirement, preserves the good

features of these theories, while satisfying the phenomenological requirements described in the text.

This idea of Higgs Exempt No-Scale (HENS) supersymmetry has many phenomenological implications worthy of consideration at current and future experimental facilities. For example, we have found that the scenario can accommodate the tantalizing (but small) deviation of $(g-2)$ of the muon compared to the SM prediction. It also suggests a near maximal leptonic signal for the Tevatron, and thus provides an excellent benchmark theory for the Tevatron to either discover this form of supersymmetry or rule out large regions of parameter space in a clean way. Furthermore, the LHC signatures are of many multi-lepton events. Perhaps the most distinctive of them is the inclusive 4ℓ channel which can effectively rule out HENS models up to gaugino mass scales that are uncomfortably large from the normal finetuning point of view. For the most part, this form of supersymmetry is rather straightforward for the LHC to find. Because of the distinctively large 4ℓ signal and the small ratio of 0ℓ to 1ℓ signal, it should be quite easy to distinguish the HENS model from other. An important exception is the lightest Higgs boson, whose mass is pressured in this scenario to be low, and thus perhaps close to the current bound of 114 GeV. Given the difficulties of finding a Higgs boson less than 120 GeV [134], discovering the Higgs boson might be one of the more challenging steps in confirming the complete structure of this theory.

We also investigated the consequences of adding right-handed neutrinos to the HENS model. This model provides a simple and phenomenologically consistent solution to the supersymmetric flavor problem. Adding heavy right-handed neutrinos, lepton flavor mixing can arise due to the neutrino Yukawa matrix in the course of RG running. We have studied the constraints on the neutrino-extended HENS model that arise from the current bounds on LFV. We have also investigated whether the baryon asymmetry can be explained by

thermal leptogenesis induced by the heavy right-handed neutrinos.

We find that the neutrino-extended HENS model can be consistent with the existing bounds on LFV in two ways. First, the neutrino Yukawa couplings that contribute to lepton flavor mixing can be very small. In the context of a seesaw generating the light neutrino masses, this corresponds to lower values of the right-handed neutrino masses, below about 10^{11} GeV. The second way to suppress LFV in the HENS model to arrange for $m^2_{H_u}$ to be small at the input scale M_{GUT}. It is this soft mass that combines with the neutrino Yukawa couplings to source flavor mixing in the RG running. Taking $m^2_{H_u} \to 0$ therefore strongly suppresses LFV, even for larger values of the heavy neutrino masses.

In models with heavy right-handed neutrinos, the baryon asymmetry of the universe can be successfully explained by (thermal) leptogenesis. For this mechanism to be effective in the HENS model, the mass of the lightest right-handed neutrino must exceed about 10^{10} GeV. This implies a tension with the constraints from LFV. For both requirements to be met, either $m^2_{H_u}$ must be somewhat small or the neutrino Yukawa matrix must have a special structure. These constraints will be strengthened by current and upcoming searches for lepton flavor violation.

Our focus has been on enabling a theoretical idea (HENS) to be compatible with additional phenomenological requirements (neutrino masses and small LFV) and explanatory opportunities (baryon asymmetry). However, it should be noted that even though the HENS idea started out by minimizing LFV in low-scale supersymmetric theories, full compatibility with nature reintroduced flavor violations through neutrino Yukawa effects. This is a generic feature of supersymmetric theories that explicitly incorporate neutrino masses in the spectrum. As explained above, we find LFV bounds nontrivial to satisfy if the baryon asymmetry of the universe originates from thermal leptogenesis with hierarchical right-handed neutrinos. In our view, this highlights in yet another context the importance

of making progress in LFV experiments whose non-zero signal upon reaching better sensitivity will be complementary to the knowledge gained from high-energy LHC experiments and will be necessary to unravel the underlying theory.

We also considered the constraints placed on the HENS model from vacuum stability. Due to the large tachyonic Higgs soft masses that can emerge in this model, there often arise local vacuum states deeper than the standard electroweak minimum. Many points that are consistent with collider phenomenological constraints (described in Ref. [14]) are ruled out because they lead to an overly short-lived SM vacuum.

The most dangerous vacuum feature is a UFB-3 direction involving the stau fields. We have also found a new CCB-4 saddle point that facilitates tunneling to the UFB-3 direction. As a result, vacuum tunneling rates tend to be too fast for larger values of $\tan\beta$. At lower values of $\tan\beta$, tunneling to a CCB-4 direction involving stop fields rules out a very small portion of the parameter space, with the rest of the parameter space being safely long-lived.

We conclude that the HENS models with a neutralino LSP and larger values of $\tan\beta = 30$ are mostly ruled out subject to our assumptions about the input scale and gaugino mass universality. On the other hand, minimal gaugino mediation and the HENS models without a neutralino LSP may still have a sufficiently long-lived electroweak vacuum state at larger values of $\tan\beta$. For moderat values of $\tan\beta$, such as $\tan\beta = 10$, the constraints from vacuum tunneling are much weaker, and most of the parameter space that is consistent with collider lower-energy bounds remains viable.

APPENDICES

APPENDIX A

Sample Point Parameters

In this appendix, we list the relevant properties of the sample points A, B, C, D, E chosen for $\tan\beta = 10$ and $M_{1/2} = 500$ GeV. The locations of these points in the $SgnSqrt(m^2_{H_u} \pm m^2_{H_d})$ plane are shown in Figs. 4.3 and 4.4. We also list properties of the points A', B', C', D', E' corresponding to $\tan\beta = 30$ and $M_{1/2} = 500$ GeV.

	A	B	C	D	E
$SgnSqrt(-)$	-1480	-1103	-530	-1087	-712
$SgnSqrt(+)$	-820	-921	-900	-2138	1197
μ	1150	1033	868	1523	278
M_{A^0}	1465	1156	764	854	1060
M_1	210	210	210	210	209
M_2	389	389	389	389	398
$m_{\chi_1^0}$	209	209	209	210	193
$m_{\chi_2^0}$	385	385	383	387	266
$m_{\chi_3^0}$	1152	1034	871	1525	283
$m_{\chi_4^0}$	1156	1040	878	1527	420
$m_{\chi_1^\pm}$	385	385	383	387	254
$m_{\chi_2^\pm}$	1157	1041	878	1528	419
$m_{\tilde{\nu}_e}$	223	274	315	281	304
$m_{\tilde{e}_L}$	237	285	325	292	314
$m_{\tilde{e}_R}$	384	312	223	308	249
$m_{\tilde{\nu}_\tau}$	217	272	315	288	298
$m_{\tilde{\tau}_1}$	221	261	214	261	233
$m_{\tilde{\tau}_2}$	383	328	331	352	310
$m_{\tilde{g}}$	1156	1155	1152	1161	1151
$m_{\tilde{t}_1}$	901	875	837	1027	719
$m_{\tilde{t}_2}$	1069	1046	1017	1163	955
$m_{\tilde{u}_L}$	1019	1016	1012	1007	1020
$m_{\tilde{u}_R}$	933	952	969	943	972
Ωh^2	0.098	0.687	0.096	0.642	0.134

Table A.1: Model parameters and particle masses for sample points A, B, C, D, E, all with $\tan\beta = 10$ and $M_{1/2} = 500$ GeV. All dimensionful quantities in the table are listed in GeV units. The Ωh^2 values are valid computations for the assumption of standard thermal cosmological evolution and stable lightest neutralino. Viability of points B and D require alterations to the standard assumptions.

	A'	B'	C'	D'	E'
$SgnSqrt(-)$	-1595	-1019	-501	-1334	-1270
$SgnSqrt(+)$	-3241	-2219	-1601	-2981	-2084
μ	2195	1547	1153	2003	1542
M_{A^0}	1031	768	522	826	1045
M_1	212	211	211	212	211
M_2	391	390	390	391	390
$m_{\chi_1^0}$	212	211	210	212	211
$m_{\chi_2^0}$	390	388	387	390	388
$m_{\chi_3^0}$	2197	1549	1156	2005	1544
$m_{\chi_4^0}$	2197	1550	1159	2006	1546
$m_{\chi_1^\pm}$	390	388	387	390	388
$m_{\chi_2^\pm}$	2197	1551	1159	2006	1547
$m_{\tilde{\nu}_e}$	220	287	318	256	260
$m_{\tilde{e}_L}$	234	298	327	270	272
$m_{\tilde{e}_R}$	403	296	219	353	342
$m_{\tilde{\nu}_\tau}$	384	360	357	394	315
$m_{\tilde{\tau}_1}$	320	272	233	324	232
$m_{\tilde{\tau}_2}$	643	494	425	599	482
$m_{\tilde{g}}$	1168	1162	1154	1168	1161
$m_{\tilde{t}_1}$	1235	1043	924	1179	1038
$m_{\tilde{t}_2}$	1393	1165	1063	1321	1160
$m_{\tilde{u}_L}$	1004	1008	1008	1005	1009
$m_{\tilde{u}_R}$	908	946	964	926	935
Ωh^2	0.105	0.521	0.0954	0.749	0.104

Table A.2: Model parameters and particle masses for sample points A', B', C', D', E', all with $\tan\beta = 30$ and $M_{1/2} = 500$ GeV. All dimensionful quantities in the table are listed in GeV units. The Ωh^2 values are valid computations for the assumption of standard thermal cosmological evolution and stable lightest neutralino. Viability of points B' and D' require alterations to the standard assumptions.

APPENDIX B

Light Neutrino Parameters

Neutrino experiments have measured the value of two independent neutrino mass differences: the solar neutrino mass, $\Delta m^2_{\odot}$, and the atmospheric neutrino mass, $\Delta m^2_{@}$. The 2σ ranges of these mass differences are [68]

$$\Delta m^2_{@} = |m^2_{\nu_3} - m^2_{\nu_2}| = (2.1 - 2.7) \times 10^{-3}\text{eV}^2 \tag{B.1}$$

$$\Delta m^2_{\odot} = m^2_{\nu_2} - m^2_{\nu_1} = (7.3 - 8.1) \times 10^{-5}\text{eV}^2. \tag{B.2}$$

Since the sign of the atmospheric mass difference is undetermined, the hierarchy of the neutrino masses is unknown.

With two known mass differences and three light neutrinos, we can parametrize the masses of all three neutrinos in terms of a single parameter m_3. In the case of a normal hierarchy (NH), we have

$$m_3 = m_3,\ m_2 = \sqrt{m_3^2 - \Delta m^2_{@}},\ m_1 = \sqrt{m_3^2 - \Delta m^2_{@} - \Delta m^2_{\odot}}. \tag{B.3}$$

Demanding that the mass of the lightest right-handed neutrino be real, we obtain a lower bound on the heaviest left-handed neutrino of

$$m_3 = \sqrt{\Delta m^2_{@} + \Delta m^2_{\odot}} \simeq (0.047 - 0.053)\text{eV}. \tag{B.4}$$

We focus on the normal hierarchy in the present work, but we expect our results will be qualitatively the same for an inverted hierarchy (IH).

Whenever we fix a set of low energy neutrino parameters in our analysis, we consider the normal hierarchy with neutrino masses of

$$m_1 = 9.0 \times 10^{-4}\,\text{eV},\ m_2 = 9.0 \times 10^{-3}\,\text{eV},\ m_3 = 5.0 \times 10^{-2}\,\text{eV}. \tag{B.5}$$

For the mixing angles in the U-matrix, defined in Eq. (5.4), we use the central values of θ_{12} and θ_{23}, and set $\theta_{13} = 0$.

$$\theta_{12} = 35^\circ,\ \theta_{13} = 0^\circ,\ \theta_{23} = 45^\circ. \tag{B.6}$$

These light neutrino parameters are the low-scale values. We do not consider additional RG running of the light neutrino masses. As shown in [119], the RG effects will only make a difference of $10 - 15\%$. This will not qualitatively alter our results.

APPENDIX C

Sample Mass Spectrum

We list in Table C.1 the high-scale input HENS model parameters for points A and B discussed in the text. We also list some of the relevant low-scale model parameters obtained by RG running using SuSpect 2.34 [39]. In Table C.2 we collect the relevant superpartner masses corresponding to points A and B. Again, these were obtained using SuSpect 2.34 [39].

Parameter	A (GeV)	B (GeV)
$M_{1/2}$	300	300
$\tan\beta$	10	10
$SgnSqrt(m^2_{H_u})$	-668	-100
$SgnSqrt(m^2_{H_d})$	-511	-359
$sgn(\mu)$	$+$	$+$
M_1	123	122
M_2	231	230
μ	666	401
M_{A^0}	851	566
$m^2_{\tilde{L}_{1,2}}$	148	192
$m^2_{\tilde{E}_{1,2}}$	221	140

Table C.1: High-scale HENS model input parameters and selected low-scale output parameters for the sample points A and B discussed in the text.

Particle	A (GeV)	B (GeV)	Particle	A (GeV)	B (GeV)
$m_{\chi_1^0}$	120	118	$m_{\tilde{\nu}_e}$	134	180
$m_{\chi_2^0}$	230	219	$m_{\tilde{e}_L}$	155	197
$m_{\chi_3^0}$	667	407	$m_{\tilde{e}_R}$	225	146
$m_{\chi_4^0}$	673	425	$m_{\tilde{\nu}_\tau}$	131	179
$m_{\chi_1^\pm}$	230	219	$m_{\tilde{\tau}_1}$	136	132
$m_{\chi_2^\pm}$	674	425	$m_{\tilde{\tau}_2}$	231	201

Table C.2: Low-scale superpartner masses for the sample points A and B discussed in the text.

BIBLIOGRAPHY

BIBLIOGRAPHY

[1] H. Goldberg, Phys. Rev. Lett. **50**, 1419 (1983).

[2] For reviews, see for example H. E. Haber and G. L. Kane, Phys. Rept. **117**, 75 (1985); S. P. Martin, hep-ph/9709356; D. J. H. Chung et al., Phys. Rept. **407**, 1 (2005) [hep-ph/0312378];

[3] M. A. Luty, arXiv:hep-th/0509029.

[4] T. P. Cheng and L. F. Li, Phys. Rev. Lett. **45**, 1908 (1980).

[5] F. Gabbiani, E. Gabrielli, A. Masiero and L. Silvestrini, Nucl. Phys. B **477**, 321 (1996) [arXiv:hep-ph/9604387].

[6] M. Drees, R. Godbole and P. Roy, *Hackensack, USA: World Scientific (2004) 555 p*

[7] J. F. Gunion, H. E. Haber and M. Sher, Nucl. Phys. B **306**, 1 (1988).

[8] M. Claudson, L. J. Hall and I. Hinchliffe, Nucl. Phys. B **228**, 501 (1983).

[9] J. A. Casas, A. Lleyda and C. Munoz, Nucl. Phys. B **471**, 3 (1996) [arXiv:hep-ph/9507294].

[10] A. Riotto and E. Roulet, Phys. Lett. B **377**, 60 (1996) [arXiv:hep-ph/9512401].

[11] A. Kusenko, P. Langacker and G. Segre, Phys. Rev. D **54**, 5824 (1996) [arXiv:hep-ph/9602414].

[12] J. R. Ellis, J. Giedt, O. Lebedev, K. Olive and M. Srednicki, Phys. Rev. D **78**, 075006 (2008) [arXiv:0806.3648 [hep-ph]].

[13] S. Komine and M. Yamaguchi, Phys. Rev. D **63**, 035005 (2001) [hep-ph/0007327]. C. Balazs and R. Dermisek, JHEP **0306**, 024 (2003) [hep-ph/0303161].

[14] J. L. Evans, D. E. Morrissey and J. D. Wells, Phys. Rev. D **75**, 055017 (2007) [hep-ph/0611185].

[15] For a review, see A. B. Lahanas and D. V. Nanopoulos, Phys. Rept. **145**, 1 (1987); A. B. Lahanas, "No scale supergravity: A Viable scenario for understanding the SUSY CERN-TH-7092-93 *Lectures given at International School of Subnuclear Physics: 31th Course: From Supersymmetry to the Origin of Space-Time, Erice, Italy, 4- 12 Jul 1993*

[16] E. Cremmer, S. Ferrara, C. Kounnas and D. V. Nanopoulos, Phys. Lett. B **133**, 61 (1983).

[17] J. R. Ellis, A. B. Lahanas, D. V. Nanopoulos and K. Tamvakis, Phys. Lett. B **134**, 429 (1984).

[18] J. R. Ellis, C. Kounnas and D. V. Nanopoulos, Nucl. Phys. B **241**, 406 (1984).

[19] J. R. Ellis, C. Kounnas and D. V. Nanopoulos, Nucl. Phys. B **247**, 373 (1984).

[20] See, for example, N. Weiner, hep-ph/0106097; C. Csaki, G. D. Kribs and J. Terning, Phys. Rev. D **65**, 015004 (2002) [hep-ph/0107266].

[21] E. Witten, Phys. Lett. B **155**, 151 (1985). P. G. Camara, L. E. Ibanez and A. M. Uranga, Nucl. Phys. B **689**, 195 (2004) [hep-th/0311241]. K. Choi, A. Falkowski, H. P. Nilles and M. Olechowski, Nucl. Phys. B **718**, 113 (2005) [hep-th/0503216].

[22] L. Randall and R. Sundrum, Nucl. Phys. B **557**, 79 (1999) [hep-th/9810155]. G. F. Giudice, M. A. Luty, H. Murayama and R. Rattazzi, JHEP **9812**, 027 (1998) [hep-ph/9810442].

[23] C. Csaki, arXiv:hep-ph/0404096.

[24] M. E. Peskin and D. V. Schroeder, *Reading, USA: Addison-Wesley (1995) 842 p*

[25] M. A. Luty and R. Sundrum, Phys. Rev. D **65**, 066004 (2002) [hep-th/0105137]. M. Luty and R. Sundrum, Phys. Rev. D **67**, 045007 (2003) [hep-th/0111231]. M. Ibe, K. I. Izawa, Y. Nakayama, Y. Shinbara and T. Yanagida, Phys. Rev. D **73**, 015004 (2006) [hep-ph/0506023]. M. Ibe, K. I. Izawa, Y. Nakayama, Y. Shinbara and T. Yanagida, Phys. Rev. D **73**, 035012 (2006) [hep-ph/0509229].

[26] M. Schmaltz and R. Sundrum, hep-th/0608051.

[27] G. Perez, T. S. Roy and M. Schmaltz, arXiv:0811.3206 [hep-ph].

[28] K. Konishi, Phys. Lett. B **135**, 439 (1984).

[29] H. Murayama, Y. Nomura and D. Poland, Phys. Rev. D **77**, 015005 (2008) [arXiv:0709.0775 [hep-ph]].

[30] A. E. Nelson and M. J. Strassler, JHEP **0009**, 030 (2000) [hep-ph/0006251].

[31] A. E. Nelson and M. J. Strassler, JHEP **0207**, 021 (2002) [hep-ph/0104051].

[32] T. Kobayashi and H. Terao, Phys. Rev. D **64**, 075003 (2001) [hep-ph/0103028].

[33] T. Kobayashi, H. Nakano, T. Noguchi and H. Terao, Phys. Rev. D **66**, 095011 (2002) [hep-ph/0202023].

[34] K. R. Dienes, E. Dudas and T. Gherghetta, Phys. Lett. B **436**, 55 (1998) [hep-ph/9803466]; K. R. Dienes, E. Dudas and T. Gherghetta, Nucl. Phys. B **537**, 47 (1999) [hep-ph/9806292].

[35] A. E. Nelson and M. J. Strassler, Phys. Rev. D **56**, 4226 (1997) [hep-ph/9607362].

[36] M. Schmaltz and W. Skiba, Phys. Rev. D **62**, 095005 (2000) [arXiv:hep-ph/0001172]; M. Schmaltz and W. Skiba, Phys. Rev. D **62**, 095004 (2000) [arXiv:hep-ph/0004210].

[37] D. E. Kaplan, G. D. Kribs and M. Schmaltz, Phys. Rev. D **62**, 035010 (2000) [hep-ph/9911293]; Z. Chacko, M. A. Luty, A. E. Nelson and E. Ponton, JHEP **0001**, 003 (2000) [hep-ph/9911323].

[38] S. P. Martin and M. T. Vaughn, Phys. Rev. D **50**, 2282 (1994) [hep-ph/9311340].

[39] A. Djouadi, J. L. Kneur and G. Moultaka, [hep-ph/0211331].

[40] W. M. Yao *et al.* [Particle Data Group], J. Phys. G **33**, 1 (2006).

[41] E. Brubaker *et al.* [Tevatron Electroweak Working Group], hep-ex/0608032.

[42] E. Barberio *et al.* [Heavy Flavor Averaging Group (HFAG)], hep-ex/0603003.

[43] S. Komine, T. Moroi and M. Yamaguchi, Phys. Lett. B **507**, 224 (2001) [hep-ph/0103182].

[44] T. Moroi, Phys. Rev. D **53**, 6565 (1996) [Erratum-ibid. D **56**, 4424 (1997)] [hep-ph/9512396].

[45] R. Barate *et al.* [LEP Working Group for Higgs boson searches], Phys. Lett. B **565**, 61 (2003) [hep-ex/0306033].

[46] D. E. Morrissey and J. D. Wells, Phys. Rev. D **74**, 015008 (2006) [hep-ph/0512019].

[47] See R. Barbieri and G. F. Giudice, Nucl. Phys. B **306**, 63 (1988), and references thereto.

[48] A. Gould, B. T. Draine, R. W. Romani and S. Nussinov, Phys. Lett. B **238**, 337 (1990); A. De Rujula, S. L. Glashow and U. Sarid, Nucl. Phys. B **333**, 173 (1990); S. Dimopoulos, D. Eichler, R. Esmailzadeh and G. D. Starkman, Phys. Rev. D **41**, 2388 (1990).

[49] T. Falk, K. A. Olive and M. Srednicki, Phys. Lett. B **339**, 248 (1994) [hep-ph/9409270].

[50] L. J. Hall, T. Moroi and H. Murayama, Phys. Lett. B **424**, 305 (1998) [hep-ph/9712515]. N. Arkani-Hamed, L. J. Hall, H. Murayama, D. R. Smith and N. Weiner, Phys. Rev. D **64**, 115011 (2001) [hep-ph/0006312]. D. Hooper, J. March-Russell and S. M. West, Phys. Lett. B **605**, 228 (2005) [hep-ph/0410114]. T. Asaka, K. Ishiwata and T. Moroi, Phys. Rev. D **73**, 051301 (2006) [hep-ph/0512118]. S. Gopalakrishna, A. de Gouvea and W. Porod, JCAP **0605**, 005 (2006) [hep-ph/0602027].

[51] For a nice review of these scenarios, see: J. L. Feng, Annals Phys. **315** (2005) 2.

[52] P. Gondolo, J. Edsjo, P. Ullio, L. Bergstrom, M. Schelke and E. A. Baltz, JCAP **0407**, 008 (2004) [astro-ph/0406204].

[53] D. N. Spergel *et al.*, [astro-ph/0603449].

[54] For some recent examples, see G. Gelmini, P. Gondolo, A. Soldatenko and C. E. Yaguna, Phys. Rev. D **74**, 083514 (2006) [hep-ph/0605016]. D. E. Morrissey and J. D. Wells, hep-ph/0606234.

[55] D. S. Akerib *et al.*, Nucl. Instrum. Meth. A **559**, 390 (2006).

[56] J. R. Ellis, A. D. Linde and D. V. Nanopoulos, Phys. Lett. B **118**, 59 (1982).

[57] See, for example, M. Dine, R. Kitano, A. Morisse and Y. Shirman, Phys. Rev. D **73**, 123518 (2006) [hep-ph/0604140], and references therein.

[58] J. L. Feng, S. f. Su and F. Takayama, Phys. Rev. D **70**, 063514 (2004) [hep-ph/0404198]; J. L. Feng, S. Su and F. Takayama, Phys. Rev. D **70**, 075019 (2004) [hep-ph/0404231].

[59] J. L. Evans, D. E. Morrissey and J. D. Wells, Phys. Rev. D **75**, 055017 (2007) [arXiv:hep-ph/0611185].

[60] See, for example, H. Baer and X. Tata, Phys. Rev. D **47**, 2739 (1993); S. Mrenna, G. L. Kane, G. D. Kribs and J. D. Wells, Phys. Rev. D **53**, 1168 (1996) [hep-ph/9505245]; V. D. Barger, C. Kao and T. j. Li, Phys. Lett. B **433**, 328 (1998) [hep-ph/9804451]; E. Accomando, R. Arnowitt and B. Dutta, Phys. Lett. B **475**, 176 (2000) [hep-ph/9811300]; V. D. Barger and C. Kao, Phys. Rev. D **60**, 115015 (1999) [hep-ph/9811489]; J. D. Lykken and K. T. Matchev, Phys. Rev. D **61**, 015001 (2000) [hep-ph/9903238].

[61] K. T. Matchev and D. M. Pierce, Phys. Rev. D **60**, 075004 (1999) [hep-ph/9904282]; K. T. Matchev and D. M. Pierce, Phys. Lett. B **467**, 225 (1999) [hep-ph/9907505].

[62] H. Baer, M. Drees, F. Paige, P. Quintana and X. Tata, Phys. Rev. D **61**, 095007 (2000) [hep-ph/9906233].

[63] F. E. Paige, S. D. Protopopescu, H. Baer and X. Tata, hep-ph/0312045.

[64] H. Baer, A. Belyaev, T. Krupovnickas and X. Tata, Phys. Rev. D **65**, 075024 (2002) [hep-ph/0110270].

[65] H. Baer, C. h. Chen, F. Paige and X. Tata, Phys. Rev. D **52**, 2746 (1995) [hep-ph/9503271].

[66] H. Baer, C. h. Chen, F. Paige and X. Tata, Phys. Rev. D **53**, 6241 (1996) [hep-ph/9512383].

[67] ATLAS detector and physics performance. Technical design report. Vol. 2, CERN-LHCC-99-15, ATLAS-TDR-15, May 1999.

[68] For recent reviews of neutrino physics, see:
R. N. Mohapatra *et al.*, Rept. Prog. Phys. **70**, 1757 (2007) [hep-ph/0510213]; R. N. Mohapatra and A. Y. Smirnov, Ann. Rev. Nucl. Part. Sci. **56**, 569 (2006) [hep-ph/0603118]; A. Strumia and F. Vissani, [hep-ph/0606054].

[69] F. Borzumati and A. Masiero, Phys. Rev. Lett. **57**, 961 (1986).

[70] M. Fukugita and T. Yanagida, Phys. Lett. B **174**, 45 (1986).

[71] M. A. Luty, Phys. Rev. D **45**, 455 (1992).

[72] F. R. Klinkhamer and N. S. Manton, Phys. Rev. D **30**, 2212 (1984).

[73] V. A. Kuzmin, V. A. Rubakov and M. E. Shaposhnikov, Phys. Lett. B **155**, 36 (1985).

[74] A. D. Sakharov, Pisma Zh. Eksp. Teor. Fiz. **5**, 32 (1967) [JETP Lett. **5**, 24 (1967 SOPUA,34,392-393.1991 UFNAA,161,61-64.1991)].

[75] E. J. Chun, J. L. Evans, D. E. Morrissey and J. D. Wells, Phys. Rev. D **79**, 015003 (2009) [arXiv:0804.3050 [hep-ph]].

[76] S. Pascoli, S. T. Petcov and C. E. Yaguna, Phys. Lett. B **564**, 241 (2003) [hep-ph/0301095]; S. Pascoli, S. T. Petcov and W. Rodejohann, Phys. Rev. D **68**, 093007 (2003) [hep-ph/0302054].

[77] P. H. Chankowski, J. R. Ellis, S. Pokorski, M. Raidal and K. Turzynski, Nucl. Phys. B **690** 297 (2004) [hep-ph/0403180].

[78] S. T. Petcov, W. Rodejohann, T. Shindou and Y. Takanishi, Nucl. Phys. B **739**, 208 (2006) [hep-ph/0510404].

[79] S. Antusch, E. Arganda, M. J. Herrero and A. M. Teixeira, JHEP **0611**, 090 (2006) [hep-ph/0607263].

[80] M. Maltoni, T. Schwetz, M. A. Tortola and J. W. F. Valle, New J. Phys. **6**, 122 (2004) [hep-ph/0405172].

[81] G. L. Fogli, E. Lisi, A. Marrone and A. Palazzo, Prog. Part. Nucl. Phys. **57**, 742 (2006) [hep-ph/0506083].

[82] B. Pontecorvo, Sov. Phys. JETP **6**, 429 (1957) [Zh. Eksp. Teor. Fiz. **33**, 549 (1957)].

[83] Z. Maki, M. Nakagawa and S. Sakata, Prog. Theor. Phys. **28**, 870 (1962).

[84] J. A. Casas and A. Ibarra, Nucl. Phys. B **618**, 171 (2001) [hep-ph/0103065].

[85] S. T. Petcov, S. Profumo, Y. Takanishi and C. E. Yaguna, Nucl. Phys. B **676**, 453 (2004) [hep-ph/0306195].

[86] J. Hisano, T. Moroi, K. Tobe, M. Yamaguchi and T. Yanagida, Phys. Lett. B **357**, 579 (1995) [hep-ph/9501407]; J. Hisano, T. Moroi, K. Tobe and M. Yamaguchi, Phys. Rev. D **53**, 2442 (1996) [hep-ph/9510309].

[87] J. Hisano and D. Nomura, Phys. Rev. D **59**, 116005 (1999) [hep-ph/9810479].

[88] I. Masina and C. A. Savoy, Nucl. Phys. B **661**, 365 (2003) [hep-ph/0211283].

[89] J. L. Feng, A. Rajaraman and B. T. Smith, Phys. Rev. D **74**, 015013 (2006) [hep-ph/0512172].

[90] R. R. de Austri, R. Trotta and L. Roszkowski, JHEP **0605**, 002 (2006) [hep-ph/0602028]; B. C. Allanach, Phys. Lett. B **635**, 123 (2006) [hep-ph/0601089]; B. C. Allanach, C. G. Lester and A. M. Weber, JHEP **0612**, 065 (2006) [hep-ph/0609295]; B. C. Allanach, K. Cranmer, C. G. Lester and A. M. Weber, JHEP **0708**, 023 (2007) [0705.0487 [hep-ph]].

[91] M. L. Brooks *et al.* [MEGA Collaboration], Phys. Rev. Lett. **83**, 1521 (1999) [hep-ex/9905013].

[92] B. Aubert *et al.* [BABAR Collaboration], Phys. Rev. Lett. **95**, 041802 (2005) [hep-ex/0502032].

[93] K. Hayasaka *et al.* [Belle Collaboration], 0705.0650 [hep-ex].

[94] B. Aubert *et al.* [BABAR Collaboration], Phys. Rev. Lett. **96**, 041801 (2006) [hep-ex/0508012].

[95] E. Komatsu *et al.* [WMAP Collaboration], arXiv:0803.0547 [astro-ph].

[96] A. Riotto, arXiv:hep-ph/9807454.

[97] G. 't Hooft, Phys. Rev. Lett. **37**, 8 (1976).

[98] A. Abada, S. Davidson, A. Ibarra, F. X. Josse-Michaux, M. Losada and A. Riotto, JHEP **0609**, 010 (2006) [hep-ph/0605281].

[99] A. Abada, S. Davidson, F. X. Josse-Michaux, M. Losada and A. Riotto, JCAP **0604**, 004 (2006) [hep-ph/0601083].

[100] E. Nardi, Y. Nir, J. Racker and E. Roulet, JHEP **0601**, 068 (2006) [hep-ph/0512052].

[101] E. Nardi, Y. Nir, E. Roulet and J. Racker, JHEP **0601**, 164 (2006) [hep-ph/0601084].

[102] E. Nardi, J. Racker and E. Roulet, JHEP **0709**, 090 (2007) [0707.0378 [hep-ph]].

[103] S. Blanchet and P. Di Bari, arXiv:0807.0743 [hep-ph].

[104] S. Davidson and A. Ibarra, Phys. Lett. B **535**, 25 (2002) [hep-ph/0202239].

[105] G. F. Giudice, A. Notari, M. Raidal, A. Riotto and A. Strumia, Nucl. Phys. B **685**, 89 (2004) [hep-ph/0310123].

[106] T. Hambye, Y. Lin, A. Notari, M. Papucci and A. Strumia, Nucl. Phys. B **695**, 169 (2004) [hep-ph/0312203].

[107] M. Bolz, A. Brandenburg and W. Buchmuller, Nucl. Phys. B **606**, 518 (2001) [Erratum-ibid. B **790**, 336 (2008)] [hep-ph/0012052].

[108] W. Buchmuller, K. Hamaguchi and J. Kersten, Phys. Lett. B **632**, 366 (2006) [hep-ph/0506105]. W. Buchmuller, J. Kersten and K. Schmidt-Hoberg, JHEP **0602**, 069 (2006) [hep-ph/0512152]. W. Buchmuller, L. Covi, J. Kersten and K. Schmidt-Hoberg, JCAP **0611**, 007 (2006) [hep-ph/0609142].

[109] M. Kawasaki, K. Kohri and T. Moroi, Phys. Rev. D **71**, 083502 (2005) [astro-ph/0408426].

[110] M. Flanz, E. A. Paschos and U. Sarkar, Phys. Lett. B **345**, 248 (1995) [Erratum-ibid. B **382**, 447 (1996)] [hep-ph/9411366]; M. Flanz, E. A. Paschos, U. Sarkar and J. Weiss, Phys. Lett. B **389**, 693 (1996) [hep-ph/9607310].

[111] L. Covi, E. Roulet and F. Vissani, Phys. Lett. B **384**, 169 (1996) [hep-ph/9605319].

[112] A. Pilaftsis, Phys. Rev. D **56**, 5431 (1997) [hep-ph/9707235].

[113] A. Pilaftsis and T. E. J. Underwood, Nucl. Phys. B **692**, 303 (2004) [hep-ph/0309342].

[114] T. Hambye, J. March-Russell and S. M. West, JHEP **0407**, 070 (2004) [arXiv:hep-ph/0403183].

[115] T. Asaka, K. Hamaguchi, M. Kawasaki and T. Yanagida, Phys. Lett. B **464**, 12 (1999) [hep-ph/9906366]; T. Asaka, K. Hamaguchi, M. Kawasaki and T. Yanagida, Phys. Rev. D **61**, 083512 (2000) [hep-ph/9907559].

[116] G. F. Giudice, M. Peloso, A. Riotto and I. Tkachev, JHEP **9908**, 014 (1999) [hep-ph/9905242]; G. F. Giudice, A. Riotto and A. Zaffaroni, Nucl. Phys. B **710**, 511 (2005) [hep-ph/0408155]; G. F. Giudice, L. Mether, A. Riotto and F. Riva, 0804.0166 [hep-ph].

[117] T. Mori, Nucl. Phys. Proc. Suppl. **169**, 166 (2007).

[118] J. L. . Hewett *et al.*, hep-ph/0503261.

[119] S. Antusch, J. Kersten, M. Lindner and M. Ratz, Nucl. Phys. B **674**, 401 (2003) [hep-ph/0305273].

[120] M. Quiros, Helv. Phys. Acta **67**, 451 (1994).

[121] M. S. Carena, M. Quiros and C. E. M. Wagner, Phys. Lett. B **380**, 81 (1996) [arXiv:hep-ph/9603420]; M. Carena, G. Nardini, M. Quiros and C. E. M. Wagner, arXiv:0809.3760 [hep-ph].

[122] M. Dine, L. Randall and S. D. Thomas, Phys. Rev. Lett. **75**, 398 (1995) [arXiv:hep-ph/9503303].

[123] C. Balazs and R. Dermisek, JHEP **0306**, 024 (2003) [arXiv:hep-ph/0303161].

[124] J. R. Ellis, K. A. Olive and Y. Santoso, Phys. Lett. B **539**, 107 (2002) [arXiv:hep-ph/0204192]; J. R. Ellis, T. Falk, K. A. Olive and Y. Santoso, Nucl. Phys. B **652**, 259 (2003) [arXiv:hep-ph/0210205];

[125] H. Baer, A. Mustafayev, S. Profumo, A. Belyaev and X. Tata, JHEP **0507**, 065 (2005) [arXiv:hep-ph/0504001].

[126] W. Buchmuller, J. Kersten and K. Schmidt-Hoberg, JHEP **0602**, 069 (2006) [arXiv:hep-ph/0512152]; W. Buchmuller, L. Covi, J. Kersten and K. Schmidt-Hoberg, arXiv:hep-ph/0609142.

[127] S. R. Coleman, Phys. Rev. D **15**, 2929 (1977) [Erratum-ibid. D **16**, 1248 (1977)].

[128] C. G. . Callan and S. R. Coleman, Phys. Rev. D **16**, 1762 (1977).

[129] S. R. Coleman, V. Glaser and A. Martin, Commun. Math. Phys. **58**, 211 (1978).

[130] A. Kusenko, Phys. Lett. B **358**, 51 (1995) [arXiv:hep-ph/9504418];

[131] T. Konstandin and S. J. Huber, JCAP **0606**, 021 (2006) [arXiv:hep-ph/0603081].

[132] M. J. Duncan and L. G. Jensen, Phys. Lett. B **291**, 109 (1992).

[133] J. Mathews and R.L. Walker, *Mathematical Methods of Physics* (Addison, 1970).

[134] S. Asai *et al.* (ATLAS Collaboration), Eur. Phys. J. C **32S2**, 19 (2004) [hep-ph/0402254]. S. Abdullin *et al.* (CMS Collaboration), Eur. Phys. J. C **39S2**, 41 (2005).